AN ABSTRACT OF THE THESIS OF

Jeffrey W. Schnick for the degree of Doctor of Philosophy in Physics presented on July 5, 1988.

Title: A Potential Model Investigation of the Low-Energy Antikaon-Nucleon Interaction and Antikaon-Nucleus Bound States

Abstract approved: Redacted for privacy 11 July 1988

Rubin H. Landau

The parameters of separable coupled channels s-wave potentials for the strong $\overline{K}N$ interaction are determined from low energy K^-p scattering data with additional constraints from $\pi^-p \rightarrow \pi\Sigma K^0$ production data. The shifts and widths of the Coulomb bound states in kaonic hydrogen are calculated with these potentials and compared with experiment. Optical potentials are constructed from $\overline{K}N$ t-matrices derived from the separable potentials and these optical potentials are used to calculate kaonic helium and kaonic carbon shifts and widths which are also compared with experiment.

A Potential Model Investigation of the Low-Energy Antikaon-Nucleon Interaction and Antikaon-Nucleus Bound States

by

Jeffrey W. Schnick

A Thesis submitted to

Oregon State University

in partial fulfillment of the
requirements for the degree of

Doctor of Philosophy

Completed July 5, 1988

Commencement June 1989

APPROVED:

Redacted for privacy 11 July 1988

Professor of Physics in charge of major

Redacted for privacy 7/22/88

Head of Department of Physics

Redacted for privacy

Dean of Graduate School

Date thesis presented July 5, 1988

Typed by Jeffrey W. Schnick for Jeffrey W. Schnick

ACKNOWLEDGEMENTS

This thesis is dedicated to Marie, Sara, and Natalie.

I am extremely thankful to Dr. Rubin H. Landau for providing me with exactly the right amount of guidance in selecting this topic of research and seeing it through. It has been very rewarding to work with someone with his patience, understanding, dedication, and professionalism. I thank Dr. Landau and Mrs. Landau for the friendship they have shared with my family.

I thank Beato Cheng for initiating this research. I thank Milton Sagen, Guangliang He, and Paul Fink for their many hours of helpful discussion and for all the assistance they provided me on this project. I thank Dr. Rubin H. Landau, Dr. Shaul Levi, Dr. Victor A. Madsen, Dr. David J. Griffiths, and Dr. Albert W. Stetz for their critical review of the material and their excessive cooperation with respect to scheduling requirements.

I thank the United States Department of Energy for research report.

Table of Contents

List of Figures

Figure | Page

Figure Page

List of Tables

A Potential Model Investigation of the Low-Energy Antikaon-Nucleon Interaction and Antikaon-Nucleus Bound States

Chapter 1

Introduction

1.1 Historical Sketch

The negatively charged antikaon held early promise as a good projectile for probing the nuclear surface. It is absorbed on one nucleon and thus reactive enough that it would be unlikely to penetrate the nucleus before interacting with it. Early attempts [1]–[14] at determining the distribution of nucleons near the surface of the nucleus by means of K^--nucleus experiments [15]–[22] slowly revealed the fact that the elementary antikaon-nucleon interaction needed further study if any information on nuclear matter distribution was to be gained from these experiments. Studies of the antikaon-nucleon interaction [6,23] turned up a puzzle which has rendered the antikaon useless as a

probe of the nucleus. The puzzle came about from the fact that conventional interpretations of low energy K^-p scattering experiments predicted a K^-p atom which was less bound because of the strong force than it would be if the interaction was purely Coulombic, while direct measurement of the kaonic hydrogen energy shift [24]–[26] showed it to be more bound. Associated with the puzzle is the presence of an s-wave isospin-0 resonance in the $\pi\Sigma$ system. Historically, this resonance has been known as the Y_0^* resonance. The modern nomenclature for it is $\Lambda(1405)$. The $\pi\Sigma$ system couples strongly to the K^-p system. The $\pi\Sigma$ threshold (sum of the masses of the two particles) lies 100 MeV below the K^-p threshold and the $\Lambda(1405)$ resonance lies 30 MeV below.

The nature of the $\Lambda(1405)$ is not well understood. Most likely it is either a conventional $\pi\Sigma$ resonance, a $\overline{K}N$ bound state, an elementary three-quark state, or some combination of these. Whatever it is, its existence makes the K^-p system both difficult to understand and interesting to study.

1.2 Point of View

This study represents an attempt to determine what nature has to tell us about the K^-p interaction —nature as opposed to a particular theory or model. We have operated within a model, and with a certain set of hypotheses, but the hope is that the model is general enough to reveal the physics of the actual interaction.

Our choice of theoretical tools and point of view is as follows: We use a potential model in order to build in the correct probabilistic features of

Quantum Mechanics. We solve a Lippmann-Schwinger equation which for the nonrelativistic case is just the integral form of the Schrödinger equation and for the relativistic case corresponds to the Blankenbecler-Sugar equation with certain simplifying assumptions. The potential is chosen to be sophisticated enough to include the important physics —coupled channels, separate isospin parts, nonlocality, and energy dependence— yet simple enough to make it a useful tool —separable Yamaguchi— and general enough to avoid prejudicing the results. In that this study is an attempt to understand nature we rely heavily on published experimental results. In this spirit we accept the kaonic hydrogen experiments at face value even though they have received much criticism [27,28]. In order to get further information on the subthreshold behavior of the K^-p scattering amplitude we also use the results of x-ray experiments on heavier kaonic atoms in an optical potential model. Further, we employ a final state interaction model to include information from the $\pi^-p \to \pi\Sigma K^0$ production experiment. All of these experiments provide important input to supplement the results of low-energy K^-p scattering.

We do not include the results of Nuclear-Coulomb interference experiments. These experiments can in principle provide valuable information. They give the scattering amplitude itself as opposed to the square modulus of the scattering amplitude. Unfortunately, the the results of the experiments carried out at low energies are ambiguous. Specifically, Coulomb-Nuclear interference shows the sign of the real part of the K^-p scattering amplitude to be positive in [29] for kaon laboratory momenta between 100 and 175 MeV/c and negative in [30] for kaon laboratory momenta between 100 and 200 MeV/c where the errors quoted are such that both experiments

yield a scattering amplitude for which the real part is consistent with negative, positive or zero values. At high energies the results are unambiguous. In reference [31] the K^-p scattering amplitude is given down to 0.9 GeV. Extrapolations have been carried out [31,32] with results that support the interpretation of low energy scattering experiments and thus contradict the kaonic hydrogen data[1]. The extrapolations are carried out over an enormous energy range however and further work in this area is needed before they can be considered definitive. The present work is not valid at the high energies for which nuclear Coulomb interference data is available and it is for this reason that we do not test our results against the interference data.

1.3 Goals

The purpose of this study is to gain information on the structure of the $\overline{K}N$ interaction. In particular, we attempt to shed some light on the puzzle regarding the kaonic hydrogen shift. To gain this information we address the following questions: What is the nature of the scattering amplitude as a complex analytic function of incident and outgoing momenta and total energy? Can the interaction be described in terms of mesons and baryons or is a more microscopic model required, such as one involving quarks? The answer to this question can be expected to shed some light on the nature of the $\Lambda(1405)$ resonance. Is it important to use relativistic kinematics in attempting to describe the interaction? In answering these questions we gain

[1] In [32] Martin has included one "data point" at a K^- lab momentum of 335 MeV/c calculated from other workers' differential cross sections published in [33].

some useful insights which can be generalized and applied to other systems.

Chapter 2

K^-p Scattering

2.1 Experiment

In scattering negatively charged antikaons from protons, several final states are possible. The hadronic reactions important at low energies are:

$$\begin{aligned} K^-p &\rightarrow K^-p \\ &\rightarrow \overline{K}^o n \\ &\rightarrow \pi^+\Sigma^- \\ &\rightarrow \pi^o\Sigma^o \\ &\rightarrow \pi^-\Sigma^+ \\ &\rightarrow \pi^o\Lambda^o \end{aligned} \tag{2.1}$$

The branching ratios for other hadronic interactions such as

$$\begin{aligned} K^-p &\rightarrow \Sigma^-\pi^0\pi^+ \\ &\rightarrow \Sigma^+\pi^0\pi^- \end{aligned}$$

and for electromagnetic interactions such as

$$\begin{aligned} K^- p &\rightarrow \Sigma^0 \gamma \\ &\rightarrow \Lambda \gamma \end{aligned}$$

are so small (down by at least three orders of magnitude) as to allow one to neglect the coupling to these channels in analyzing the scattering to the dominant channels.

Scattering cross sections for the important reactions indicated above have been measured in a number of experiments. These low energy $K^- p$ scattering experiments are challenging. The difficulty lies in the short path lengths traveled by the particles in the final state. These tracks are on the order of millimeters in length. Modern electronic detection apparatus are unsuitable. Almost all the experiments are carried out using bubble chambers[2]. Tens of thousands of photographs are analyzed to yield only hundreds of events from which cross sections are determined. Several groups [29],[33]–[40] have taken on the challenge with results for the total cross section of the reactions indicated in equation 2.1 in fairly good agreement.

In the experiment, low-energy kaons impinge upon a liquid hydrogen target. The kaons interact with (among other things) the protons in the target. The incoming K^- and the charged particles produced in the interaction cause the supercooled liquid hydrogen to vaporize along their paths leaving a trail of bubbles. The target is in a magnetic field so the trajectory of the charged

[2]Some early data is available from emulsion experiments.

particles reveals their identity. Photographs of the tracks are taken and analyzed. The cross section for a given reaction is given by

$$\sigma = \frac{n}{l\rho}$$

where n is the number of events observed, l is the measured K^- track length and ρ is the number of protons per unit volume. Cutoff criteria are applied to the data for both momentum and scattering angle.

A cutoff in laboratory momentum at a value of approximately 100 MeV/c is made because at lower momenta the track lengths of the particles in the final state are on the order of or smaller than the size of a single bubble (≈ 0.25 mm) and the events are indistinguishable from "at rest" events.

The angular cutoff varies quite a bit from experiment to experiment. A typical value is a laboratory angle of ten degrees about the forward direction. At smaller angles the cross section is swamped by the Coulomb cross section.

Coulomb corrections made in the published total cross sections differ from experiment to experiment. In some experiments the combined Coulomb plus nuclear cross section is given where only data from angles greater than the cutoff angle is included. In other cases, the pure Coulomb cross section is subtracted and cutoff angles are chosen to exclude much of the data from forward angles as well as backward angles to remove effects of Coulomb-nuclear interference. The experimental data [29],[33]–[40] used in this work is shown in Figure 1. The agreement of the results from different experiments indicates that at the precision to which this data has been obtained, the exact nature of the methods employed in dealing with the Coulomb interaction is of no great importance.

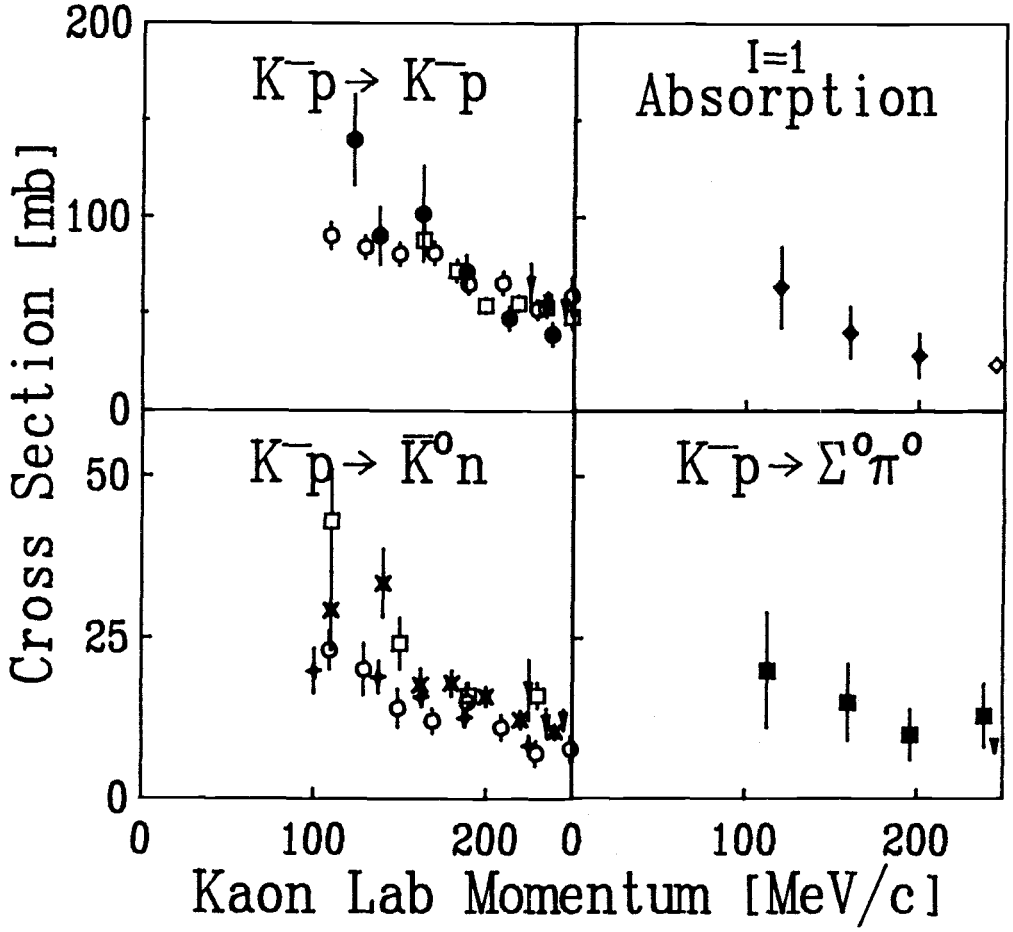

Figure 1. Cross Sections as measured by: plusses, [34]; filled circles, [29]; filled triangles, [33]; open circles, [35]; filled squares, [38]; open squares, [39]; crosses, [40]. The $I = 1$ absorption data are derived from: open lozenges, [36,37]; closed lozenges, [38,39].

The range of kaon lab momenta that can be used in a pure s-wave analysis of the data is limited. As mentioned, data for kaon lab momenta below about 100 MeV/c does not exist. Although the elastic and charge exchange ($K^-p \rightarrow \overline{K}^0 n$) are found to be isotropic at kaon lab momenta below 280 MeV/c [29,34,35,39], p-wave contributions to the reactions $K^-p \rightarrow \pi^{\pm}\Sigma^{\mp}$ have been reported [39] at kaon lab momenta as low as 150 MeV/c. Earlier experiments suggested that this reaction was isotropic for all momenta below 280 MeV/c [29,35]. Figure 2 depicts the production angular distribution measured by [39,41] for the reaction $K^-p \rightarrow \pi^{\pm}\Sigma^{\mp}$ at various lab momenta. In reference [41] the anisotropic nature of this data is given as evidence for the contribution of p-waves at 150 MeV/c. We submit it as evidence that the p-wave contribution can be neglected at kaon lab momenta below 250 MeV/c as the distribution is nearly constant. We use scattering data for kaon lab momenta below 250 MeV/c.

2.2 Method used in determining scattering amplitudes

In describing the theoretical methods used in obtaining scattering amplitudes we first give the basic ideas in the framework of single channel scattering and then extend the formalism so that it applies to K^-p scattering. In this manner we can provide a brief review of simple scattering while laying down the conventions used in this work.

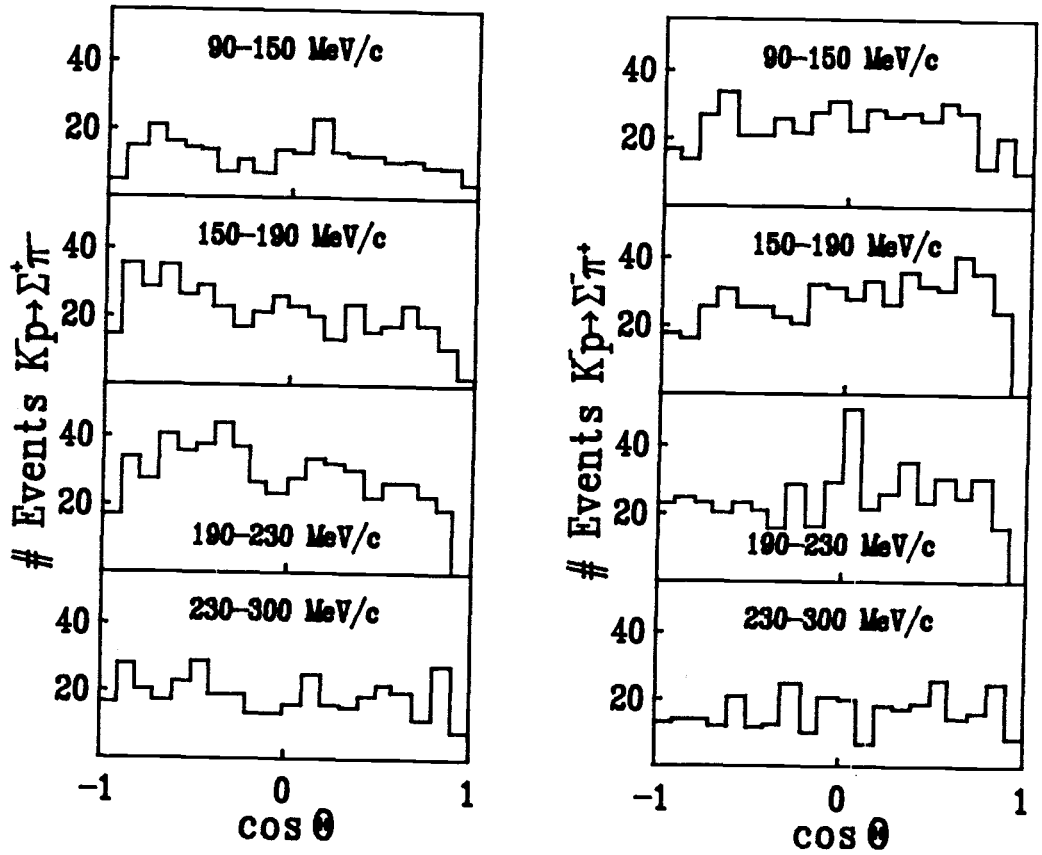

Figure 2. Angular distribution of $K^- p \to \pi^{\pm}\Sigma^{\mp}$ events for various kaon lab momenta as measured by [39,41].

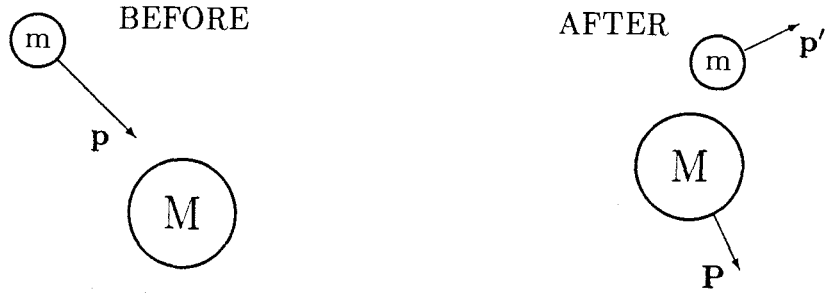

Figure 3. The Scattering experiment depicted in the laboratory frame.

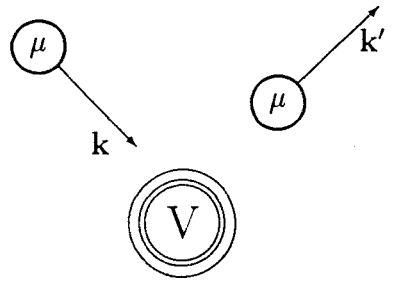

Figure 4. The equivalent one body scattering problem for the relative position of two interacting bodies.

2.2.1 Single Channel Scattering Theory

The physical situation to be analyzed is one in which a projectile of mass m with momentum $\mathbf{p}$ interacts with a target of mass M which is at rest. (See Figure 3.) The projectile has a final momentum $\mathbf{p}'$ and the target a final momentum $\mathbf{P}$. Viewed in the Center of Momentum frame we can treat the problem as one in which a single particle interacts with a potential which is fixed in space. (See Figure 4.) We solve the scattering problem in

momentum space using time independent scattering theory. In this theory, the cross section can be obtained from the on shell scattering amplitude $f_E(\mathbf{k}', \mathbf{k})$ where:

$$\begin{aligned} \mathbf{k} &= \text{incoming momentum} \\ \mathbf{k}' &= \text{outgoing momentum} \\ E &= \text{energy of the problem} \end{aligned}$$

The integrated elastic cross section is given in terms of the scattering amplitude as

$$\sigma = 4\pi |f|^2$$

and the total cross section is given by the optical theorem as

$$\sigma_{total} = \frac{4\pi}{k} \mathrm{Im} f(\theta = 0)$$

where θ is the angle between $\mathbf{k}$ and $\mathbf{k}'$. The scattering amplitude f can be obtained from the T-matrix by the relation

$$f = -4\pi^2 (\hbar c)(\mu c^2) T$$

where the T-matrix is the solution of the Lippmann-Schwinger equation

$$\langle \mathbf{k}' | T | \mathbf{k} \rangle = \langle \mathbf{k}' | V | \mathbf{k} \rangle + (\hbar c)^3 \int d^3p \, \langle \mathbf{k}' | V | \mathbf{p} \rangle \, G_E(\mathbf{p}) \, \langle \mathbf{p} | T | \mathbf{k} \rangle \qquad (2.2)$$

In this equation the transition amplitude for an initial plane wave state of momentum $\mathbf{k}$ to yield, after the interaction, a final plane wave state of momentum $\mathbf{k}'$ is given as a sum of the potential operator evaluated between initial and final states and an integral which represents the sum over all intermediate states of the probability amplitude for an incoming state to make

a transition to an intermediate state of momentum $\mathbf{p}$, to propagate in that state, and then to connect to the final state via the potential operator. The propagator G is given by

$$G_E(\mathbf{p}) = \frac{1}{E - E(\mathbf{p}) + i\epsilon}$$

where E is again the energy of the problem and

$$E(\mathbf{p}) = \frac{p^2}{2\mu}$$

is the nonrelativistic kinetic energy of the particle in the intermediate state $|\mathbf{p}\rangle$. For the relativistic case we use

$$E(\mathbf{p}) = \sqrt{p^2 + m^2} + \sqrt{p^2 + M^2} - (m + M)$$

Rewriting the Lippmann-Schwinger equation in terms of functions we have:

$$T(\mathbf{k}', E, \mathbf{k}) = V(\mathbf{k}', \mathbf{k}) + (\hbar c)^3 \int d^3p \frac{V(\mathbf{k}', \mathbf{p})\, T(\mathbf{p}, E, \mathbf{k})}{E - E(\mathbf{p}) + i\epsilon}$$

For the special case[3] in which the interaction is independent of the azimuthal angle ϕ (see Figure 5) we can make the expansions:

$$\begin{aligned} V(\mathbf{k}', \mathbf{k}) &= \sum_{l=0}^{\infty} (2l+1) V_l(k', E, k)\, P_l(\cos\theta) \\ T(\mathbf{k}', E, \mathbf{k}) &= \sum_{l=0}^{\infty} (2l+1) T_l(k', E, k)\, P_l(\cos\theta) \end{aligned}$$

We can then write the Lippmann-Schwinger equation for a given l value as:

[3]This special case occurs when the interaction can be described by a central potential, in particular for cases in which there is no spin-orbit interaction. Since we consider only the $l = 0$ terms of the following expansions we lose no generality in ignoring the spin-orbit interaction.

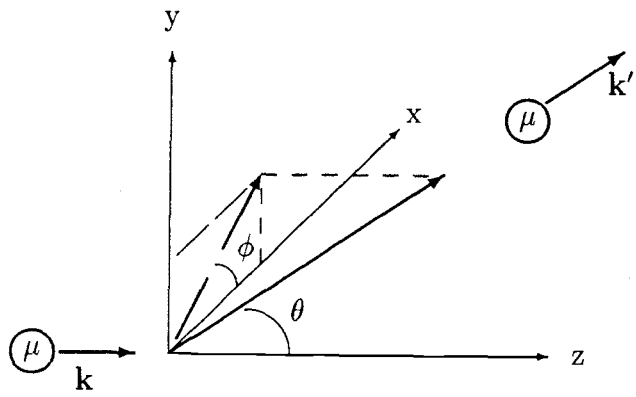

Figure 5. Definition of the angles in the scattering problem.

$$T_l(k', E, k) = V_l(k', k) + 4\pi \int dp\, p^2 \frac{V_l(k', p)\, T_l(p, E, k)}{E - E(p) + i\epsilon} \qquad (2.3)$$

For the $K^- p$ scattering that we shall be investigating, the energy is so low that only the $l = 0$ contribution to the sum for T above need be considered.

Our method consists of choosing an analytical form for $V_{l=0}(k', k)$ which has some parameters whose values are initially unknown. The choice of the analytic form is based on the physics of the problem. The unknown parameters are determined by first fixing the parameters at some arbitrary values, solving the Lippmann-Schwinger equation for the T-matrix, calculating the scattering amplitude and cross sections, comparing the cross sections with experiment, and adjusting the potential parameters and repeating until the calculated cross sections agree with those measured experimentally.

2.2.2 The Coupled Channels Nature of the Problem

In the discussion of the experiments it was revealed that in scattering negatively charged antikaons from protons there are six important final states. In the simplest analysis one could, for this problem, employ the single channel formalism described above by using the following arguments: In that the strong interaction conserves isospin, an isospin basis is suitable. For isospin-0 there are only two final states:

$$\begin{aligned} \overline{K}N &\rightarrow \overline{K}N \\ &\rightarrow \pi\Sigma \end{aligned}$$

and for $I = 1$ three final states:

$$\begin{aligned} \overline{K}N &\rightarrow \overline{K}N \\ &\rightarrow \pi\Sigma \\ &\rightarrow \pi\Lambda \end{aligned}$$

If we are only interested in the $K^-p \rightarrow K^-p$ interaction we could give the potential an imaginary (absorptive) part to account for the coupling to the other channel(s). Thus we could solve a single channel problem for $I = 0$, another one for $I = 1$ and determine the $K^-p \rightarrow K^-p$ scattering amplitude by combining the results. This approach has the drawback that too much of the physics is buried in the imaginary part of the potential. Experiment reveals an isospin-0 resonance in the $\pi\Sigma$ channel which has important consequences on the K^-p channel (including the possible existence of a virtual $\overline{K}N$ nuclear bound state). Cross sections for $\overline{K}N \rightarrow \pi\Sigma$ have been measured

directly and it is easier to incorporate the results of these measurements in our calculations by considering the isospin-0 $\pi\Sigma$ channel explicitly. Further, although the strong interaction conserves isospin, it acts always in concert with the Coulomb interaction which does not conserve isospin. We would like to take into account the gross effect of this symmetry breaking in the low energy region of interest. This means taking into account the mass difference between the K^-p and $\overline{K}^0n$ systems. Now, there is little or no structure in the $\pi\Lambda$ or isospin-1 $\pi\Sigma$ channels so it is O.K. to take these into account with an imaginary part of the potential. The $\pi\Sigma$ thresholds all occur so far below the region of interest (100 MeV below the K^-p threshold) that we can ignore the mass differences between these channels. Thus in the simplest analysis which still includes the important physics we need to consider three final states explicitly:

$$\begin{aligned} K^-p &\rightarrow K^-p \\ &\rightarrow \overline{K}^0n \\ &\rightarrow \pi\Sigma \text{ (Isospin-0)} \end{aligned}$$

Again, the potential must include an imaginary part to take into account the coupling to $\pi\Lambda$ and isospin-1 $\pi\Sigma$ final states.

2.2.3 Coupled Channels Theory

Having established the need for a multichannel calculation for the specific problem at hand, we now elucidate the extensions to the single channel meth-

ods that are needed to handle the coupled channels problem. We explain the extensions in a simple two channel problem and later implement them in the K^-p system. To make the discussion more concrete we consider the following interactions:

$$\begin{aligned}
\overline{K}N &\rightarrow \overline{K}N \\
\overline{K}N &\rightarrow \pi\Sigma \\
\pi\Sigma &\rightarrow \pi\Sigma \\
\pi\Sigma &\rightarrow \overline{K}N
\end{aligned}$$

The plan here is to write the Lippmann-Schwinger equation for each interaction and show how the resulting set of coupled integral equations can be combined into a single matrix equation. Using subscript "1" to denote the $\overline{K}N$ system and "2" to denote the $\pi\Sigma$ system we can write the Lippmann-Schwinger equations as:

$$\begin{aligned}
T_{11}(k',E,k) &= V_{11}(k',k) + 4\pi \int dp\, p^2 \frac{V_{11}(k',p)\, T_{11}(p,E,k)}{E - E_1(p) + i\epsilon} \\
&\quad + 4\pi \int dp\, p^2 \frac{V_{12}(k',p)\, T_{21}(p,E,k)}{E - E_2(p) + i\epsilon} \\
T_{12}(k',E,k) &= V_{12}(k',k) + 4\pi \int dp\, p^2 \frac{V_{12}(k',p)\, T_{22}(p,E,k)}{E - E_2(p) + i\epsilon} \\
&\quad + 4\pi \int dp\, p^2 \frac{V_{11}(k',p)\, T_{12}(p,E,k)}{E - E_1(p) + i\epsilon} \\
T_{21}(k',E,k) &= V_{21}(k',k) + 4\pi \int dp\, p^2 \frac{V_{21}(k',p)\, T_{11}(p,E,k)}{E - E_1(p) + i\epsilon} \\
&\quad + 4\pi \int dp\, p^2 \frac{V_{22}(k',p)\, T_{21}(p,E,k)}{E - E_2(p) + i\epsilon} \\
T_{22}(k',E,k) &= V_{22}(k',k) + 4\pi \int dp\, p^2 \frac{V_{22}(k',p)\, T_{22}(p,E,k)}{E - E_2(p) + i\epsilon} \\
&\quad + 4\pi \int dp\, p^2 \frac{V_{21}(k',p)\, T_{12}(p,E,k)}{E - E_1(p) + i\epsilon}
\end{aligned}$$

Letting the matrix

$$V \equiv \begin{bmatrix} V_{11} & V_{12} \\ V_{21} & V_{22} \end{bmatrix}$$

and

$$T \equiv \begin{bmatrix} T_{11} & T_{12} \\ T_{21} & T_{22} \end{bmatrix}$$

we can write the coupled set of equations as:

$$T(k', E, k) = V(k', k) + 4\pi \int dp\, p^2 \frac{V(k', p)\, T(p, E, k)}{E - E(p) + i\epsilon}$$

This completes our general discussion, we now turn our attention to the problem at hand.

In a theoretical description of $K^- p$ scattering one can use six coupled channels —one for each of the 2-body final states. We use and describe the method of HAW [23] which involves only three channels. The reasons, which will become clearer as we describe the method, are as follows: Using fewer channels limits the number of free parameters while still allowing one to include the important physics. HAW found that the parameters were poorly constrained by the scattering data alone (they published several different sets of parameters corresponding to equally good fits to the data). Certainly, one should not use even more parameters until further constraints can be found (as we do; see later chapters). Secondly, our work is an extension of HAW's. By starting with a similar formalism we allow easier comparison of results. Finally, determining up-to-date values for the same parameters that they used allows immediate application of our results, for instance in investigating bound states, by researchers who have used HAW's results in

the past. In order to understand HAW's method one needs to know the underlying physics.

2.2.4 Isospin

The total isospin and the third component of the isospin (I, I_3) are, for the K^-: $(\frac{1}{2}, -\frac{1}{2})$, and for the proton: $(\frac{1}{2}, \frac{1}{2})$. Thus, for the K^-p system, (I, I_3) can take on the values $(1, 0)$ and $(0, 0)$. It follows that the K^-p strong interaction Hamiltonian must include a term for $I = 1$ and $I = 0$. Since the strong interaction conserves isospin, there will be no coupling between the two. The interaction Hamiltonian $H_{intx} = H_0 P_0 + H_1 P_1$ where P_I is the projection operator for projection onto a state of pure isospin I. Evaluating the potential operator between initial and final states will thus yield a potential function which consists of the sum of an isospin-0 part and an isospin-1 part.

2.2.5 Actual Equations Solved

We operate in a charge basis as opposed to an isospin basis —the states we deal with are pairs of physical particles. The 3×3 potential matrix is a sum of isospin-0 and isospin-1 parts.

$$V = V^0 + V^1$$

The matrix elements are given by:

$$V^I_{ij} = g_I(k')\, \lambda^I_{ij}\, g_I(k)$$

with the Yukawa potential

$$g_I(r) = \frac{e^{-\beta_I r}}{r}$$

which, by Fourier transformation, yields the momentum space potential

$$g_I(k) = \frac{1}{(2\pi)^{\frac{3}{2}}} \int d^3r \, g_I(r) \, e^{-i\mathbf{k}\cdot\mathbf{r}} = \frac{\sqrt{2/\pi}}{k^2 + \beta_I^2}$$

β_I is the inverse range parameter. It is real. The λ_{ij}^I's are coupling strength parameters. These can be written in terms of coupling strength parameters for pure isospin states with the Clebsch Gordan coefficients used in expressing the physical states in terms of isospin states.

$$\begin{aligned}
\left|K^- p\right\rangle &= \frac{1}{\sqrt{2}}(|I=0\rangle_{\overline{K}N} + |I=1\rangle_{\overline{K}N}) \\
\left|\overline{K}^0 n\right\rangle &= \frac{1}{\sqrt{2}}(-|I=0\rangle_{\overline{K}N} + |I=1\rangle_{\overline{K}N}) \\
|\pi\Sigma\rangle &= |I=0\rangle_{\pi\Sigma}
\end{aligned}$$

For example,

$$\begin{aligned}
V_{K^-p\leftarrow K^-p} &= \left\langle K^- p\right| g_0(k')\lambda^0_{\overline{K}N\leftarrow\overline{K}N} g_0(k) P^0 \left|K^- p\right\rangle + \\
&\quad \left\langle K^- p\right| g_1(k')\lambda^1_{\overline{K}N\leftarrow\overline{K}N} g_1(k) P^1 \left|K^- p\right\rangle \\
&= \frac{1}{\sqrt{2}} \langle I=0| g_0(k')\lambda^0_{\overline{K}N\leftarrow\overline{K}N} g_0(k) |I=0\rangle \frac{1}{\sqrt{2}} + \\
&\quad \frac{1}{\sqrt{2}} \langle I=1| g_1(k')\lambda^1_{\overline{K}N\leftarrow\overline{K}N} g_1(k) |I=1\rangle \frac{1}{\sqrt{2}} \\
&= g_0(k') \frac{1}{2}\lambda^0_{\overline{K}N\leftarrow\overline{K}N} g_1(k) + g_1(k') \frac{1}{2}\lambda^1_{\overline{K}N\leftarrow\overline{K}N} g_1(k)
\end{aligned}$$

so that

$$\begin{aligned}
\lambda^0_{K^-p\leftarrow K^-p} &= \frac{1}{2}\lambda^0_{\overline{K}N\leftarrow\overline{K}N} \\
\lambda^1_{K^-p\leftarrow K^-p} &= \frac{1}{2}\lambda^1_{\overline{K}N\leftarrow\overline{K}N}
\end{aligned}$$

Carrying this procedure out for each of the matrix elements we find that λ matrices have the form

$$\lambda^0 = \begin{bmatrix} \frac{1}{2}\lambda^0_{\overline{K}N\leftarrow\overline{K}N} & -\frac{1}{2}\lambda^0_{\overline{K}N\leftarrow\overline{K}N} & \frac{1}{\sqrt{2}}\lambda^0_{\overline{K}N\leftarrow\pi\Sigma} \\ -\frac{1}{2}\lambda^0_{\overline{K}N\leftarrow\overline{K}N} & \frac{1}{2}\lambda^0_{\overline{K}N\leftarrow\overline{K}N} & -\frac{1}{\sqrt{2}}\lambda^0_{\overline{K}N\leftarrow\pi\Sigma} \\ \frac{1}{\sqrt{2}}\lambda^0_{\overline{K}N\leftarrow\pi\Sigma} & -\frac{1}{\sqrt{2}}\lambda^0_{\overline{K}N\leftarrow\pi\Sigma} & \lambda^0_{\pi\Sigma\leftarrow\pi\Sigma} \end{bmatrix}$$

$$\lambda^1 = \begin{bmatrix} \frac{1}{2}\lambda^1_{\overline{K}N\leftarrow\overline{K}N} & \frac{1}{2}\lambda^1_{\overline{K}N\leftarrow\overline{K}N} & 0 \\ \frac{1}{2}\lambda^1_{\overline{K}N\leftarrow\overline{K}N} & \frac{1}{2}\lambda^1_{\overline{K}N\leftarrow\overline{K}N} & 0 \\ 0 & 0 & 0 \end{bmatrix}$$

The matrix elements of λ^0 are real. The matrix elements of λ^1 include an imaginary part to take into account the coupling to the isospin-1 $\pi\Sigma$ and $\pi\Lambda$ systems. Our potential matrices thus appear as:

$$V^0 = \begin{bmatrix} \frac{1}{2}V^0_{\overline{K}N\leftarrow\overline{K}N} & -\frac{1}{2}V^0_{\overline{K}N\leftarrow\overline{K}N} & \frac{1}{\sqrt{2}}V^0_{\overline{K}N\leftarrow\pi\Sigma} \\ -\frac{1}{2}V^0_{\overline{K}N\leftarrow\overline{K}N} & \frac{1}{2}V^0_{\overline{K}N\leftarrow\overline{K}N} & -\frac{1}{\sqrt{2}}V^0_{\overline{K}N\leftarrow\pi\Sigma} \\ \frac{1}{\sqrt{2}}V^0_{\overline{K}N\leftarrow\pi\Sigma} & -\frac{1}{\sqrt{2}}V^0_{\overline{K}N\leftarrow\pi\Sigma} & V^0_{\pi\Sigma\leftarrow\pi\Sigma} \end{bmatrix}$$

$$V^1 = \begin{bmatrix} \frac{1}{2}V^1_{\overline{K}N\leftarrow\overline{K}N} & \frac{1}{2}V^1_{\overline{K}N\leftarrow\overline{K}N} & 0 \\ \frac{1}{2}V^1_{\overline{K}N\leftarrow\overline{K}N} & \frac{1}{2}V^1_{\overline{K}N\leftarrow\overline{K}N} & 0 \\ 0 & 0 & 0 \end{bmatrix}$$

The Greens Function matrix is:

$$G = \begin{bmatrix} \frac{1}{E - E_1(p) + i\epsilon} & 0 & 0 \\ 0 & \frac{1}{E - E_2(p) + i\epsilon} & 0 \\ 0 & 0 & \frac{1}{E - E_3(p) + i\epsilon} \end{bmatrix} \tag{2.4}$$

where $E_i(p)$ is given by

$$E_i(p) = \frac{p^2}{2\mu_i}$$

nonrelativistically and

$$E_i(p) = \sqrt{p^2 + m_i^2} + \sqrt{p^2 + M_i^2} - (m_i + M_i)$$

relativistically. (Again m_i is the mass of the projectile in channel i and M_i is the mass of the target.) We have included the option of using a relativistic propagator in the calculation in that since the $\pi\Sigma$ lies some 100 MeV below the $\overline{K}N$ threshold, an energy which is comparable to the pion rest mass, the pions in the $\pi\Sigma$ channel are at relativistic energies even for very low energy K^-p scattering. In the nonrelativistic calculation we take this into account approximately by defining the reduced mass in the $\pi\Sigma$ channel μ_3 so that the nonrelativistic expression for energy agrees with the relativistic expression at the K^-p threshold. This is the definition used in [23]. First, the constant p_0 is chosen such that

$$\sqrt{p_0^2 + m_3^2} + \sqrt{p_0^2 + M_3^2} = m_1 + M_1$$

Then μ_3 is chosen such that

$$\frac{p_0^2}{2\mu_3} = m_1 + M_1 - m_3 - M_3$$

For channels 1 and 2 (K^-p and $\overline{K}^0n$) the reduced mass is defined in the normal manner

$$\mu_i = \frac{m_i M_i}{m_i + M_i} \qquad i = 1, 2$$

We can write out the coupled channels Lippmann-Schwinger equation for a given value of the angular momentum quantum number l (subscript

suppressed) as

$$T_{ij}(k',k) = V_{ij}(k',k) + \sum_{n=1}^{3} 4\pi \int dp\, p^2\, V_{in}(k',p)\, G_n(p)\, T_{nj}(p,k)$$

In solving this equation we take advantage of our choice of a separable potential. To explain how this works we again revert to the single channel case. Consider $V = g(k')\lambda g(k)$ in the Lippmann-Schwinger equation

$$T = V + VGT$$

This can be expanded in a Born series as

$$T = V + VGV + VGVGV + \cdots + VGV \cdots GV + \cdots$$

Each term on the right begins with a $g(k')$ and ends with a $g(k)$. It follows that our T-matrix must have the form

$$T(k', E, k) = g(k')A_E g(k)$$

Assuming this form, our integral equation for T becomes an algebraic equation for A_E.

$$g(k')A_E g(k) = g(k')\lambda g(k) + g(k')\lambda 4\pi \int dp\, p^2\, \frac{g^2(p)\, A_E}{E - E(p) + i\epsilon}\, g(k)$$

Defining

$$B = 4\pi \int dp\, p^2\, \frac{g^2(p)}{E - E(p) + i\epsilon}$$

we have

$$A_E = \lambda + \lambda B A_E$$

$$(1 - \lambda B)A_E = \lambda$$

$$A_E = (1 - \lambda B)^{-1} \lambda \tag{2.5}$$

If we now consider our potential to be the sum of isospin-0 and isospin-1 parts

$$V = g_0 \lambda^0 g_0 + g_1 \lambda^1 g_1$$

we find that the T-matrix can be written:

$$T = \sum_{I=0,1} \sum_{J=0,1} g_I(k') \, A_E^{IJ} \, g_J(k)$$

and in analogy with equation 2.5, the A_E's are given by

$$\begin{pmatrix} A_E^{00} & A_E^{01} \\ A_E^{10} & A_E^{11} \end{pmatrix} = \left[\begin{pmatrix} 1 & 0 \\ 0 & 1 \end{pmatrix} - \begin{pmatrix} \lambda_0 & 0 \\ 0 & \lambda_1 \end{pmatrix} \begin{pmatrix} B^{00} & B^{01} \\ B^{10} & B^{11} \end{pmatrix} \right]^{-1} \begin{pmatrix} \lambda_0 & 0 \\ 0 & \lambda_1 \end{pmatrix} \tag{2.6}$$

In going to the three channel case we simply let each of the variables in equation 2.6 become 3×3 matrices. The A-matrix, for instance, becomes a 6×6 matrix which can be described as a 2×2 supermatrix of 3×3 submatrices. The 36 elements of the B-matrix are defined by:

$$B_{ij}^{IJ} = 4\pi \int dp \, p^2 \, \frac{g_I(p) g_J(p)}{E - E_i(p) + i\epsilon} \, \delta_{ij}$$

where the diagonal nature of the 3×3 submatrices is a direct result of the diagonal nature of the propagator matrix G. (See equation 2.4.) The T-matrix also becomes a 3×3 matrix with each of the elements given by:

$$T_{ij}(k', E, k) = \sum_{I=0,1} \sum_{J=0,1} g_I(k') \, A_{ij}^{IJ}(E) \, g_J(k)$$

The scattering amplitudes are given in terms of the T-matrix elements as

$$f_{ij} = -4\pi^2 (\hbar c)(\sqrt{\mu_i \mu_j} c^2) T_{ij}$$

Experimental Cross Section	Theoretical Cross Section
$\sigma_{K^-p\leftarrow K^-p}$	$4\pi\|f_{11}\|^2$
$\sigma_{\overline{K}^0n\leftarrow K^-p}$	$4\pi(k_{\overline{K}^0n}/k_{K^-p})\|f_{21}\|^2$
$\sigma_{\pi^0\Sigma^0\leftarrow K^-p}$	$(4\pi/3)(k_{\pi\Sigma}/k_{K^-p})\|f_{31}\|^2$
$\sigma_{\pi\Lambda\leftarrow K^-p}+\sigma_{\pi^+\Sigma^-\leftarrow K^-p}+$	$(4\pi/k_{K^-p})\mathrm{Im}f_{11}-4\pi\|f_{11}\|^2-$
$\sigma_{\pi^-\Sigma^+\leftarrow K^-p}-2\sigma_{\pi^0\Sigma^0\leftarrow K^-p}$	$4\pi(k_{\overline{K}^0n}/k_{K^-p})\|f_{21}\|^2-4\pi(k_{\pi\Sigma}/k_{K^-p})\|f_{31}\|^2$

Table 1. Formulas for the cross sections.

Expressions for the cross sections in terms of the scattering amplitudes are given in Table 1. The last entry in the table represents the isospin-1 absorption cross section. The experimental isospin-1 absorption cross section is actually a derived quantity. It is a linear combination of measured cross sections.

2.3 Results (Low Energy K^-p Scattering)

In Figure 6 we show a nonrelativistic fit to the low energy scattering cross sections. The $K^-p \to K^-p$ scattering amplitude corresponding to the the nonrelativistic fit is shown in Figure 7. Figures 8 and 9 show a relativistic fit to the cross sections and the corresponding K^-p elastic scattering amplitude. These represent the best fits to the data. The cross section data constrains the scattering amplitudes only in the energy range 1438.5–1470.5 MeV as indicated in Figures 7 and 9. We are interested in the behavior of the scattering amplitudes below this energy —in particular, the value of the $K^-p \to K^-p$

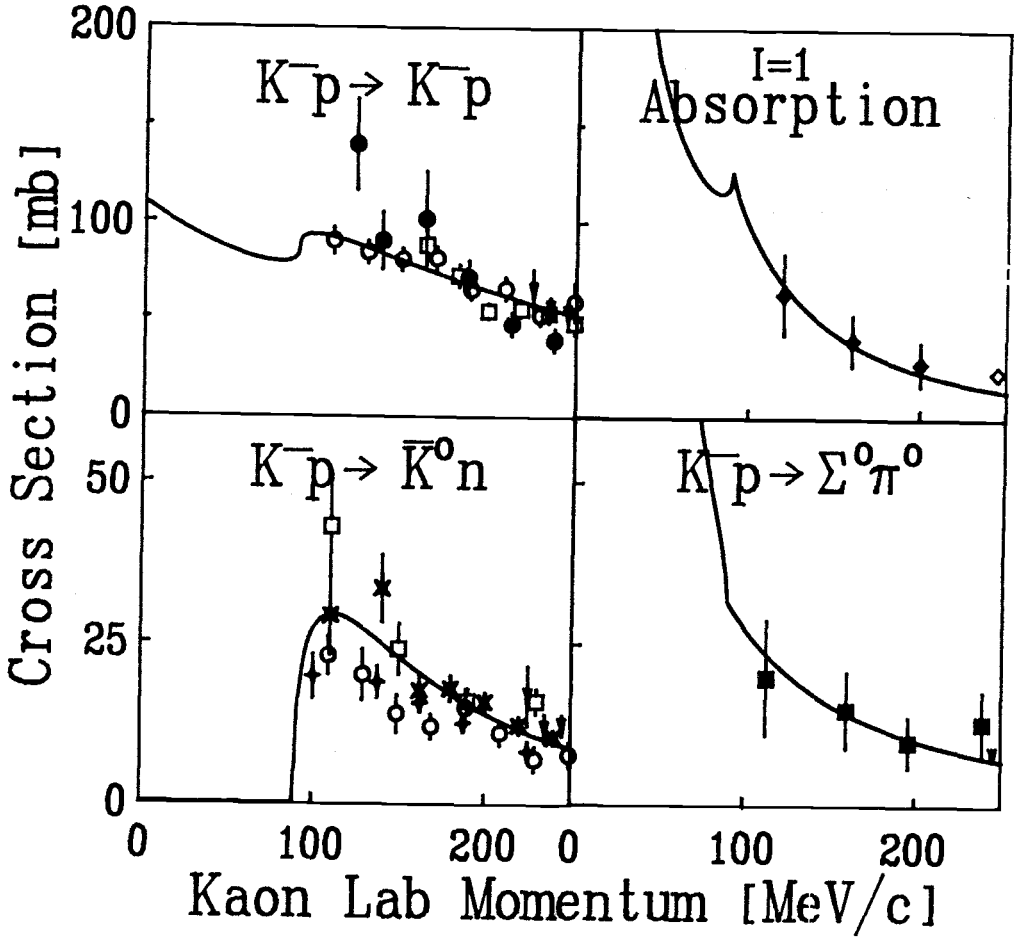

Figure 6. Calculated cross sections for a nonrelativistic fit to the indicated data. The data are the same as in Figure 1.

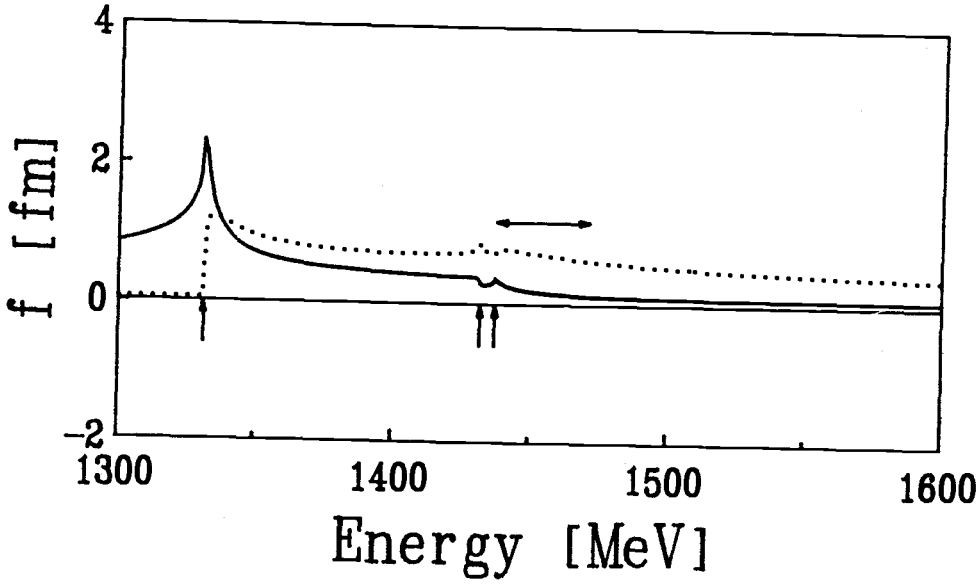

Figure 7. The K^-p elastic scattering amplitude corresponding to a nonrelativistic fit to the low energy scattering data only. The solid curve represents the real part of the amplitude and the dotted line represents the imaginary part. Vertical arrows indicate threshold energies for the $\Sigma\pi$, K^-p, and $\overline{K}^0n$ channels in order from left to right. Double arrows show the range of energies for which the scattering amplitude is constrained by the low energy scattering data.

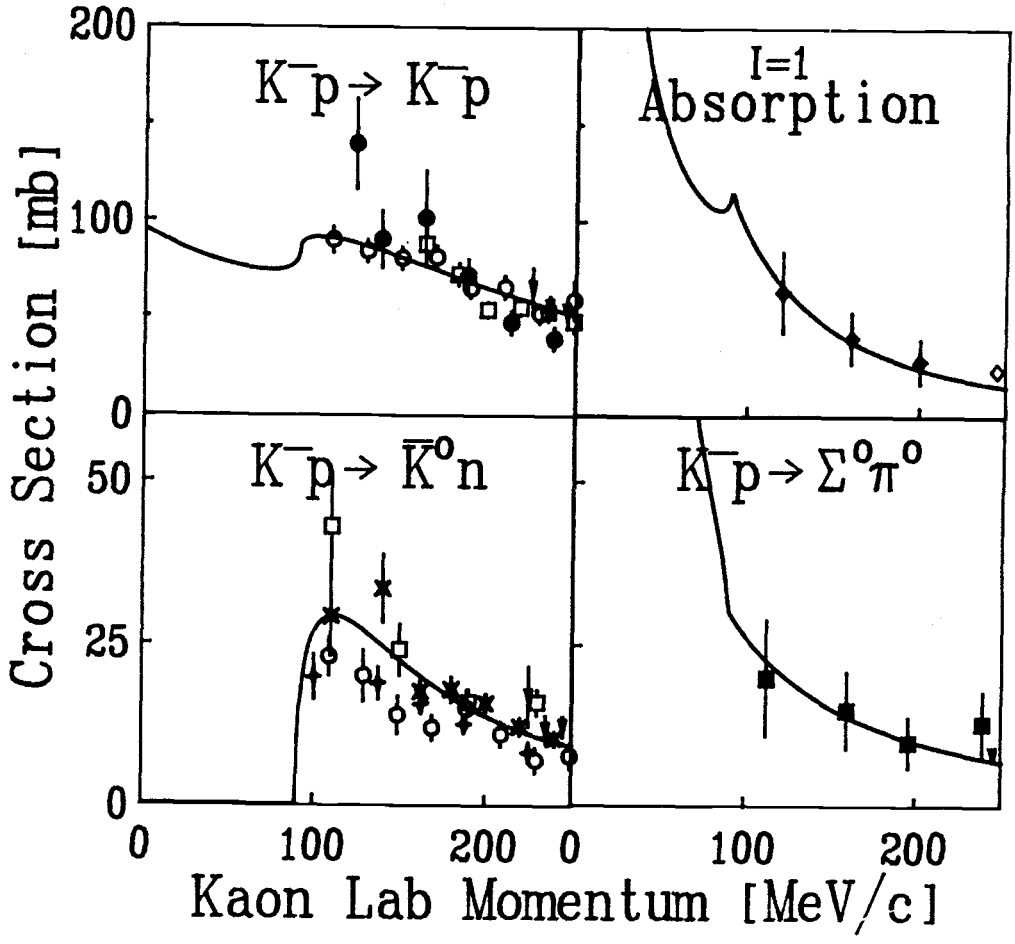

Figure 8. Calculated cross sections for a relativistic fit to the indicated data. The data are the same as in Figure 1.

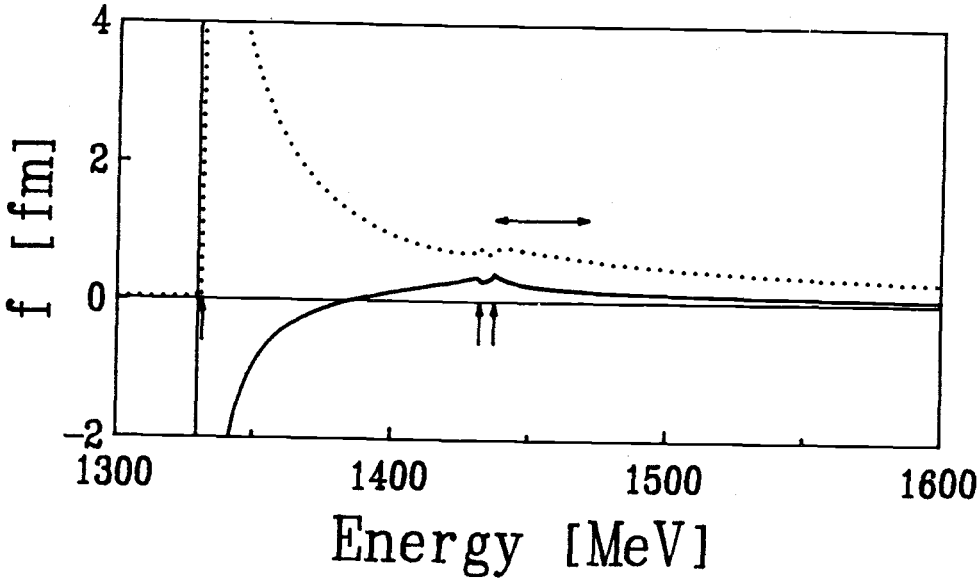

Figure 9. The K^-p elastic scattering amplitude corresponding to a relativistic fit to the low energy scattering data only. The solid curve represents the real part of the amplitude and the dotted line represents the imaginary part. Vertical arrows indicate threshold energies for the $\Sigma\pi$, K^-p, and $\overline{K}^0n$ channels in order from left to right. Double arrows show the range of energies for which the scattering amplitude is constrained by the low energy scattering data.

scattering amplitude just below the K^-p threshold at the K^-p Coulomb bound state energy. It is desirable therefore, to check the consistency of our scattering amplitudes with other data. Such data is available but computing the observables from the theoretical scattering amplitudes is not as straight forward as in the low-energy K^-p scattering case. We postpone discussion of the physical significance of our results until after completion of the consistency checks. The chi-squared per degree of freedom for these two fits is on the order of 10^{-2}. Recall that for a good fit $\chi^2/^oF \approx 1$. These fits are too good. The potential parameters are underdetermined by the data. Scattering amplitudes with different behavior than that shown in Figures 7 and 9 also fit the data well. It is clear that other experimental data is needed to obtain an understanding of the antikaon-proton interaction.

Chapter 3

$\pi^- p \rightarrow \pi^{\pm}\Sigma^{\mp}K^0$ at 1.69 GeV/c

In order to build subthreshold constraints into our scattering amplitudes we consider the reaction $\pi^- p \rightarrow \pi^{\pm}\Sigma^{\mp}K^0$ at a laboratory momentum of 1.69 GeV/c (2025 MeV center of mass energy). This reaction has been investigated experimentally by Thomas et al. [42]. It provides indirect information on $\pi\Sigma$ scattering. In that direct $\pi\Sigma$ scattering experiments are beyond the state of the art, this type of experiment ($\pi^- p \rightarrow \pi^{\pm}\Sigma^{\mp}K^0$) is our best source of information on $\pi\Sigma$ scattering in the low energy regime. It can be used to constrain the $\pi\Sigma$ scattering amplitude at two body center of momentum energies below the $K^- p$ threshold within following model: In the absence of any final state interactions amongst the π, Σ, or K^0 it is assumed that the distribution of momenta among the final state particles is governed solely by phase space considerations. That is, the $\pi^- p$ interaction itself does not prejudice the momentum distribution. Further, if we assume that the interaction of the K^0 with either of the other two particles can be neglected, or in other words, that the K^0 is a spectator with respect to final state interactions,

then the deviation of the momentum distribution from the pure phase space distribution is accounted for by the $\pi\Sigma$ interaction alone. (The energy at which the experiment was carried out was deliberately chosen so that the interaction between the K^0 and the other particles in the final state would have little structure and the distribution would thus be dominated by the resonance in the $\pi\Sigma$ channel.)

Thomas et al. [43] give the $\pi\Sigma$ experimental mass spectrum for this interaction as a histogram of the number of observed $\pi^- p \to \pi^\pm \Sigma^\mp K^0$ events versus the total energy in the $\pi\Sigma$ center of momentum, i.e. the "Mass" of a $\pi\Sigma$ pseudoparticle. The histogram is shown in Figure 10. We can calculate this mass spectrum theoretically within the model just described, up to an undetermined overall normalization factor. In practice, this normalization factor is determined by setting the integral of the theory spectrum (total number of events) equal to the integral of the measured spectrum.

3.1 Computing the $\pi^- p \to \pi^\pm \Sigma^\mp K^0$ Spectrum

We can state the problem as: Given the scattering amplitude for $\pi^\pm \Sigma^\mp \to \pi^\pm \Sigma^\mp$ as a function of the total energy in the $\pi\Sigma$ center of mass, find the number of events $\pi^- p \to \pi^\pm \Sigma^\mp K^0$ as a function of the same variable.

The shape of the spectrum is given by the transition probability dw_3 where the "3" indicates a three body final state.

$$dw_3 = |M_{fi}|^2 \, \rho_3^I(E, M_\Lambda) \tag{3.7}$$

$|M_{fi}|^2$ is the square modulus of the invariant transition amplitude and ρ_3^I is the three body invariant phase space function of E, the total energy in the

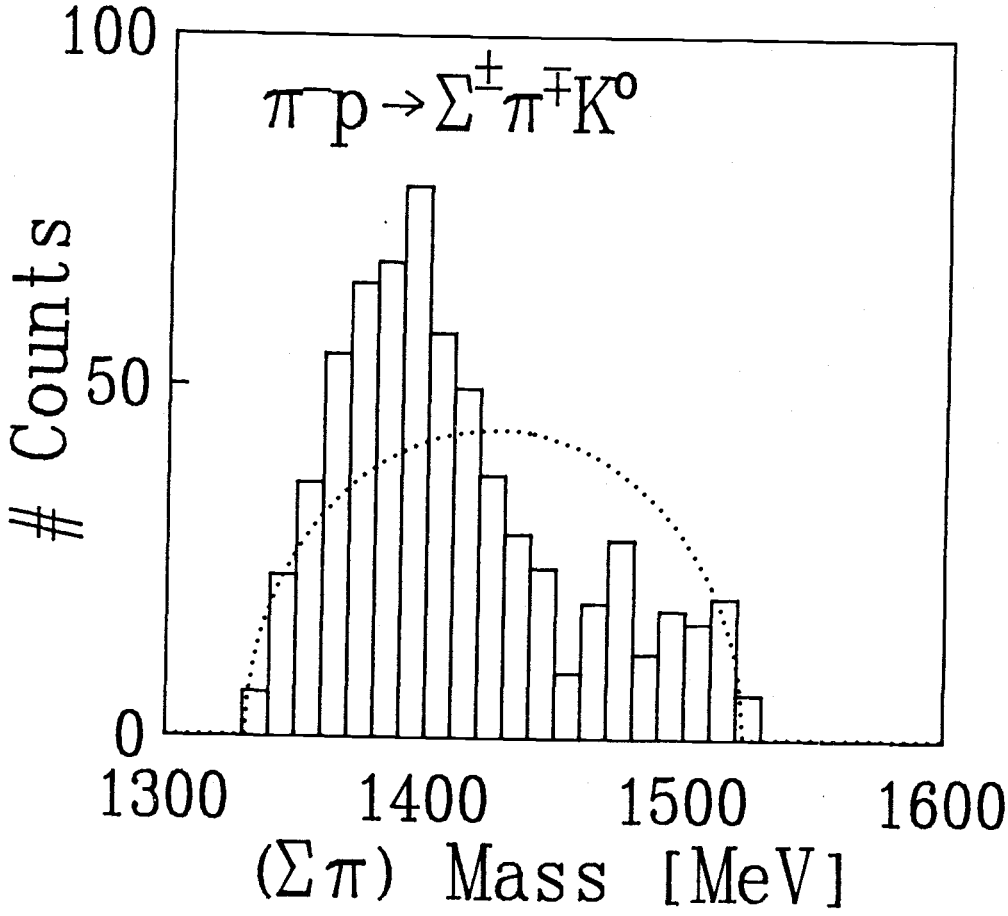

Figure 10. The $\pi\Sigma$ mass spectrum. The histogram is the experimentally measured spectrum [43]. The dotted line represents the phase space curve for the interaction.

three body center of mass frame and M_Λ, the total energy of the pion and the sigma particle in the $\pi\Sigma$ center of mass.

At this point we need to consider the fact that in our calculation of the $\pi^\pm\Sigma^\mp \to \pi^\pm\Sigma^\mp$ scattering amplitudes we considered the potential to be the sum of isospin-0 and isospin-1 parts only. The physical $\pi^\pm\Sigma^\mp$ states are actually linear combinations of isospin-0, 1 and 2. The isospin-2 part does not appear in the K^-p scattering problem because the K^-p system has no isospin-2 component[4]. The $\pi^\pm\Sigma^\mp$ produced in the reaction $\pi^-p \to \pi^\pm\Sigma^\mp K^0$ does have an isospin-2 component. We extend the model to handle this situation by assuming no energy dependence of the interaction for the isospin-2 part. (This is one further manifestation of our assumption regarding the dominance of the $\pi\Sigma$ isospin-0 resonance on the distribution of particles in the final state.) The π^-p state can be written in terms of isospin states as

$$\left|\pi^-p\right\rangle = \sqrt{\frac{1}{3}}\left|\frac{3}{2},-\frac{1}{2}\right\rangle - \left|\frac{1}{2},-\frac{1}{2}\right\rangle$$

where the kets on the right represent states of total isospin I and the third component of isospin I_3 as $|I,I_3\rangle$. A final $\pi^-\Sigma^+K^0$ state for which the $\pi^-\Sigma^+$ particle pair is in an isospin-0 state is given by

$$\left\langle(\pi^-\Sigma^+)_{I=0}K^0\right| = \left\langle\frac{1}{2},-\frac{1}{2}\right|$$

For isospin-1 we have

$$\left\langle(\pi^-\Sigma^+)_{I=1}K^0\right| = \sqrt{\frac{2}{3}}\left\langle\frac{3}{2},-\frac{1}{2}\right| + \sqrt{\frac{1}{3}}\left\langle\frac{1}{2},-\frac{1}{2}\right|$$

[4]The Coulomb interaction can mix in an isospin-2 component but we consider only the gross effect of isospin symmetry breaking by the Coulomb force, namely the mass differences among particles of the same isospin multiplet.

and for isospin-2

$$\left\langle (\pi^-\Sigma^+)_{I=2}K^0\right| = \sqrt{\frac{3}{5}}\left\langle \frac{5}{2},-\frac{1}{2}\right| + \sqrt{\frac{2}{5}}\left\langle \frac{3}{2},-\frac{1}{2}\right|$$

Thus the fraction of $\langle(\pi^-\Sigma^+)_{I=0}K^0|$ is

$$\begin{aligned} f_{I=0} &= \frac{\langle(\pi^-\Sigma^+)_{I=0}K^0|\pi^-p\rangle}{\text{sum}} \\ &= 5/6 \end{aligned}$$

where

$$\begin{aligned} \text{sum} = &\left\langle (\pi^-\Sigma^+)_{I=0}K^0|\pi^-p\right\rangle + \left\langle (\pi^-\Sigma^+)_{I=1}K^0|\pi^-p\right\rangle + \\ &\left\langle (\pi^-\Sigma^+)_{I=2}K^0|\pi^-p\right\rangle \end{aligned}$$

Likewise

$$\begin{aligned} f_{I=1} &= 0 \\ f_{I=2} &= 1/6 \end{aligned}$$

We find the same results for the final state $\pi^+\Sigma^-$. Thus, we can write the transition probability to the three body final state as

$$dw_3^N = \frac{5}{6}dw_3^N(I=0) + \frac{1}{6}dw_3^N(I=2)$$

where the N signifies the fact that the probabilities have been normalized to yield the same total number of events as were observed in the experiment.

For either isospin, the transition probability can be written as in equation 3.7. In computing $dw_3(I=2)$ we take $|M_{fi}|^2$ to be a constant so that the transition probability is proportional to the phase space factor

$$\rho_3^I(E, M_\Lambda) = \frac{1}{E}P(E, M_\Lambda, m_{K^0})P(M_\Lambda, m_\Sigma, m_\pi)$$

where the function P is defined by [44]

$$P(E, m_1, m_2) = \left\{ \frac{[E^2 - (m_1 + m_2)^2]\,[E^2 - (m_1 - m_2)^2]}{4E^2} \right\}^{1/2}$$

For the $I = 0$ case we need to evaluate $|M_{fi}|^2$ which can be written as [45]

$$|M_{fi}|^2 = \left(\prod_{\alpha} E_\alpha \prod_{\beta} E_\beta \right) |\langle \beta | H | \alpha \rangle|^2$$

where $\langle \beta | H | \alpha \rangle$ is the matrix element of the interaction Hamiltonian connecting an initial state α to a final state β and $\prod_\alpha E_\alpha \prod_\beta E_\beta$ is the product of the energies of each of the particles in the initial state times the product of the energies of each of the particles in the final state. These quantities can be evaluated in any reference frame but they must all be evaluated in the same reference frame. We use the final state interaction assumption that for constant total energy E

$$|\langle \beta | H | \alpha \rangle|^2 \propto |f_{\pi\Sigma \leftarrow \pi\Sigma}|^2$$

Since we know $f_{\pi\Sigma \leftarrow \pi\Sigma}$ in the $\pi\Sigma$ center of mass frame we evaluate

$$dw_3(I = 0) \propto E'_{\pi_i} E'_p E'_{\pi_f} E'_\Sigma E'_{K^0} |f_{\pi\Sigma \leftarrow \pi\Sigma}|^2 P(E, M_\Lambda, m_{K^0}) P(M_\Lambda, m_\Sigma, m_\pi)$$

in that frame. We have used a prime to indicate quantities which must be evaluated in the $\pi\Sigma$ center of mass frame. Explicit expressions for the initial pion energy E'_{π_i}, the initial proton energy E'_p, the final pion energy E'_{π_f}, the final sigma hyperon energy E'_Σ and the final kaon energy E'_{K^0} are derived in appendix A.

Some properties of dw_3 based on the behavior of ρ_3 should be pointed out. E is a constant (2025 MeV) dictated by the $\pi\Sigma$ center of mass energy

at which the experiment was carried out. $\rho_3 = 0$ for $M_\Lambda < m_\pi + M_\Sigma$ since under this condition there isn't enough energy in the $\pi\Sigma$ center of mass to produce the particles at rest. $\rho_3 = 0$ for $M_\Lambda > E - m_{K^0}$ since under this condition there isn't enough energy left over to produce the K^0 at rest. Since $dw_3 \propto \rho_3$, dw_3 has these properties too.

If we set $f_{\pi\Sigma\leftarrow\pi\Sigma} = 1$ we obtain the phase space diagram shown as the dotted curve in Figure 10 (page 34). Results for the the scattering amplitudes we have been generating are given in the "Results" section.

3.2 Results

Low-Energy K^-p Scattering and $\pi^-p \rightarrow \pi^\pm\Sigma^\mp K^0$

Requiring the $\pi\Sigma \rightarrow \pi\Sigma$ scattering amplitude to reproduce the $\pi^-p \rightarrow \pi^\pm\Sigma^\mp K^0$ spectrum proves to be a severe constraint on the T-matrix. This forces a functional form on $f_{\pi\Sigma\rightarrow\pi\Sigma}$ over a $\pi\Sigma$ center of mass energy range of some 200 MeV. In that the $\pi\Sigma$ channel is strongly coupled to the $\overline{K}N$ channels this is a strong constraint on all the scattering amplitudes.

In Figures 11 and 12 we show the computed $\pi^-p \rightarrow \pi^\pm\Sigma^\mp K^0$ mass spectrum (along with a histogram of the measured spectrum) based on the non-relativistic fit to the low energy scattering data (see Figure 6 page 27 and Figure 7 page 28) and the relativistic fit (see Figure 8 page 29 and Figure 9 page 30). We note that scattering amplitudes fit to the low-energy scattering cross sections alone yield poor fits to the spectrum. If we use the spectrum as a constraint we obtain different scattering amplitudes which still yield good fits to the low-energy scattering cross sections.

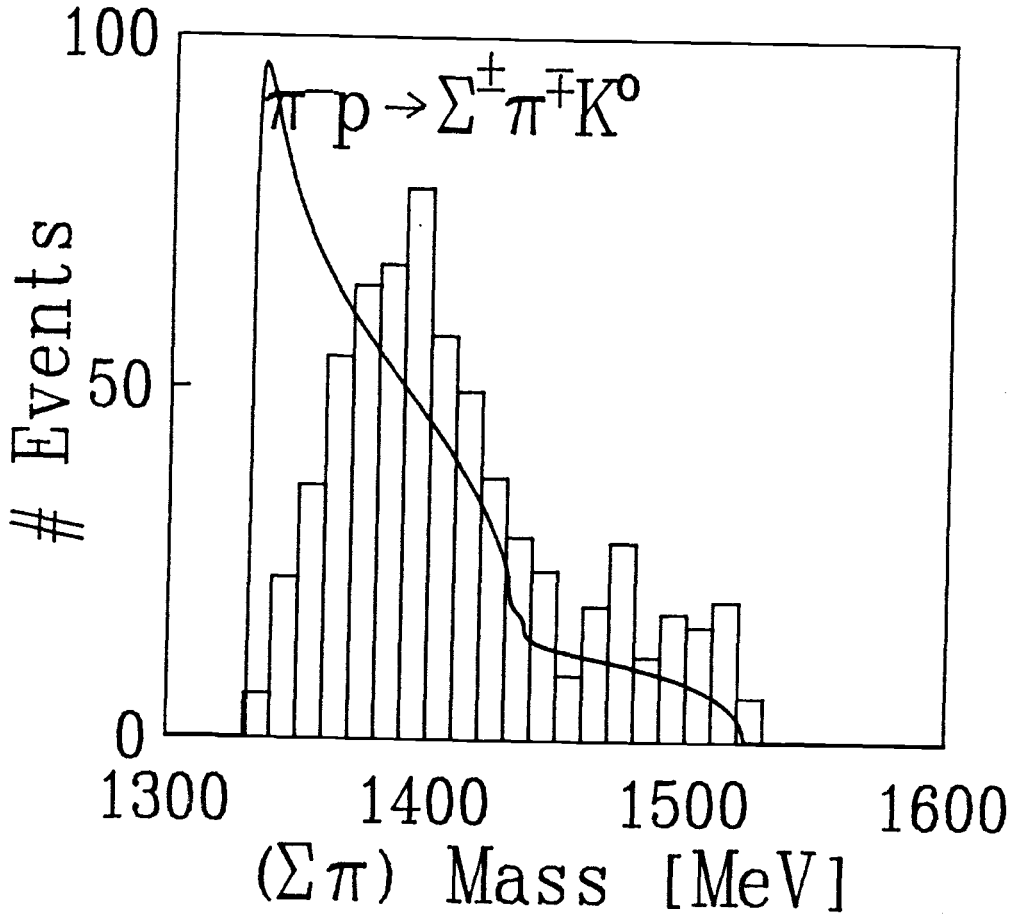

Figure 11. The $\pi\Sigma$ mass spectrum of [43] compared to predictions from a nonrelativistic fit to low-energy scattering data only.

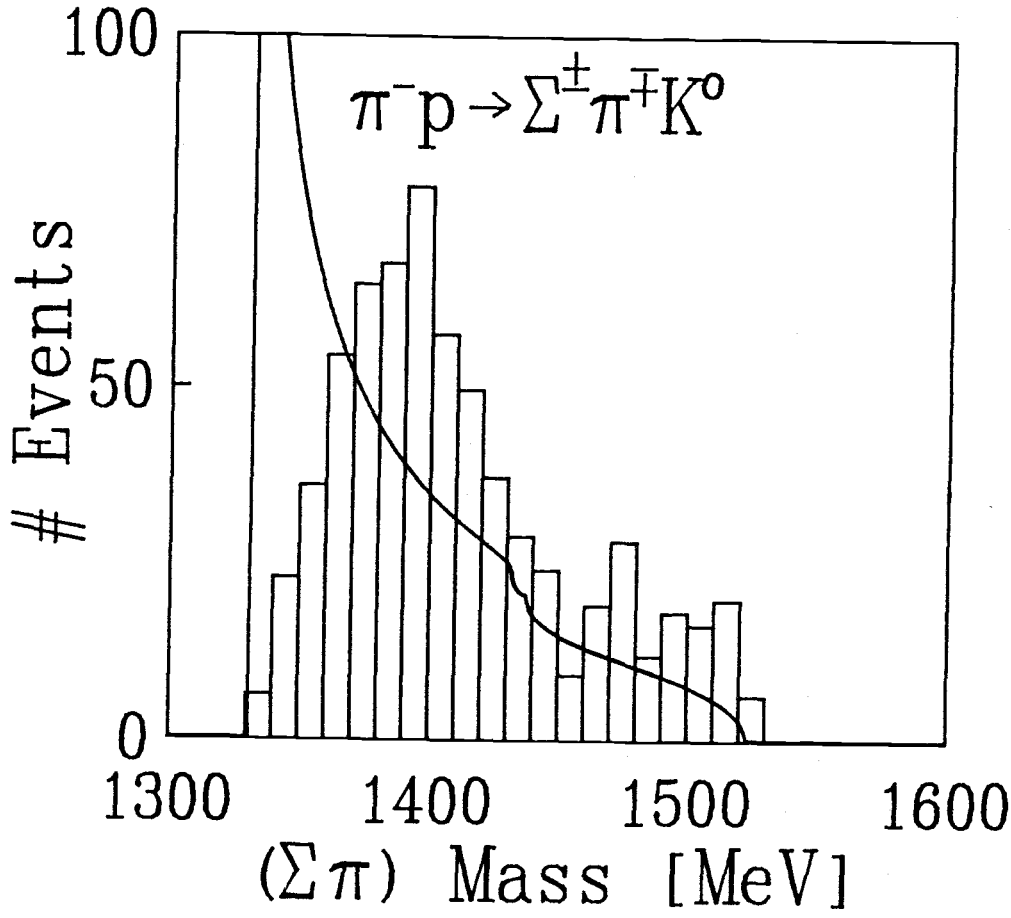

Figure 12. The $\pi\Sigma$ mass spectrum of [43] compared to predictions from a relativistic fit to low-energy scattering data only.

Fit	β_0^{-1} (fm)	λ_0^{11} (MeV^2)	λ_0^{12} (MeV^2)	λ_0^{22} (MeV^2)
nr1	0.0235	-1.47×10^8	-7.72×10^6	-2.83×10^8
nr2	0.138	-2.61×10^4	-4.88×10^4	$+3.46 \times 10^4$
nr3	0.223	-1.82×10^5	-1.54×10^5	-4.36×10^5
HAW	0.180	-3.58×10^5	-1.23×10^5	-4.52×10^5

Fit	β_1^{-1} (fm)	λ_1^{11} (MeV^2)
nr1	0.128	$-7.37 \times 10^5 - 2.14 \times 10^5 i$
nr2	0.293	$-3.88 \times 10^4 - 4.25 \times 10^4 i$
nr3	0.616	$-1.72 \times 10^4 - 1.13 \times 10^4 i$
HAW	0.500	$-6.08 \times 10^3 - 4.42 \times 10^3 i$

Table 2. Potential parameters for three nonrelativistic fits.

3.2.1 Nonrelativistic Calculation

In Figures 13–24 we show the K^-p elastic scattering amplitudes, cross sections, and $\pi^-p \to \pi\Sigma K^0$ mass spectra for each of four nonrelativistic fits to both the low energy scattering data and the $\pi\Sigma$ mass spectrum.

The first three fits were obtained in the present work and are referred to as nr1, nr2, and nr3. The last fit, obtained by Alberg, Henley, and Wilets [23] and referred to as fit HAW is shown for comparison. Table 2 gives the potential parameters corresponding to the four fits. The K^-p elastic scattering

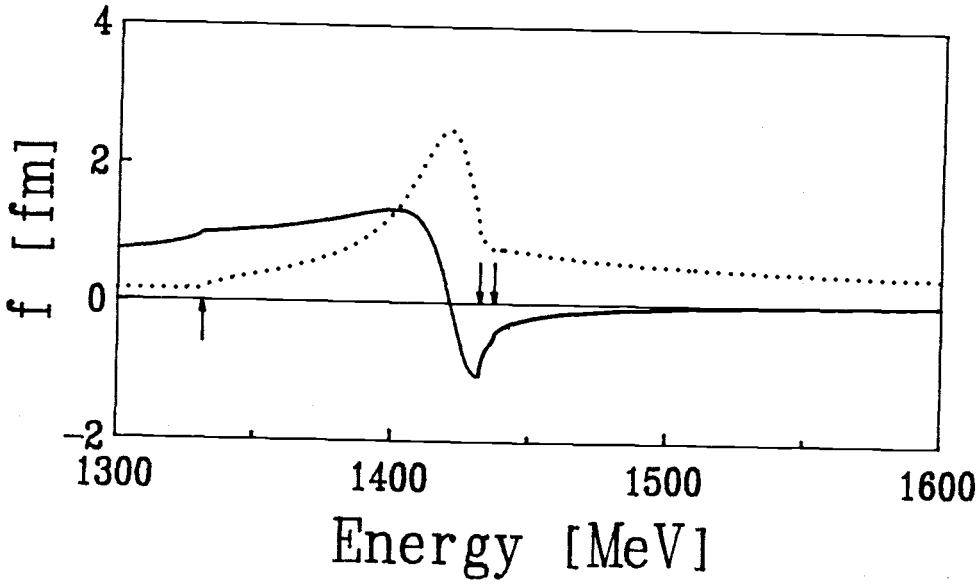

Figure 13. Real (solid) and imaginary (dotted) parts of the K^-p scattering amplitude from nonrelativistic fit nr1 to low-energy scattering data and the $\pi^-p \to \pi^\pm\Sigma^\mp K^0$ mass spectrum.

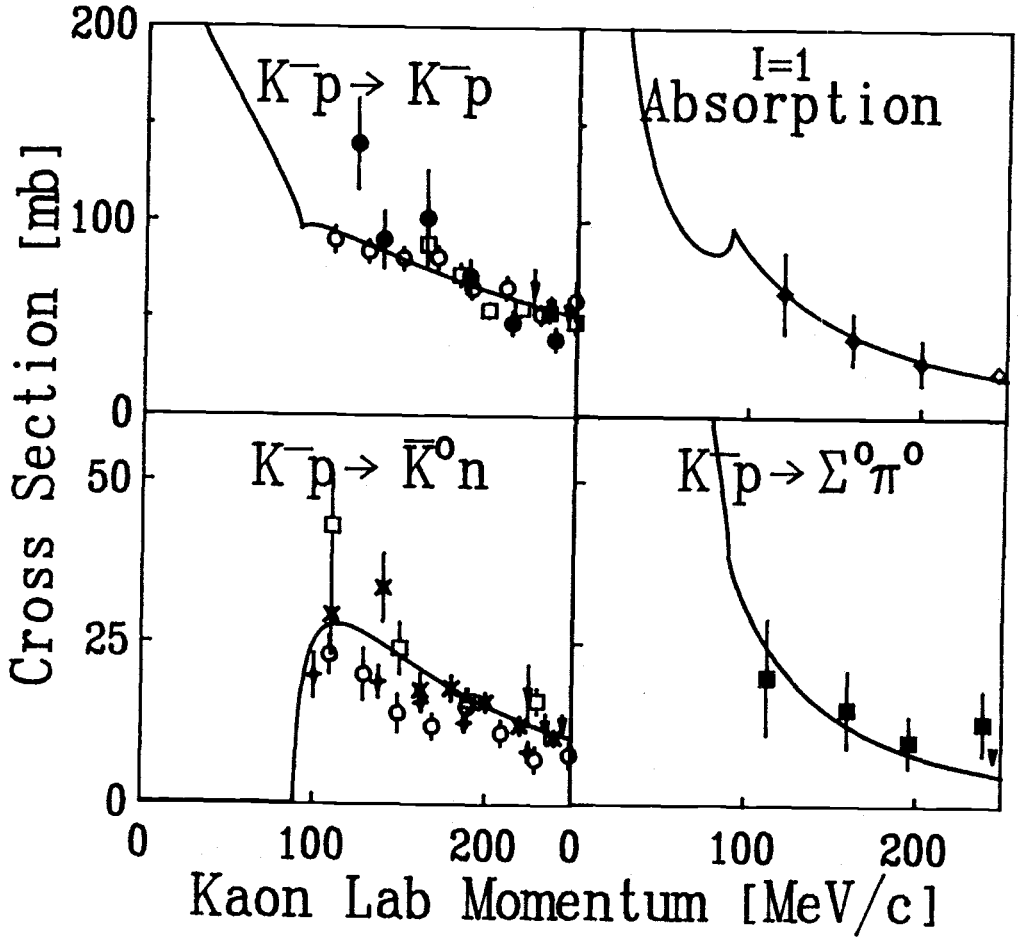

Figure 14. Cross sections from nonrelativistic fit nr1.

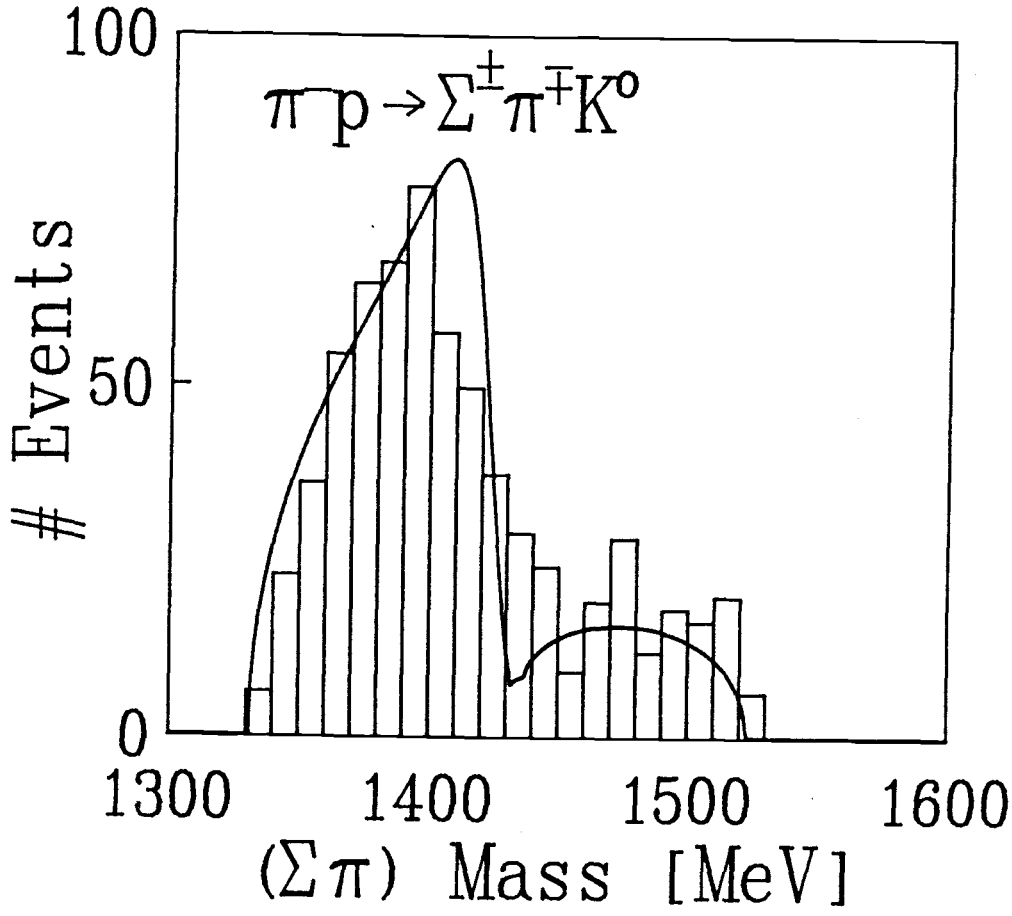

Figure 15. Mass spectrum from nonrelativistic fit nr1.

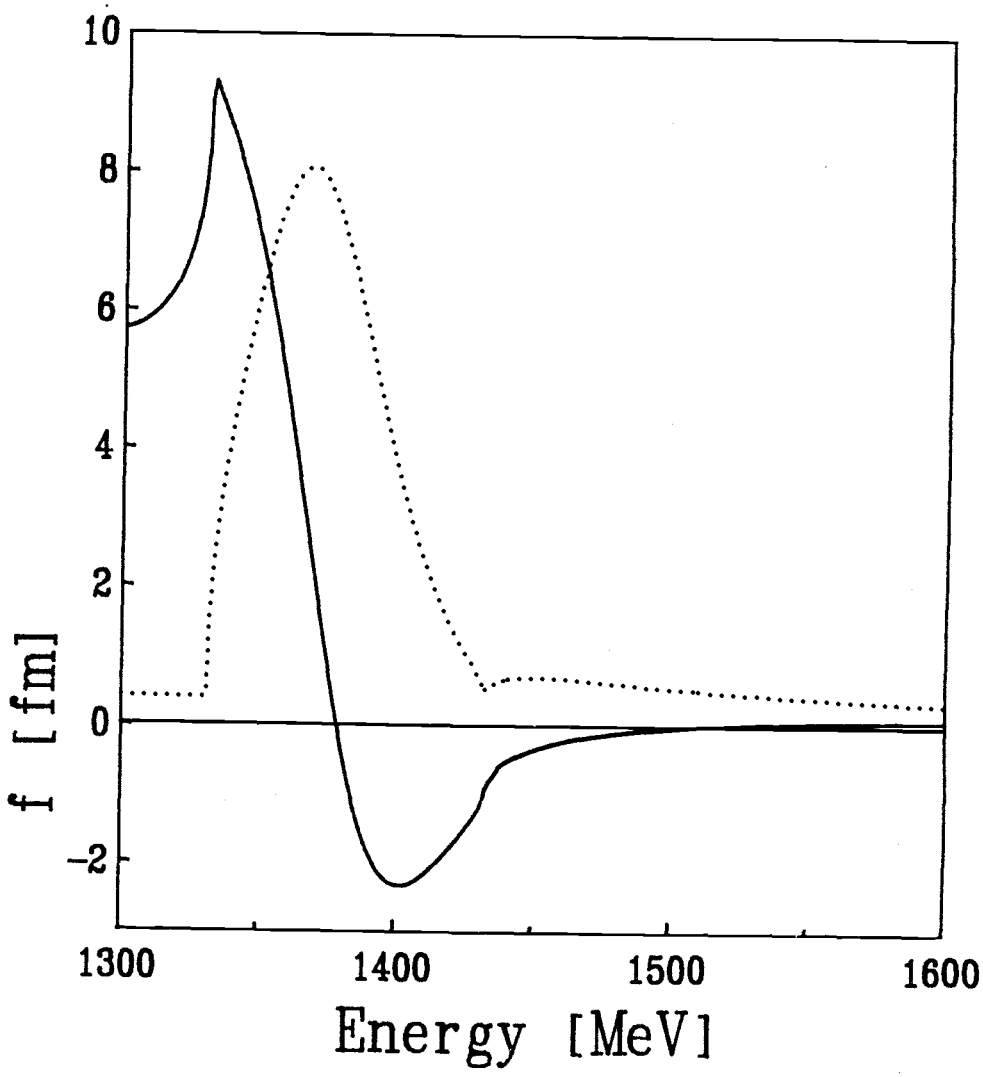

Figure 16. Real (solid) and imaginary (dotted) parts of the $K^- p$ scattering amplitude from nonrelativistic fit nr2 to low-energy scattering data and the $\pi^- p \to \pi^{\pm}\Sigma^{\mp}K^0$ mass spectrum.

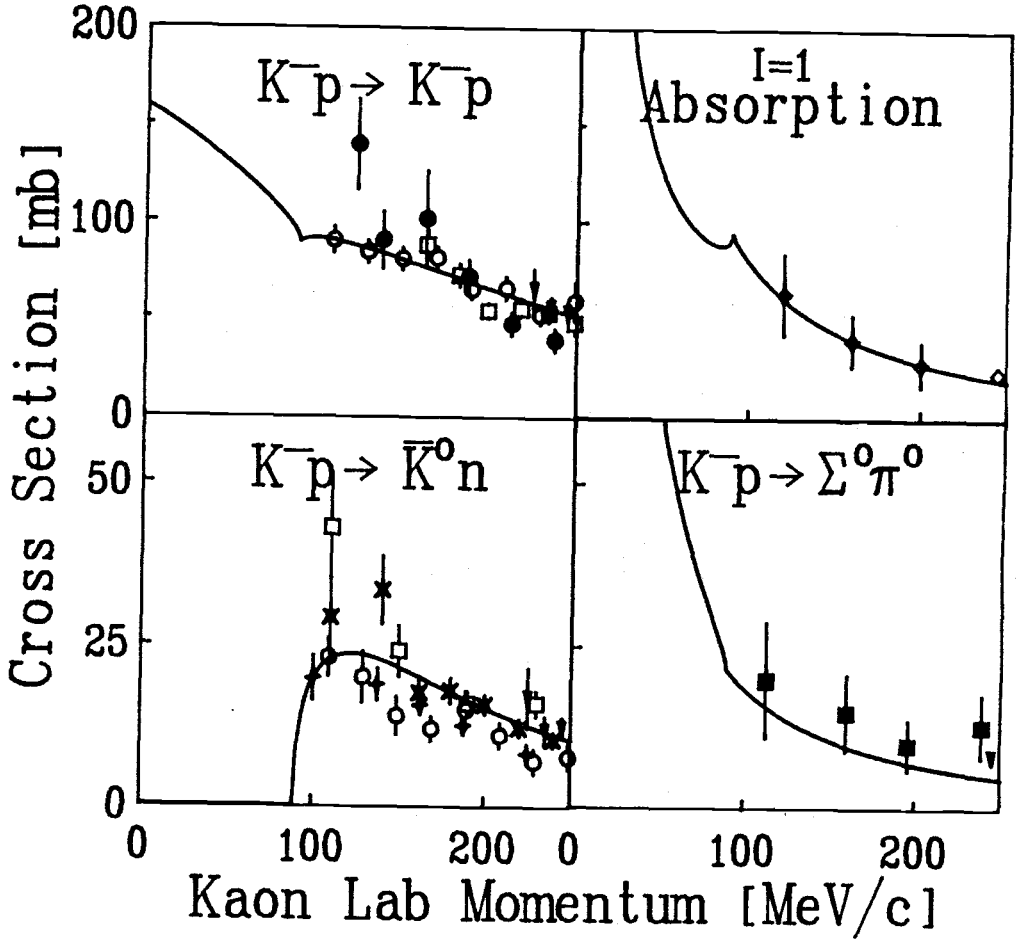

Figure 17. Cross sections from nonrelativistic fit nr2.

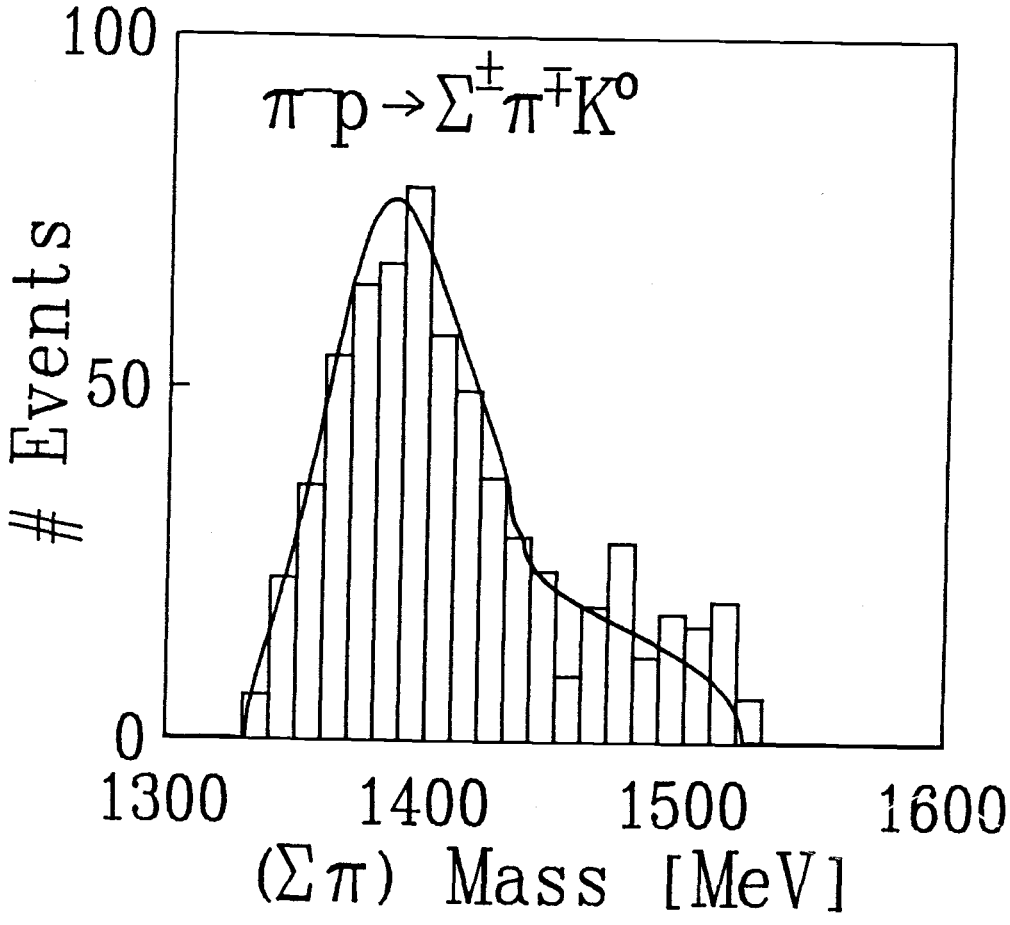

Figure 18. Mass spectrum from nonrelativistic fit nr2.

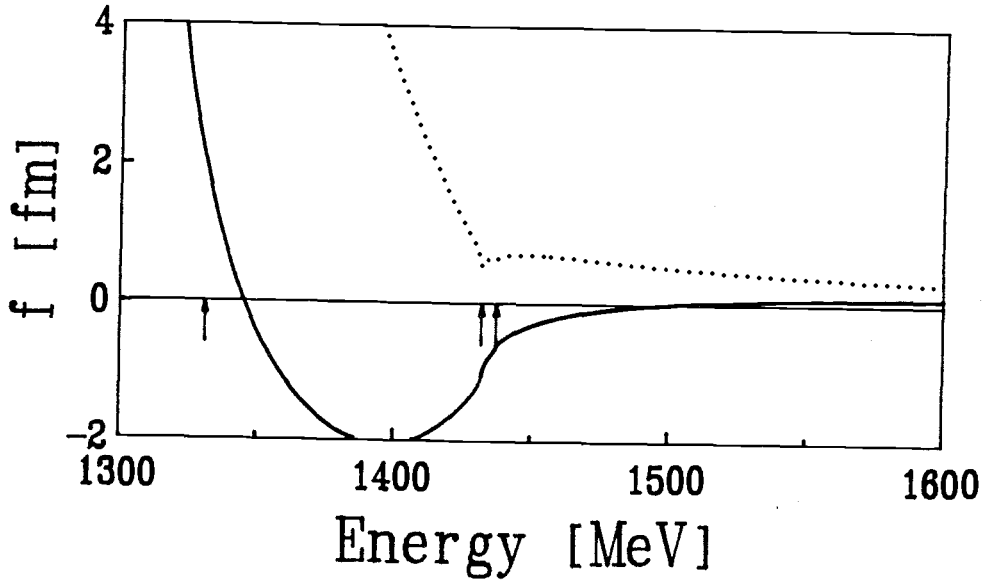

Figure 19. Real (solid) and imaginary (dotted) parts of the K^-p scattering amplitude from nonrelativistic fit nr3 to low-energy scattering data and the $\pi^-p \to \pi^\pm\Sigma^\mp K^0$ mass spectrum.

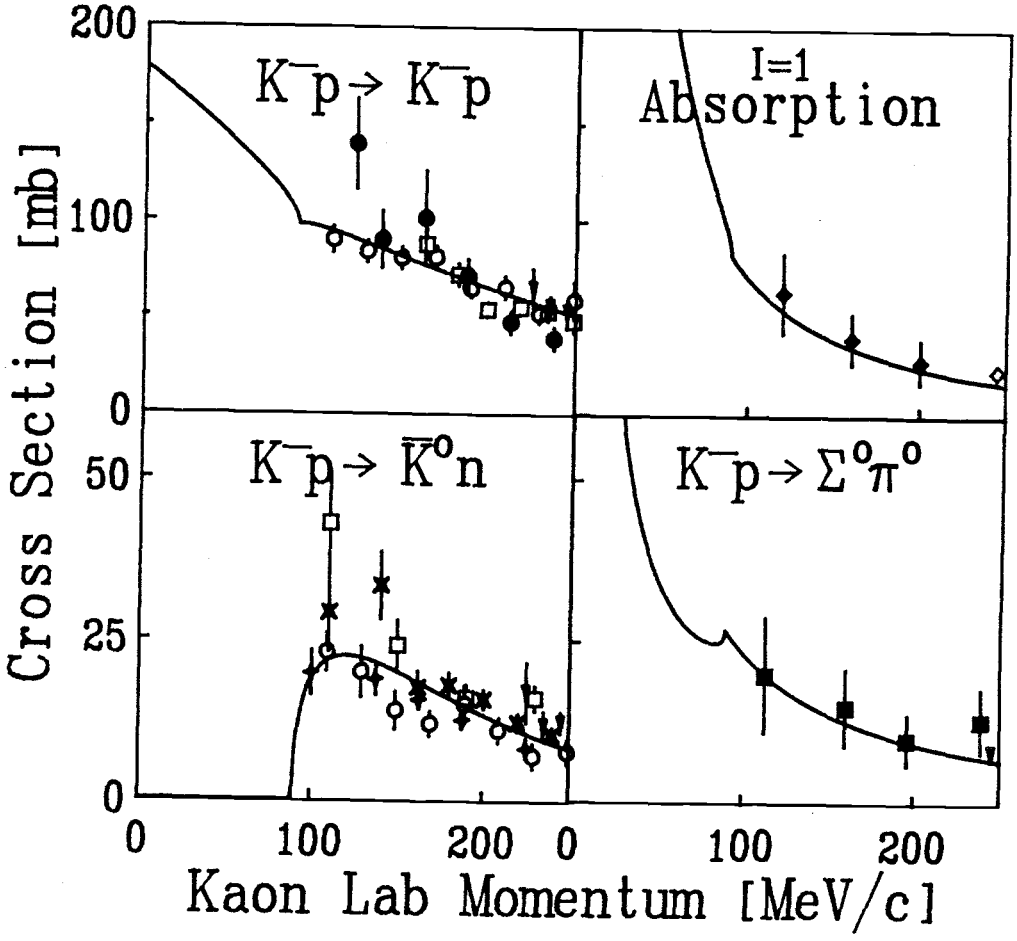

Figure 20. Cross sections from nonrelativistic fit nr3.

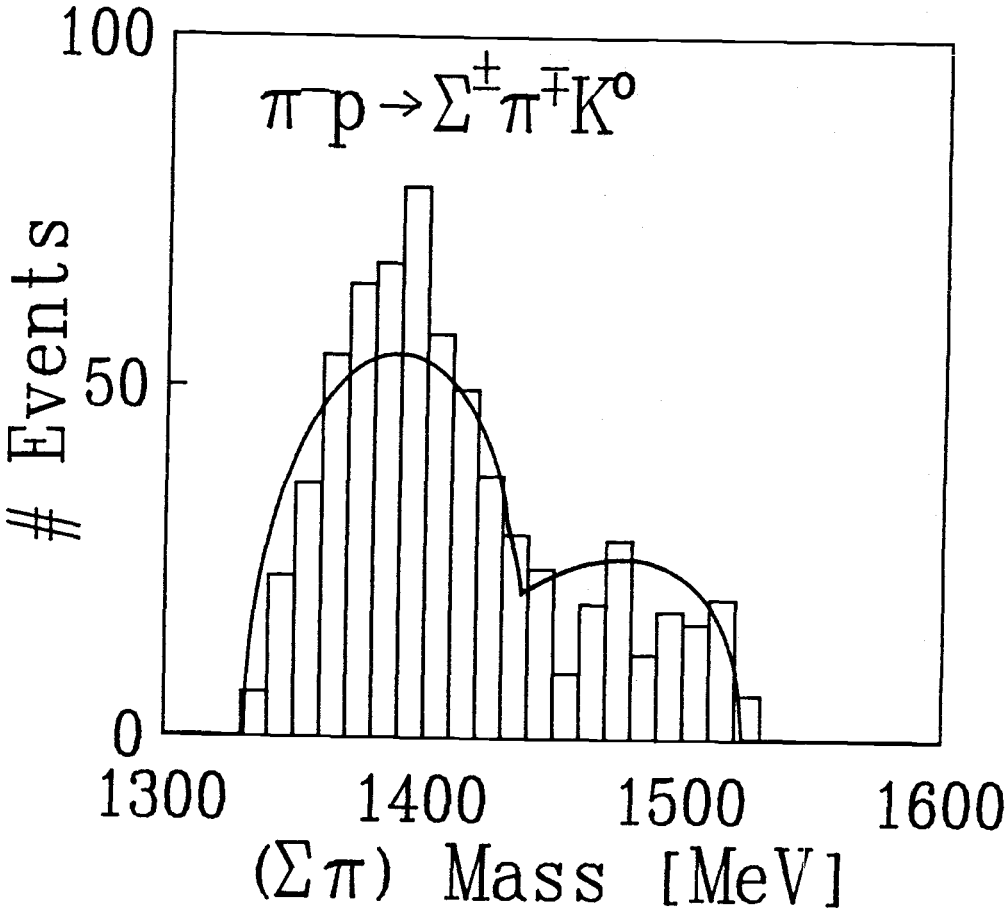

Figure 21. Mass spectrum from nonrelativistic fit nr3.

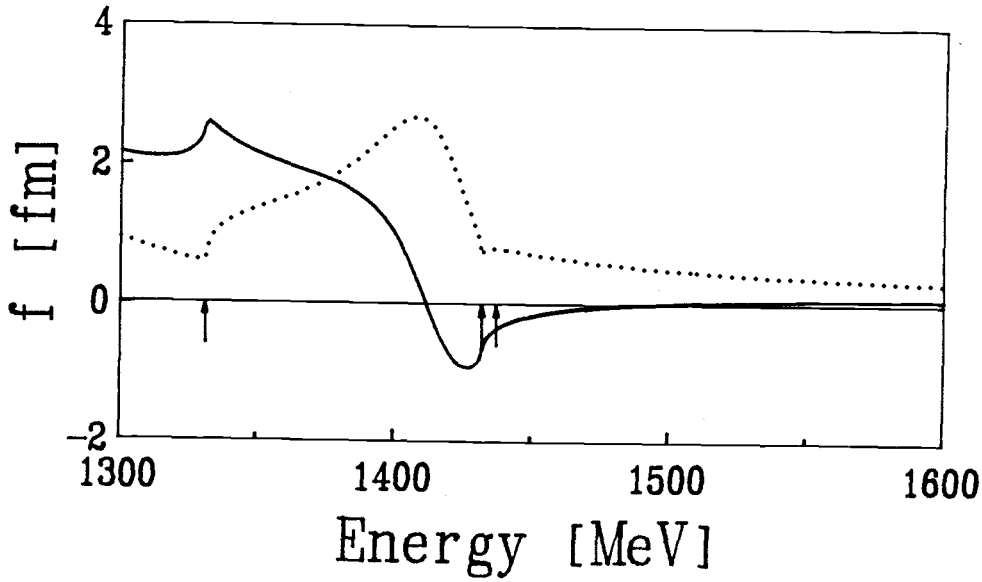

Figure 22. Real (solid) and imaginary (dotted) parts of the $K^- p$ scattering amplitude from nonrelativistic fit HAW [23] to low-energy scattering data and the $\pi^- p \to \pi^{\pm}\Sigma^{\mp}K^0$ mass spectrum.

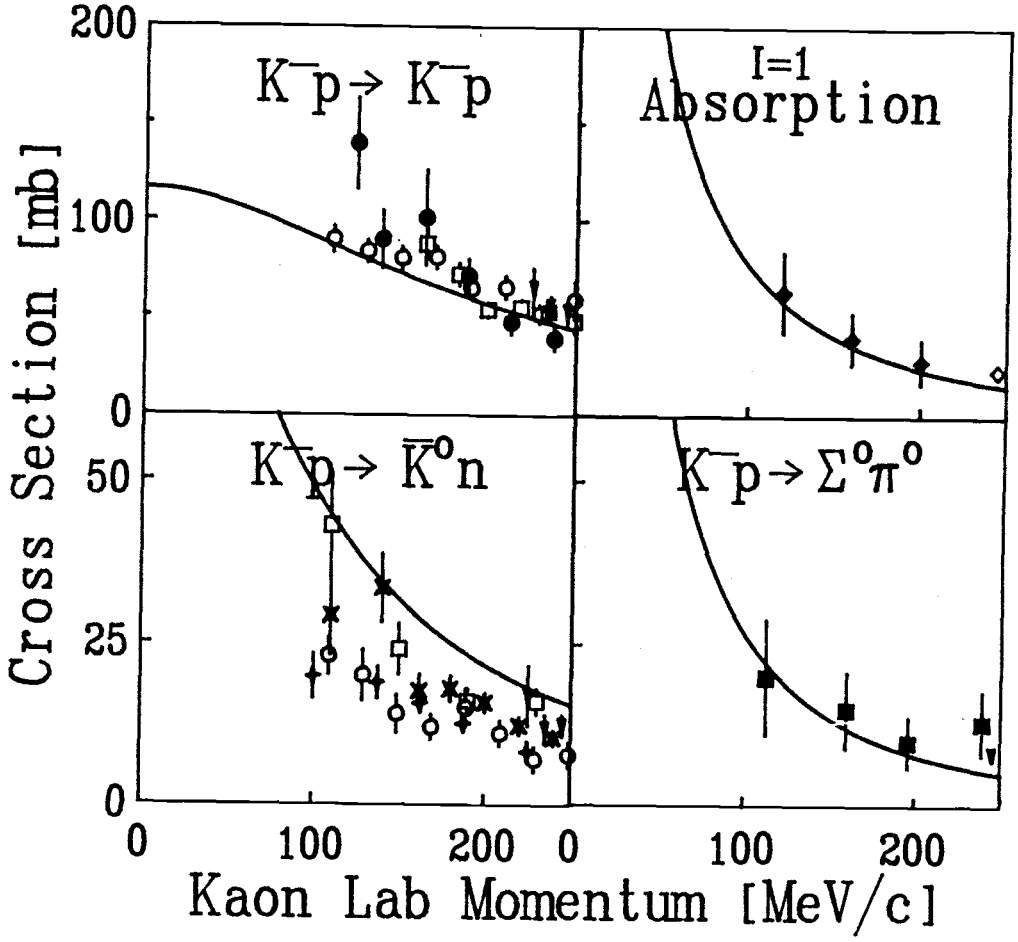

Figure 23. Cross sections from nonrelativistic fit HAW (ref. [23]).

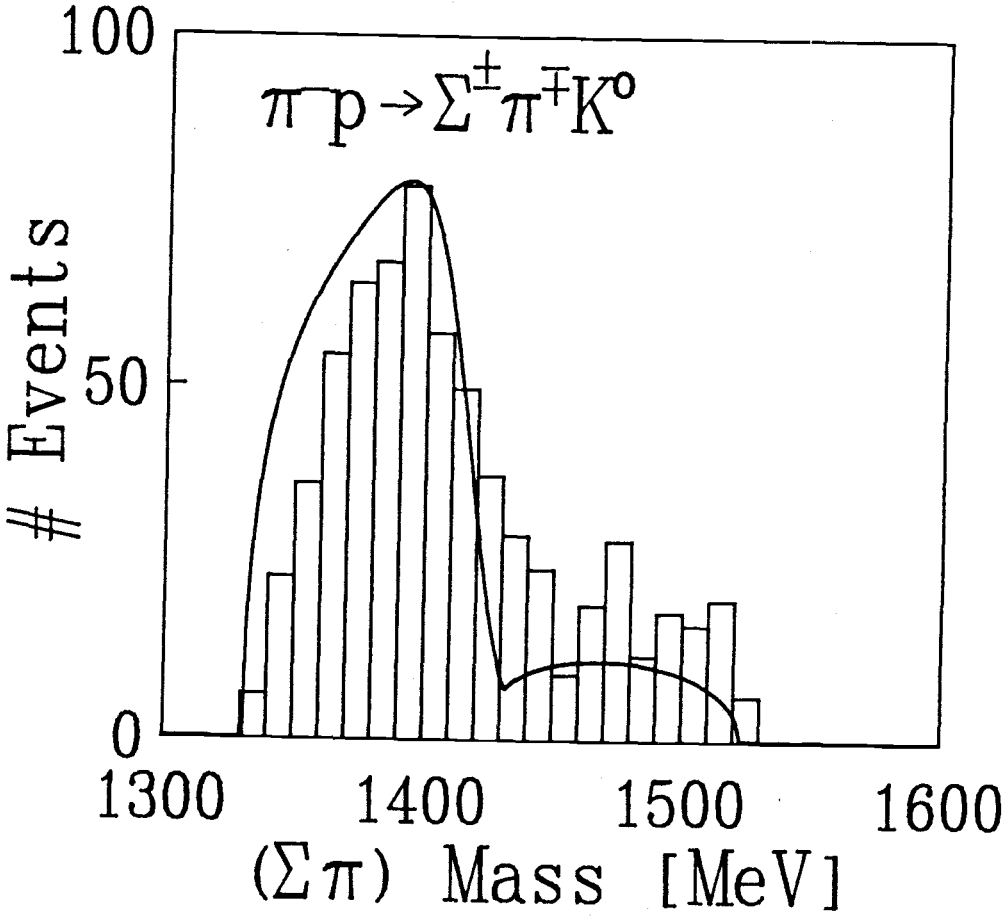

Figure 24. Mass spectrum from nonrelativistic fit HAW (ref. [23]).

Fit	Scattering Length [fm]
nr1	-1.04 + 0.96i
nr2	-1.02 + 0.48i
nr3	-1.06 + 0.55i
HAW	-0.66 + 0.71i

Table 3. The K^-p scattering lengths for nonrelativistic fits nr1, nr2, and nr3 of present work and fit HAW (fit c of ref. [23]).

lengths are given in Table 3. HAW [23] fit to the sum of the antikaon-nucleon scattering cross sections which they reproduce well though the fit to the individual cross sections is poor. The different fits of this work correspond to different chi squared minima arrived at by using different starting values for the potential parameters. In each case the chi squared per degree of freedom is about one. The scattering amplitude of Figure 13, fit nr1, is quite similar to the scattering amplitudes published by other authors [32], [42], [46] including HAW [23], Figure 22. The scattering amplitudes corresponding to fits nr2 and nr3 are also similar in shape but the zero in the real part and the peak in the imaginary part are shifted left and the magnitude of both parts is much greater in the subthreshold region.

Qualitatively, nr3 does not reproduce the spectrum as well as fits nr1 and nr2. However, the big difference between fit nr3 and the other two doesn't become apparent until one looks at the scattering amplitude for $\pi\Sigma \rightarrow \pi\Sigma$. In Figures 25–28 we show the $\pi\Sigma \rightarrow \pi\Sigma$ isospin-0 scattering amplitudes

Fit	Energy [MeV]	Width [MeV]
nr1	1410	54
nr2	1391	70
HAW	1398	64

Table 4. The $\Lambda(1405)$ resonance parameters based on fits fits nr1 and nr2 of present work and fit HAW (fit c of ref. [23]).

generated with the nr1, nr2, nr3 and HAW sets of potential parameters.

We have multiplied the amplitudes by the relative momentum in the $\pi\Sigma$ channel in order to extract the resonance parameters directly from the graphs. Fits nr1, nr2, and HAW show a clear isospin-0 resonance signal (the real part of the scattering amplitude goes through zero and the imaginary part peaks, both at the same energy). This corresponds to the $\Lambda(1405)$. The energy and width of the $\Lambda(1405)$ calculated from fits nr1, nr2, and HAW are given in Table 4. Fit nr3 reproduces the low-energy scattering data and gives a reasonable fit to the $\pi^- p \to \pi^{\pm}\Sigma^{\mp}K^0$ mass spectrum but amazingly[5], fit nr3 shows no evidence for a resonance in the $\pi\Sigma$ channel.

[5]This is amazing only because the data fit here was used to give the $\Lambda(1405)$ its four star rating — the pronounced peak in the $\pi^- p \to \pi^{\pm}\Sigma^{\mp}K^0$ mass spectrum is considered to be hard evidence for the resonance. It is not so amazing when one looks at the phase space curve (which peaks near the resonance energy) in Figure 10 and realizes that the $\overline{K}N$ channels open up at about 1430 MeV causing a dip in the distribution near that energy. The gross features of the spectrum occur in the absence of **any** $\pi\Sigma$ interaction except for the coupling to $\overline{K}N$!

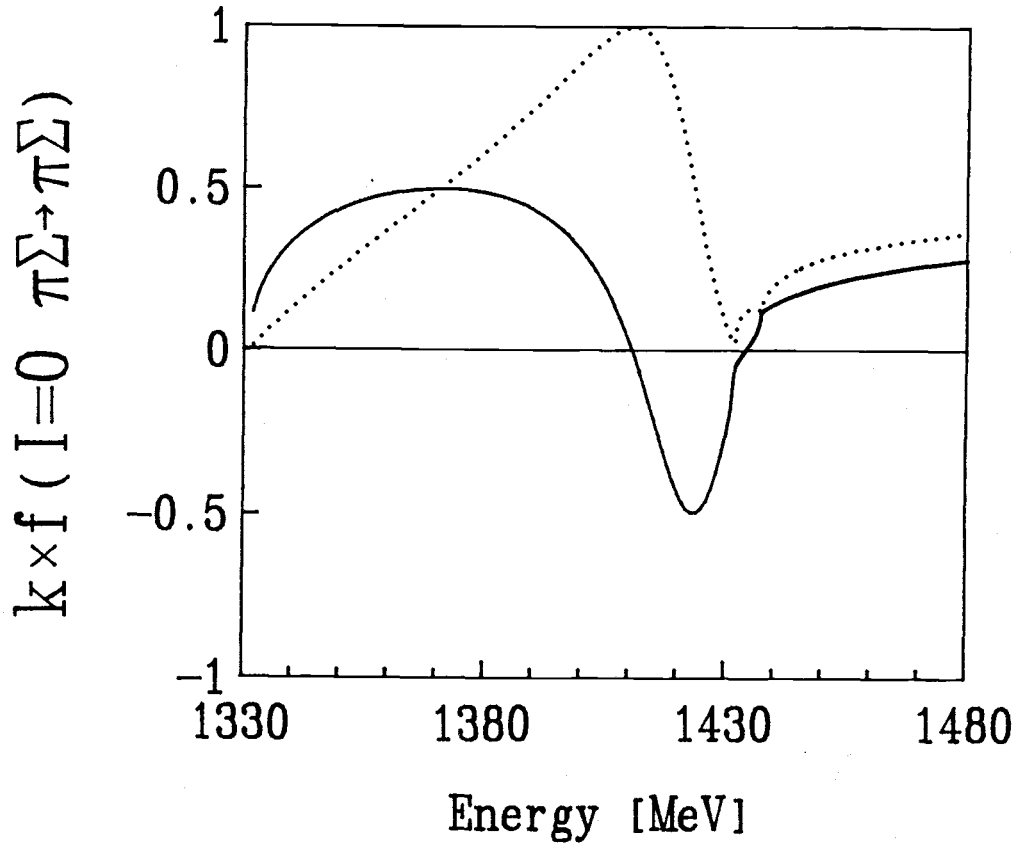

Figure 25. The isospin-0 $\pi\Sigma \to \pi\Sigma$ scattering amplitude multiplied by the relative $\pi\Sigma$ momentum and plotted as a function of the total energy in the $\pi\Sigma$ center of mass frame for fit nr1.

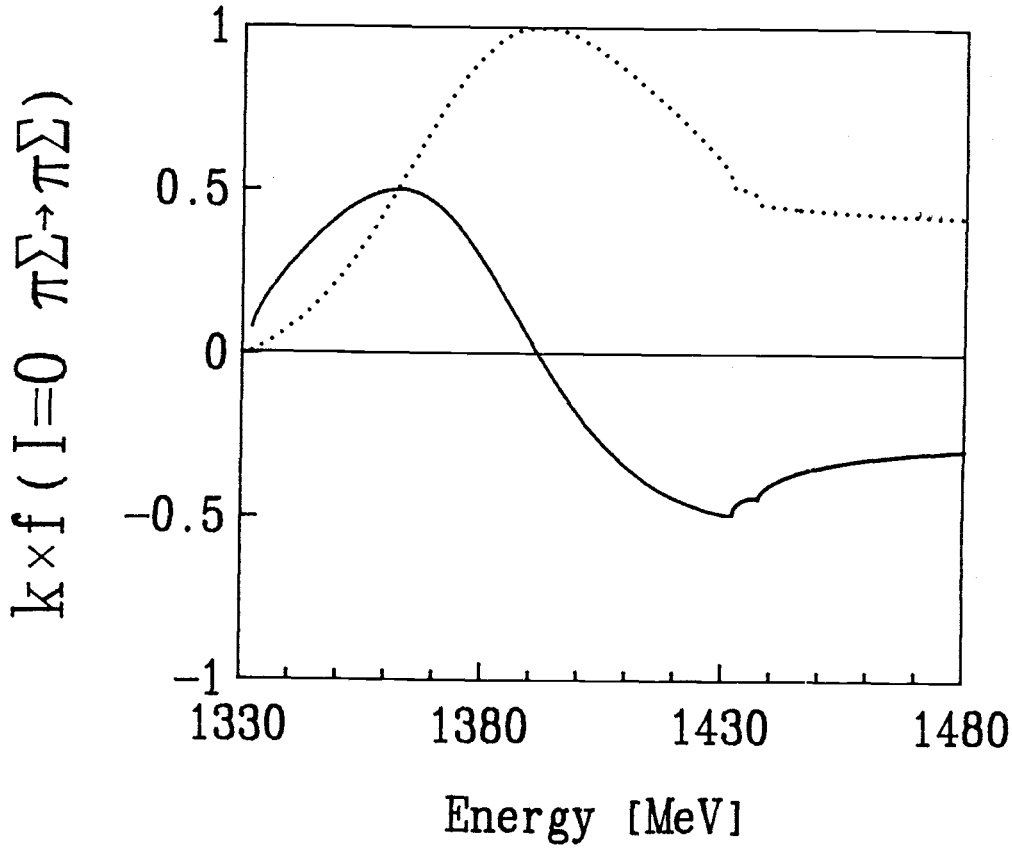

Figure 26. The isospin-0 $\pi\Sigma \to \pi\Sigma$ scattering amplitude multiplied by the relative $\pi\Sigma$ momentum and plotted as a function of the total energy in the $\pi\Sigma$ center of mass frame for fit nr2.

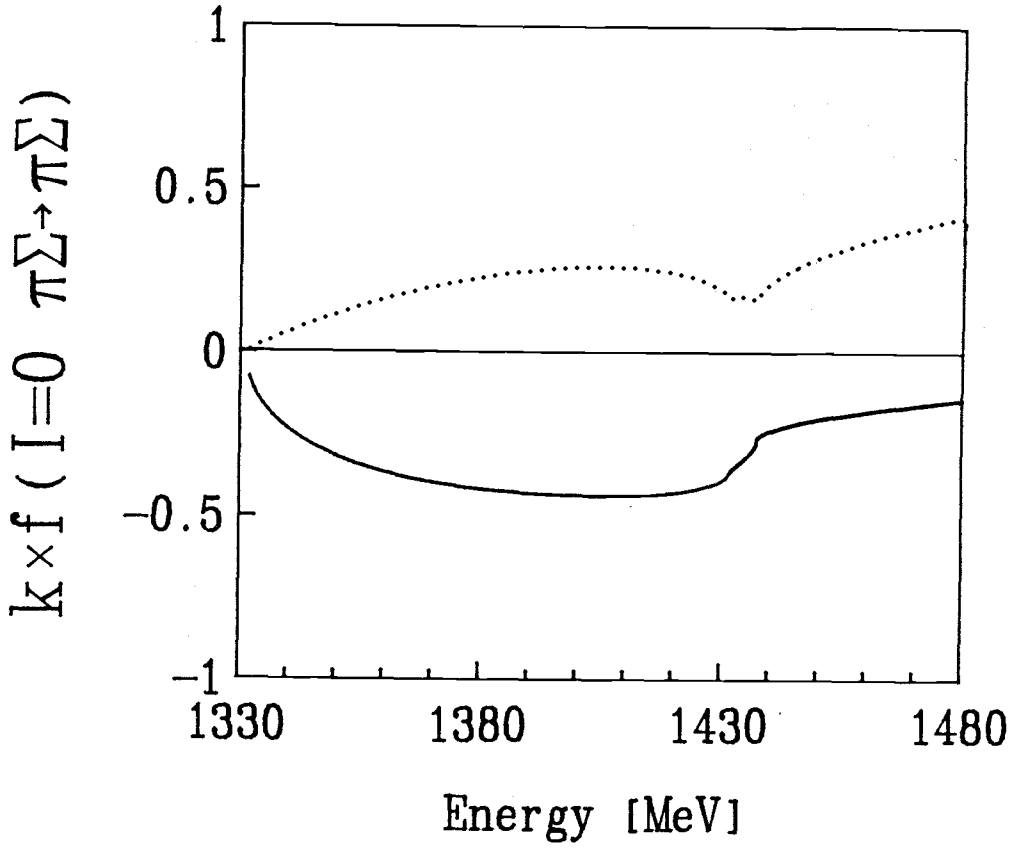

Figure 27. The isospin-0 $\pi\Sigma \to \pi\Sigma$ scattering amplitude multiplied by the relative $\pi\Sigma$ momentum and plotted as a function of the total energy in the $\pi\Sigma$ center of mass frame for fit nr3.

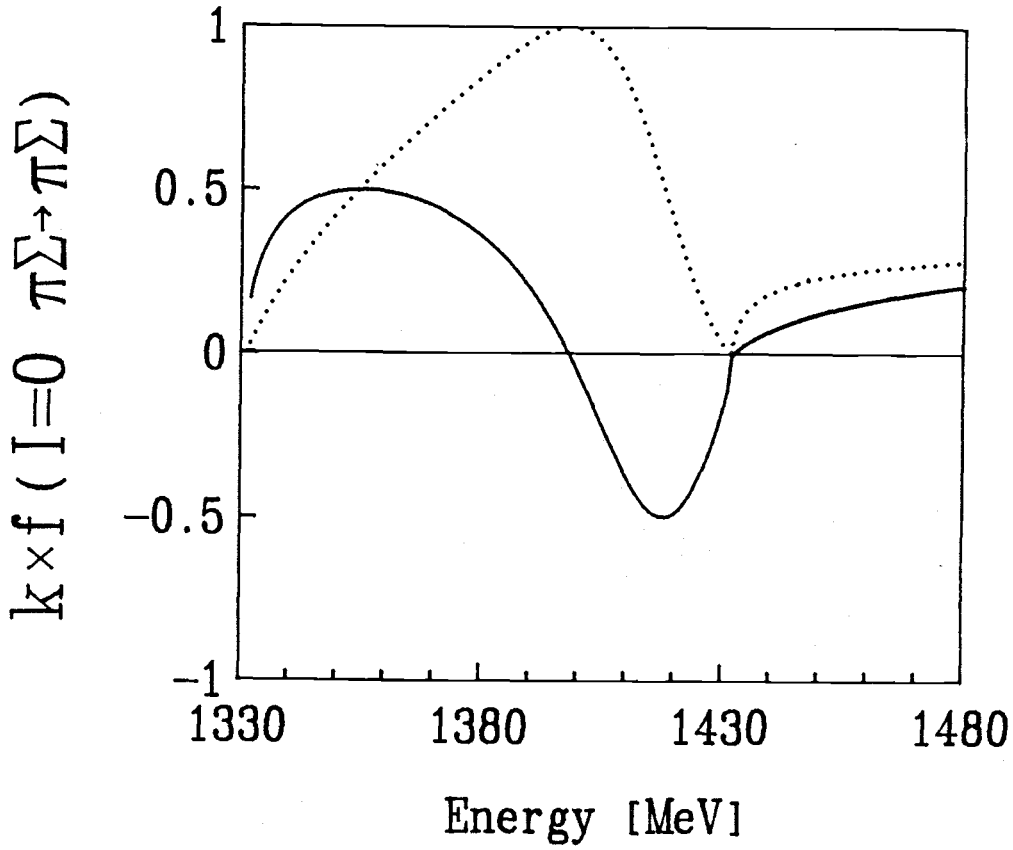

Figure 28. The isospin-0 $\pi\Sigma \to \pi\Sigma$ scattering amplitude multiplied by the relative $\pi\Sigma$ momentum and plotted as a function of the total energy in the $\pi\Sigma$ center of mass frame for fit HAW.

Fit	β_0^{-1} (fm)	λ_0^{11} (MeV^2)	λ_0^{12} (MeV^2)	λ_0^{22} (MeV^2)
r1	0.261	-2.89×10^7	$+2.99 \times 10^7$	-3.13×10^7
r2	0.0962	-1.05×10^6	-1.71×10^5	-1.29×10^6

Fit	β_1^{-1} (fm)	λ_1^{11} (MeV^2)
r1	0.223	$-1.25 \times 10^5 - 2.02 \times 10^4 i$
r2	0.0678	$-2.75 \times 10^6 - 3.77 \times 10^4 i$

Table 5. Potential parameters for two relativistic fits.

3.2.2 Relativistic Calculation

In Figures 29–34 we show the K^-p elastic scattering amplitude, the cross sections, and the $\pi^-p \to \pi^{\pm}\Sigma^{\mp}K^0$ production spectrum for two relativistic fits referred to as fits r1 and r2. The potential parameters and scattering lengths are given in Tables 5 and 6. Fit r1 represents a relativistic update

Fit	Scattering Length [fm]
r1	-0.30 + 0.81i
r2	+0.61 + 0.69i

Table 6. The K^-p scattering lengths for relativistic fits r1 and r2.

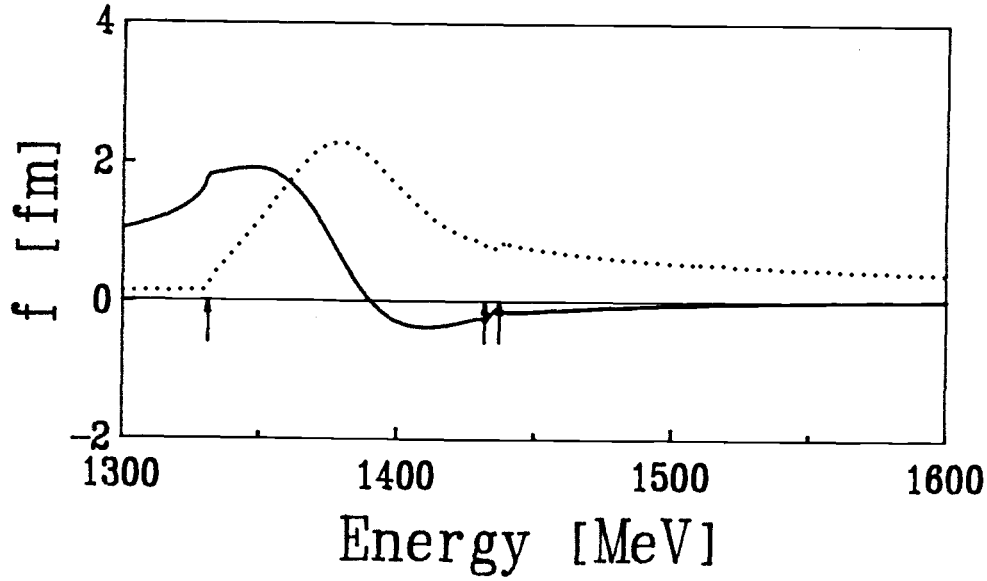

Figure 29. Real (solid) and imaginary (dotted) parts of the K^-p scattering amplitude from relativistic fit r1 to low-energy scattering data and the $\pi^-p \to \pi^\pm\Sigma^\mp K^0$ mass spectrum.

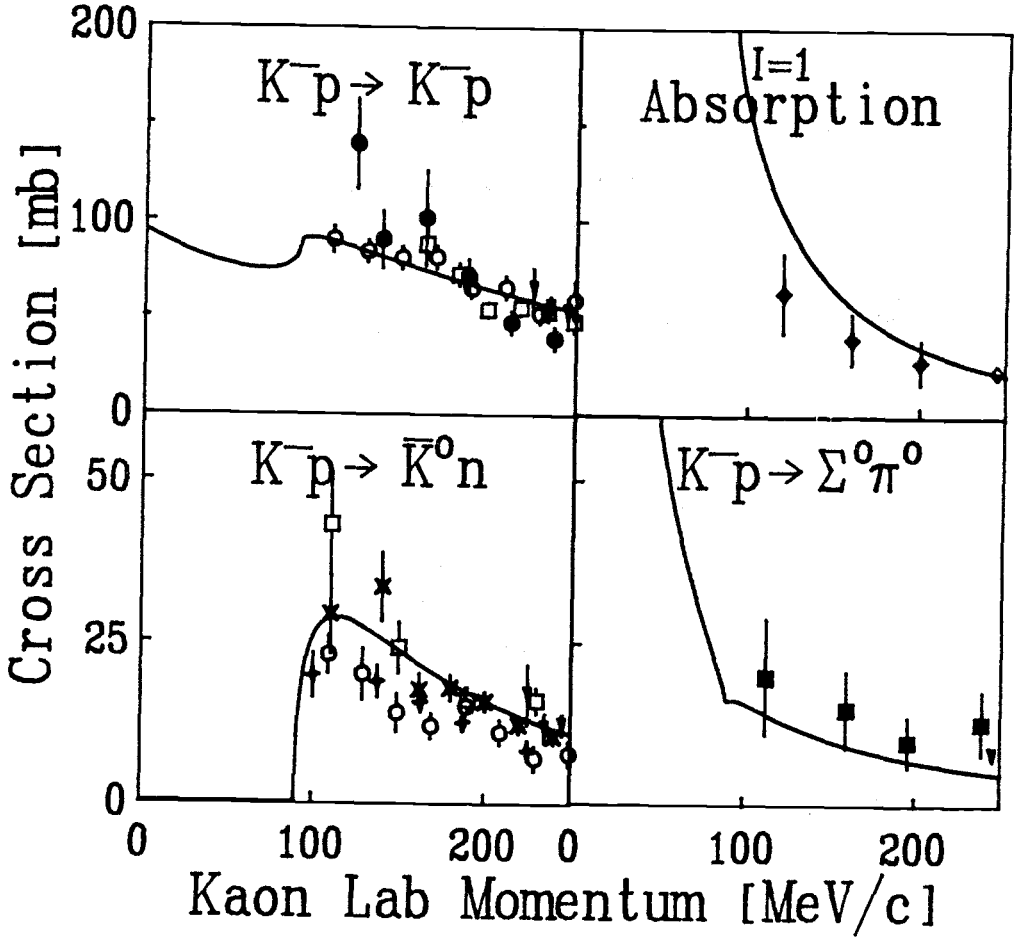

Figure 30. Cross sections from relativistic fit r1.

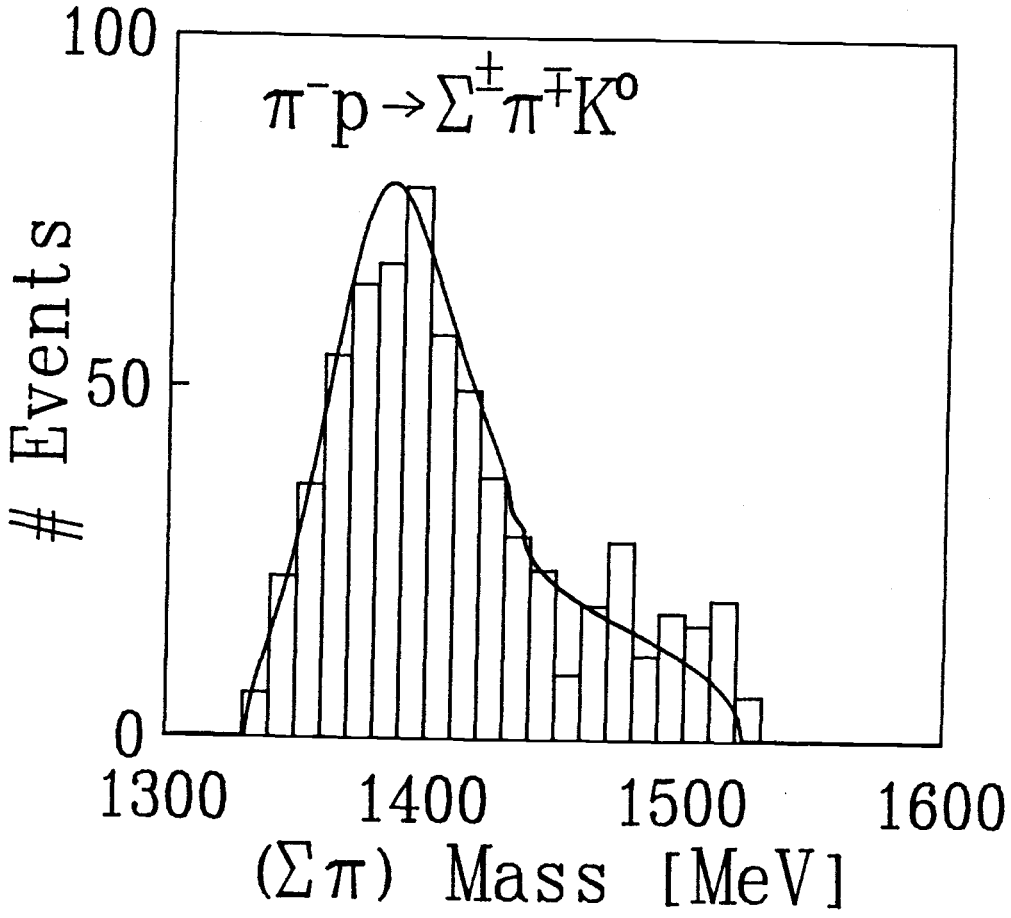

Figure 31. Mass spectrum from relativistic fit r1.

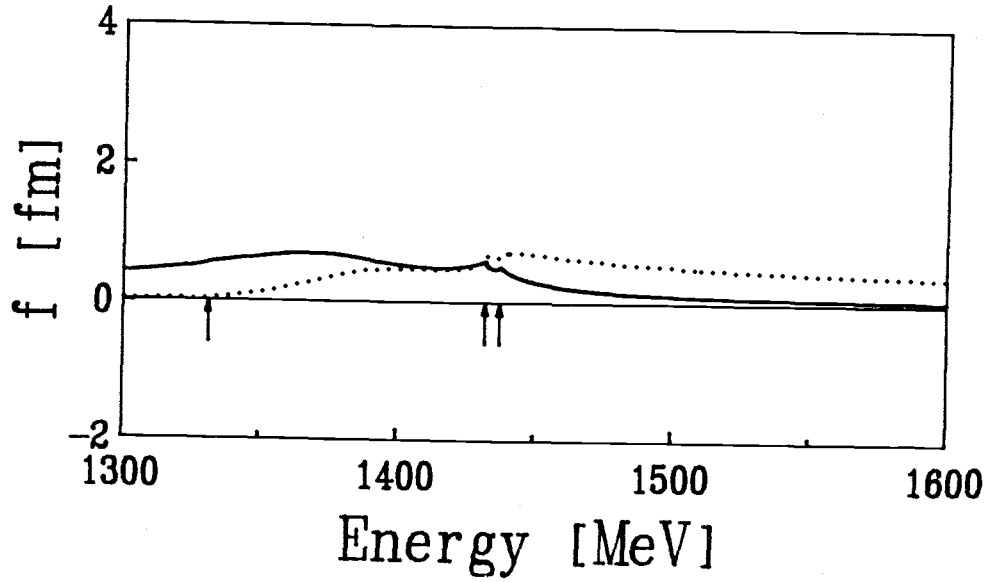

Figure 32. Real (solid) and imaginary (dotted) parts of the K^-p scattering amplitude from relativistic fit r2 to low-energy scattering data and the $\pi^-p \to \pi^{\pm}\Sigma^{\mp}K^0$ mass spectrum.

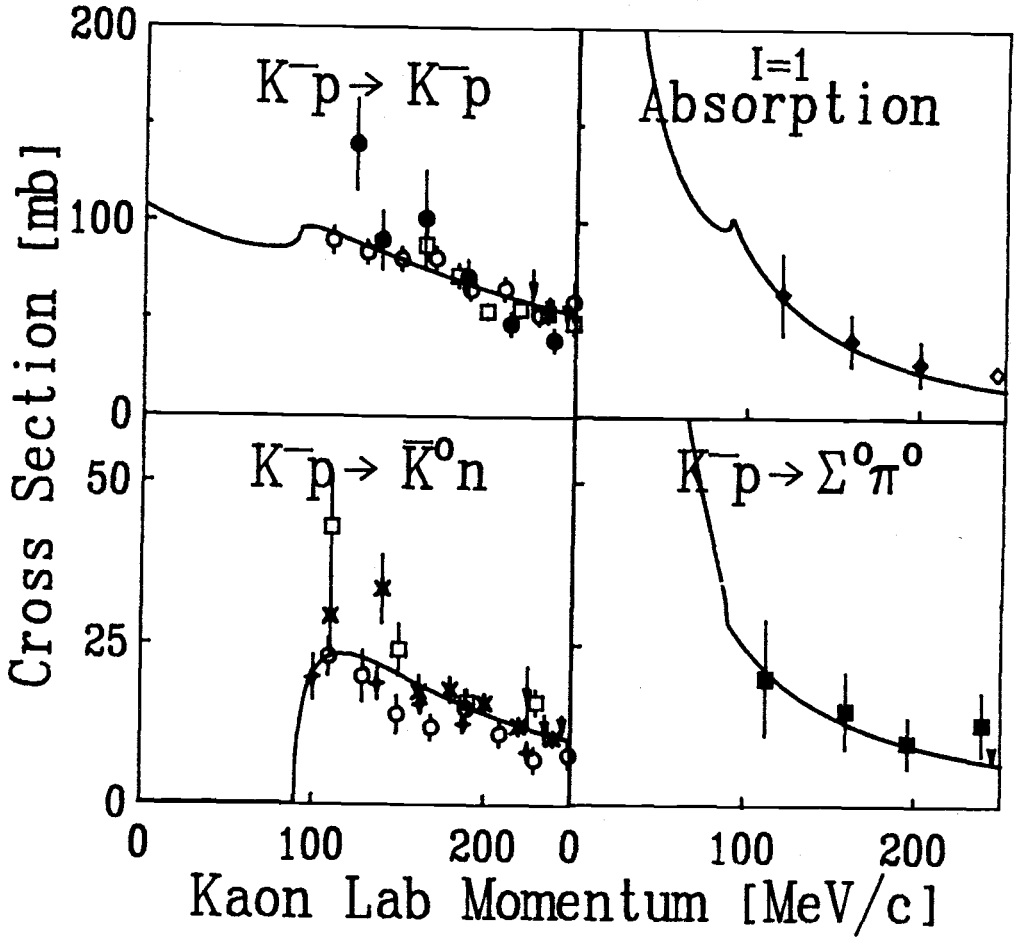

Figure 33. Cross sections from relativistic fit r2.

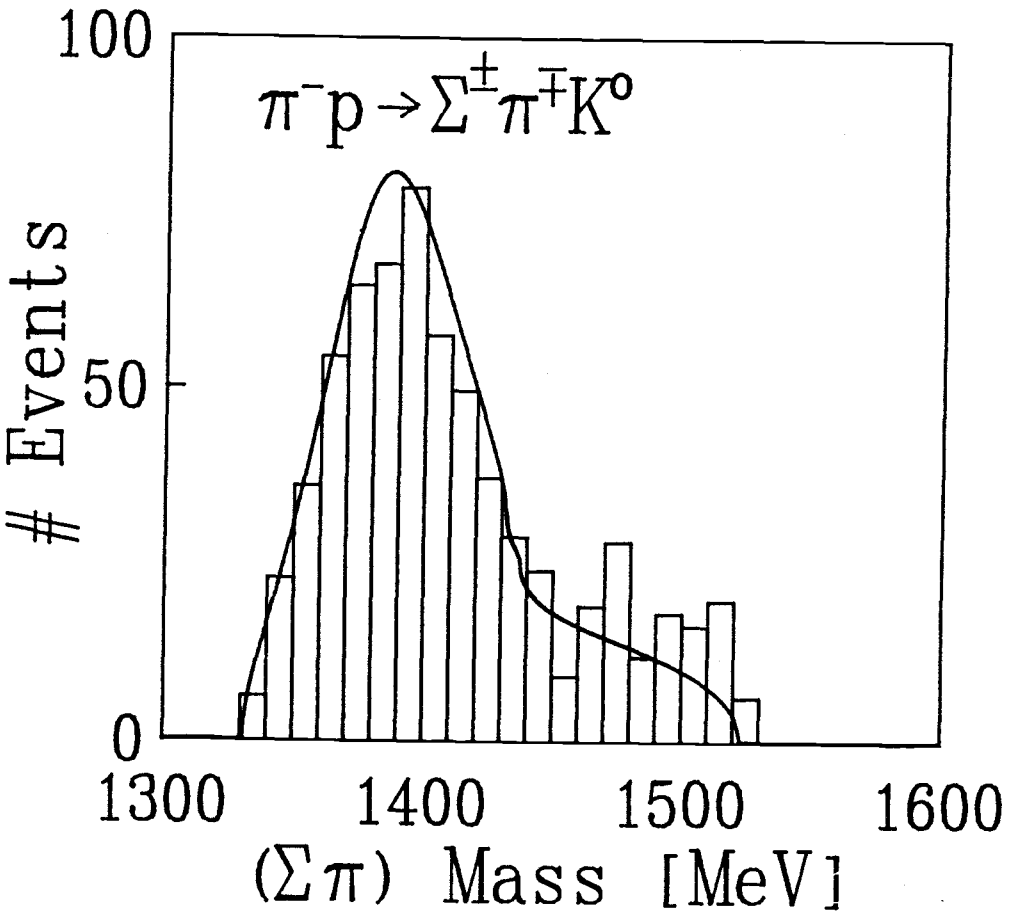

Figure 34. Mass spectrum from relativistic fit r2.

of HAW's work. We present this calculation, although it does not represent quite as good a fit to the data as the other fits, in order to show that including relativistic kinematics as we have done does not rule out scattering amplitudes of the "conventional" shape, i.e. that shape determined by other authors [23], [32], [42], and [46]. Fit r2 represents our best fit to the data. It is the result of a relativistic calculation differing from the other relativistic calculation only in that it corresponds to a different minimum χ^2. Although this result does correspond to the best fit to the data, the difference in χ^2 's is not great enough to suggest that the data is dictating this to be the "true" scattering amplitude.

We note that the real part of the new relativistic scattering amplitude, in contrast to the real part of the other scattering amplitudes, does not change sign. The difference is in the relative strengths of the isospin-0 and isospin-1 parts. In Figure 35 we show the $I = 0$ and $I = 1$ K^-p elastic scattering amplitudes separately for fit r1. Figure 36 shows the individual isospin amplitudes for fit r2. We note that the the essential difference is in the strength of the $I = 0$ amplitude. In the r1 fit, it is weaker than the $I = 1$ amplitude. In fit r2, and only in fit r2, the $I = 1$ curve dominates in the region near threshold so that the total scattering amplitude which is approximated very accurately by the sum of the two does not have any sign changes! Coupled strongly to the $\pi\Sigma$ channel as it is, one might expect the behavior of the r2 scattering amplitude to carry over into the $\pi\Sigma$ channel and thus fail to yield a $\pi\Sigma$ resonance. We find that, on the contrary, fits r1 and r2 both give a nice $\pi\Sigma$ resonance that can be identified as the $\Lambda(1405)$. In Figures 37 and 38 we show the $\pi\Sigma$ elastic scattering amplitude times the

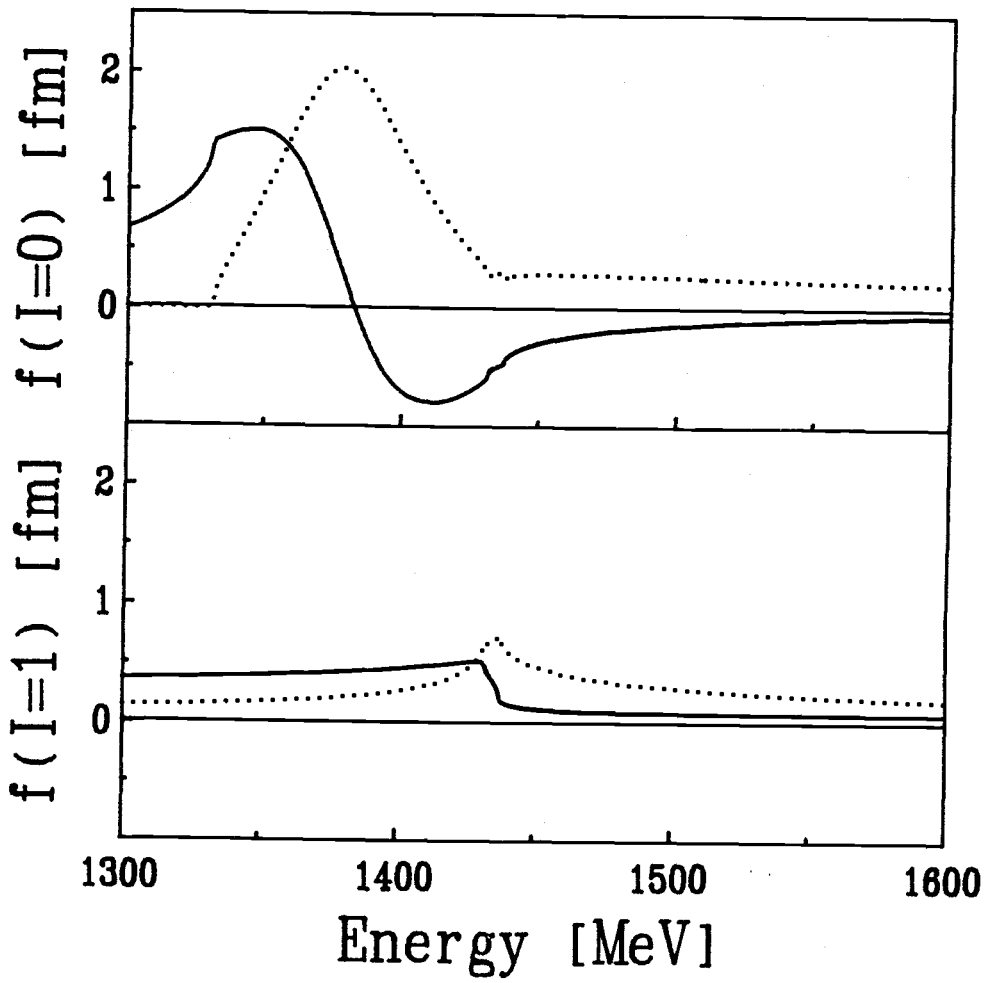

Figure 35. Real (solid) and imaginary (dotted) parts of the $\overline{K}N$ $I = 0$ (upper) and $I = 1$ (lower) elastic scattering amplitudes from relativistic fit r1 to low-energy scattering data and the $\pi^- p \to \pi^{\pm}\Sigma^{\mp}K^0$ mass spectrum.

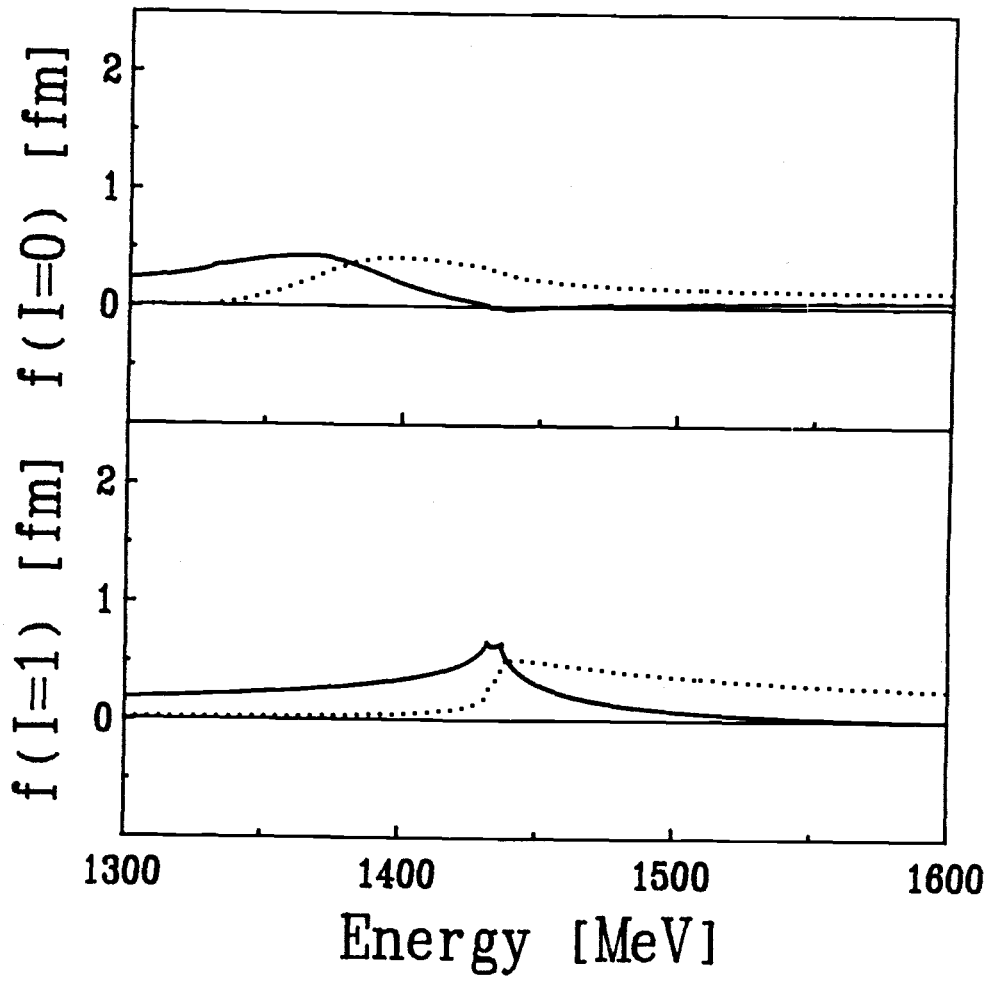

Figure 36. Real (solid) and imaginary (dotted) parts of the $\overline{K}N$ $I = 0$ (upper) and $I = 1$ (lower) elastic scattering amplitudes from relativistic fit r2 to low-energy scattering data and the $\pi^- p \to \pi^{\pm}\Sigma^{\mp}K^0$ mass spectrum.

Fit	Energy [MeV]	Width [MeV]
r1	1397	81
r2	1400	70

Table 7. The $\Lambda(1405)$ resonance parameters based on fits fits r1 and r2.

channel momentum for fits r1 and r2. The resonance behavior is apparent. The resonance parameters are given in Table 7.

Even with the strong conditions placed on the scattering amplitudes by the $\pi p \rightarrow \pi \Sigma K^0$ spectrum we still have enough variety in the calculated amplitudes that further constraints on the scattering amplitudes are needed to determine which set is correct. To this end we turn to kaonic atoms.

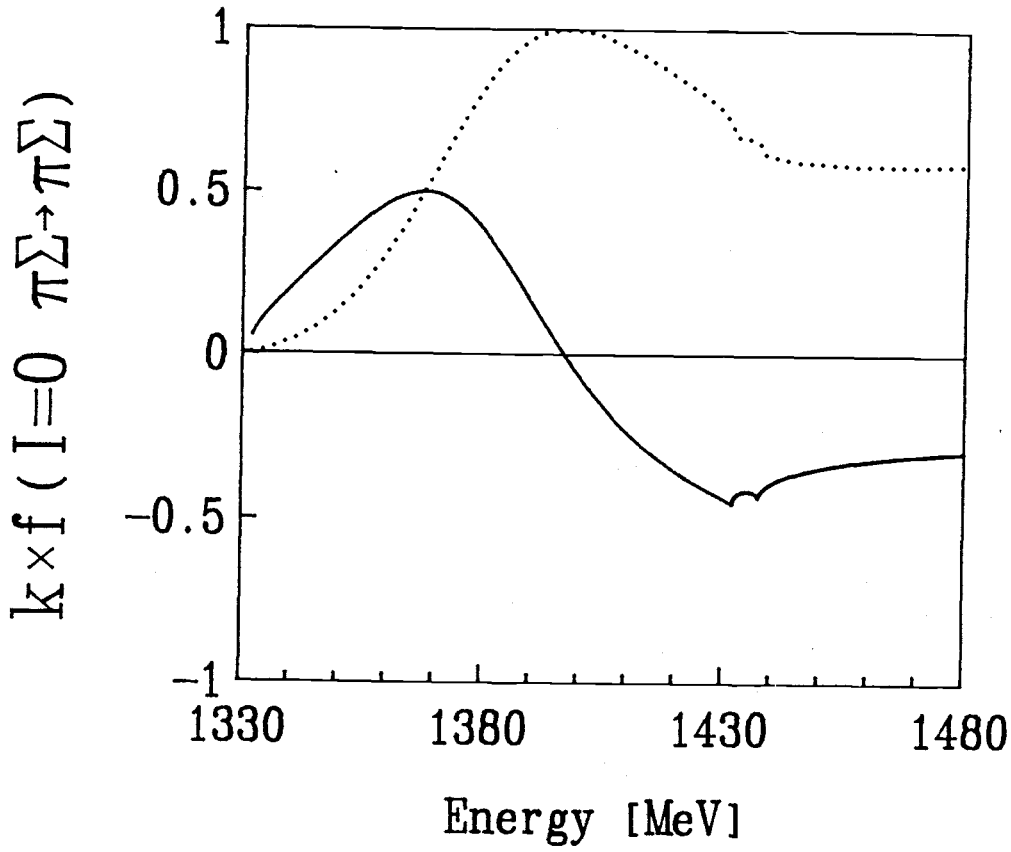

Figure 37. The isospin-0 $\pi\Sigma \to \pi\Sigma$ scattering amplitude multiplied by the relative $\pi\Sigma$ momentum and plotted as a function of the total energy in the $\pi\Sigma$ center of mass frame for fit r1.

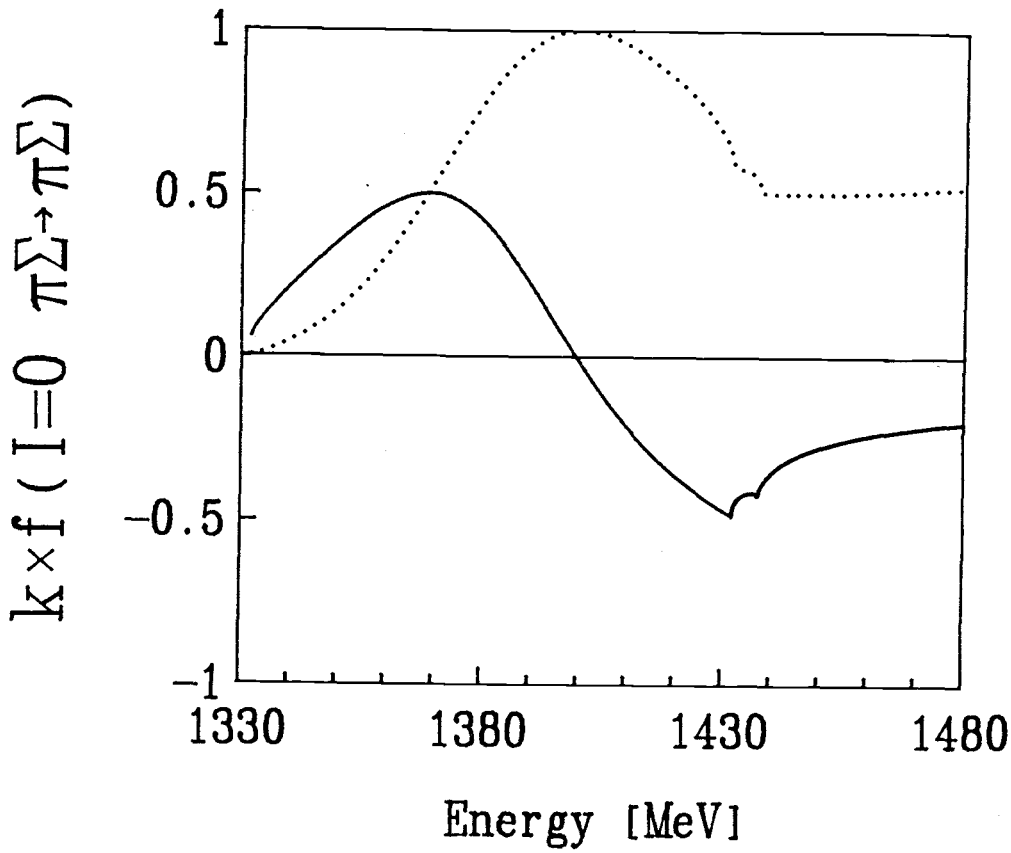

Figure 38. The isospin-0 $\pi\Sigma \to \pi\Sigma$ scattering amplitude multiplied by the relative $\pi\Sigma$ momentum and plotted as a function of the total energy in the $\pi\Sigma$ center of mass frame for fit r2.

Chapter 4

Kaonic Hydrogen

4.1 Kaonic Hydrogen Experiment

When negatively charged antikaons are allowed to impinge upon a liquid hydrogen target they slow down in the target and are captured on protons in high principal quantum number n and angular momentum quantum number l Bohr orbits. The antikaons cascade down through the various Bohr orbits, by Auger transitions until they are inside the innermost electron orbit, and then via photon emission. The Coulomb bound state which is formed in such a manner is known as kaonic hydrogen. It is a hydrogen atom with a negatively charged antikaon instead of an electron. The antikaon has mass 493.667 MeV which is roughly 1000 times the mass of the electron. Since the Bohr radius goes as $1/m$, an antikaonic hydrogen orbit is smaller, by a factor of about 10^{-3}, than the electronic hydrogen orbit of the same principal quantum number. The Bohr radius of kaonic hydrogen is 84 fm. For this reason the short range strong interaction causes a significant shift in the $1s$ level of kaonic hydrogen and also gives the level a significant width. The

shift and width in the $2p$ level are negligible and thus a measurement of the energies of the photons given off in $2p - 1s$ transitions of kaonic hydrogen can be expected to give the shift and width of the $1s$ level when these measurements are compared with the exactly calculable $1s$ levels for the pure Coulomb state.

The experiment is a very difficult one. Because of the necessary target container, photons of energies near the $2p - 1s$ transition energy (6.4 KeV) are given off by other processes which makes it very difficult to identify the $2p - 1s$. The experiment has been carried out three times [24,25,26] and although the results differ to some extent (see Figure 39), they agree in that each measurement shows the 1s state of kaonic hydrogen to be more bound than it would be in the absence of the strong force. This is in direct contradiction to the theoretical shift predicted [47]–[49] on the basis of low energy K^-p scattering experiments [29],[33]–[40]. In the next section we show how the theoretical shift is determined. Then we give the theoretical shifts based on the scattering amplitudes calculated in Sections 3.2.1 and 3.2.2. Here we emphasize that it may very well be the experiment which is in error. However, these three measurements are the only ones available and we choose to explore the consequences which follow when they are taken at face value.

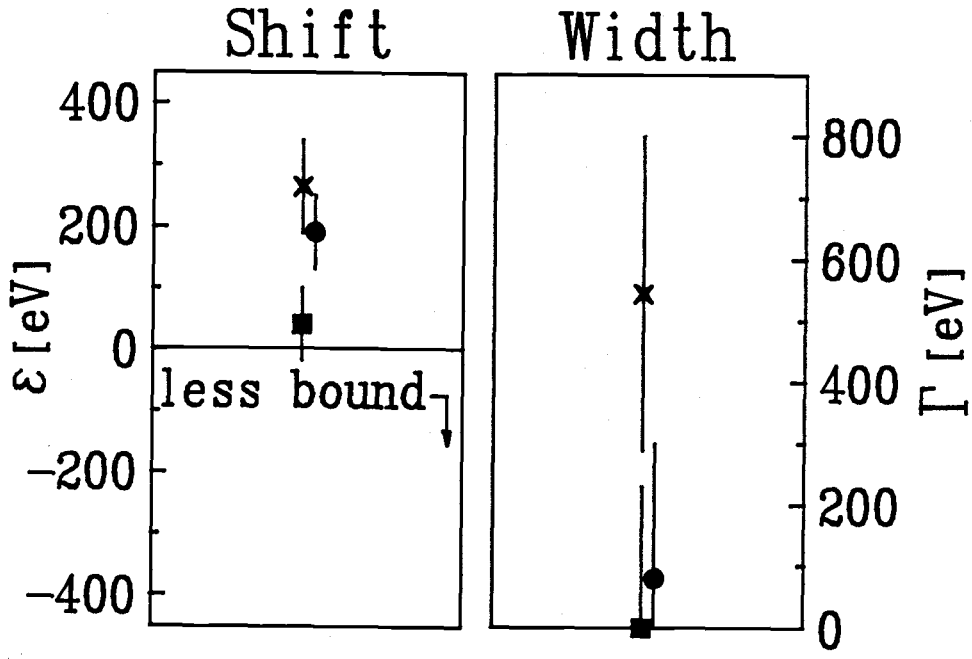

Figure 39. The shifts and widths of the 1S level in kaonic hydrogen as measured by [24] (squares), [25] (crosses), [26] (circles).

4.2 Kaonic Hydrogen Theory

In the simplist analysis the kaonic hydrogen shift and width are given by the Trueman formula [50]:

$$\frac{\triangle E_n}{E_n} = -\frac{4\, f(E_n)}{n\, R_B}$$

where $f(E_n)$ is the complex $K^- p$ scattering amplitude evaluated at E_n, the Coulomb bound-state energy of principal quantum number n , and R_B is the Bohr radius. The shift and width are given in terms of $\triangle E_n$ as:

$$\begin{aligned} \epsilon &= -Re(\triangle E_n) \\ \Gamma &= -2\, Im(\triangle E_n) \end{aligned}$$

According to this formula, the scattering amplitude must have a positive real part at threshold in order to produce a shift to the more bound (positive ϵ). Thus, if we accept the kaonic hydrogen results, the only scattering amplitude of those depicted in Figures 13, 16, 19, 22, 29, and 32 that would yield a qualitatively correct shift is the the one corresponding to fit r2. In light of these considerations the kaonic hydrogen experimental results are seen to be very useful in ruling out what would otherwise be considered physically reasonable scattering amplitudes (but only to the extent that the experimental results can be believed).

Although we have used the Trueman Formula to argue that the only physically reasonable scattering amplitude from our various fits is the one from the "New Relativistic" fit, the strong energy dependence of the $K^- p$ elastic scattering amplitude makes it necessary to carry out a more exact calculation of the shift and width in order to compare the theoretical predictions of the

shift and width based on the scattering amplitudes of section 3.2.1 and 3.2.2 with the measured values.

4.2.1 The Bound State Problem in Momentum Space

In this section we give the general methods used for solution of the momentum space bound state problem, first in terms of operators and then in terms of matrix elements or functions. Calculational details for specific applications are given in subsequent sections.

We begin with the Lippmann-Schwinger equation

$$\begin{aligned} T &= V + VGT \\ (1 - VG)T &= V \\ T &= (1 - VG)^{-1}V \end{aligned}$$

The condition for a bound state is that the T-matrix has a pole, or

$$\det(1 - VG) = 0$$

If we evaluate the operators in the Lippmann-Schwinger equation between momentum states we arrive at the integral equation given in section 2.2.1 as equation 2.2.

$$\langle \mathbf{k}' | T | \mathbf{k} \rangle = \langle \mathbf{k}' | V | \mathbf{k} \rangle + (\hbar c)^3 \int d^3p \, \langle \mathbf{k}' | V | \mathbf{p} \rangle \, G_E(\mathbf{p}) \, \langle \mathbf{p} | T | \mathbf{k} \rangle$$

Carrying out the same steps as were performed in that section we arrive at the Lippmann-Schwinger equation for a particular value of the angular momentum quantum number l as given by equation 2.3.

$$T_l(k', E, k) = V_l(k', k) + 4\pi \int dp \, p^2 \, \frac{V_l(k', p) \, T_l(p, E, k)}{E - E(p) + i\epsilon}$$

If we approximate the integral in this equation by a sum over points with weighting factor W_n this equation becomes (subscript l suppressed and E dependence understood)

$$T(k_i, k_j) = V(k_i, k_j) + \frac{2}{\pi}(\hbar c)^3 \sum_{n=1}^{N} W_n k_n^2 \frac{V(k_i, k_n)T(k_n, k_j)}{E - E(k_n) + i\epsilon}$$

which we write for convenience as

$$T_{ij} = V_{ij} + \frac{2}{\pi}(\hbar c)^3 \sum_{n=1}^{N} W_n k_n^2 V_{in} G_n T_{nj}$$

where

$$G_n \equiv \frac{1}{E - E(k_n) + i\epsilon}$$

Defining

$$M_{ij} \equiv \frac{2}{\pi}(\hbar c)^3 W_j k_j^2 V_{ij} G_j$$

we have

$$T_{ij} = V_{ij} + \sum_{n=1}^{N} M_{in} T_{nj}$$

This equation holds for any k_i, k_j; in particular for the $k_{i=1,N}$, $k_{j=1,N}$ values that occur in the sum. We can thus consider T, V, and M to be $N \times N$ matrices and write the equation in matrix form as

$$\begin{aligned} T &= V + MT \\ (1 - M)T &= V \end{aligned}$$

The condition for a bound state is thus

$$\det(1 - M) = 0 \tag{4.8}$$

where in this case $1 - M$ is a matrix whose elements can be computed for a given E so that equation 4.8 can be solved on a computer. One calculates

the determinant for various values of E until that E is found for which the determinant is 0. The grid points are chosen as those appropriate for Gaussian integration [51] and N is chosen to be large enough so that further increases in its value do not change the resulting bound state energy E.

4.2.2 The Coulomb Bound State Problem

Given the Coulomb potential in coordinate space due to a point charge at the origin

$$V^C(\mathbf{r}', \mathbf{r}) = \frac{Ze^2}{r}\delta(\mathbf{r}' - \mathbf{r})$$

we obtain, by Fourier transformation, the momentum space Coulomb potential

$$V^C(\mathbf{p}', \mathbf{p}) = -\frac{Ze^2}{2\pi^2}\frac{1}{|\mathbf{p}' - \mathbf{p}|^2}$$

The singularity at $\mathbf{p} = \mathbf{p}'$ occurs not because of the pole in the coordinate space potential at the origin but because of the infinite range of the potential. (In fact, if one uses a cutoff Coulomb potential, the momentum space wave function is non-singular. However, numerical problems arise if one chooses a realistic cutoff range, i.e. on the order of atomic distances, and if one cuts off the potential at a short enough range to alleviate these problems, the potential is no longer realistic.) In that we are interested in the potential for a particular l value we make the projection

$$\begin{aligned} V_l^C(p', p) &= -\frac{Ze^2}{2}\int_{-1}^{1}\frac{P_l(x)\,dx}{p^2 + p'^2 - 2pp'x} \\ &= \frac{Ze^2}{2pp'}Q_l(z_{pp'}) \end{aligned}$$

where

$$z_{pp'} = (p^2 + p'^2)/2pp'$$

and Q_l is the Legendre function of the second kind.

Explicit forms of Q_l for the first few l values are

$$\begin{aligned} Q_0 &= \frac{1}{2}\ln\left|\frac{z_{pp'}+1}{z_{pp'}-1}\right| \\ Q_1 &= \frac{z}{2}\ln\left|\frac{z_{pp'}+1}{z_{pp'}-1}\right| - 1 \\ Q_2 &= \frac{1}{4}(3z_{pp'}^2 - 1)\ln\left|\frac{z_{pp'}+1}{z_{pp'}-1}\right| - \frac{3z_{pp'}}{2} \end{aligned}$$

Recognizing that

$$\ln\left|\frac{z_{pp'}+1}{z_{pp'}-1}\right| = 2\ln\left|\frac{p+p'}{p-p'}\right|$$

we realize that the momentum space Coulomb potential for a given l value has a logarithmic singularity at $p = p'$. This singularity makes for a difficulty in the momentum space Coulomb bound state problem which requires special treatment. The method for handling the problem was first published by Kwon and Tabakin [52] where they give Lande credit for the technique which is therefore referred to as the Kwon Tabakin-Lande technique[6]. In the general momentum space method described in section 4.2.1, where the bound state problem is reduced to one of solving $det(1 - VG) = 0$, the difficulty with the Coulomb potential manifests itself as singular diagonal matrix elements in the potential. To remove the singularities, one has to go back to the integral

[6]Kwon and Tabakin formulated the problem in terms of wave functions. They solved the eigenvalue problem $H\Psi = E\Psi$ directly. We have incorporated their method into a reformulation of the problem in terms of the T-matrix.

form of the problem which for the case of the Coulomb interaction takes on the specific form

$$T_l(k', E, k) = V_l^C(k', k) + 4\pi \int dp\, p^2 \frac{V_l^C(k', p)\, T_l(p, E, k)}{E - E(p) + i\epsilon} \tag{4.9}$$

The Kwon Tabakin-Lande technique consists of removing the singularity by adding and subtracting a term involving the integral

$$S_l(k) = \int_0^\infty \frac{V_l^C(k', p)}{P_l(k', p)}\, dp$$

which can be evaluated analytically. The Lippmann-Schwinger equation then appears as

$$\begin{aligned} T_l(k', E, k) = \quad & V_l^C(k', k) \\ + \quad & 4\pi \int dp V_l^C(k', p) \Big[p^2 G_E(p) T_l(p, E, k) \\ & - \frac{k'^2 G_E(k') T_l(k', k)}{P_l(z_{k'p})} \Big] \\ + \quad & 4\pi k'^2 G_E(k') S_l(k') T_l(k', k) \end{aligned}$$

Now when we convert this integral equation to a matrix equation, the V matrix is nonsingular. Considering the l subscripts to be implied we have for a given l:

$$\begin{aligned} T_{ij} = \quad & V_{ij} + 4\pi \sum_{\substack{n=1 \\ n \neq i}}^{N} W_n V_{in}^C k_n^2 G_n T_{nj} \\ - \quad & 4\pi k_i^2 G_i T_{ij} \sum_{\substack{n=1 \\ n \neq i}}^{N} W_n \frac{V_{in}^C}{P_{in}} \\ + \quad & 4\pi k_i^2 G_i S_i T_{ij} \end{aligned} \tag{4.10}$$

The sum in the second term can be evaluated explicitly allowing us to define

$$\begin{aligned} V_{ii} &\equiv S_i - \sum_{\substack{n=1 \\ n\neq i}}^{N} W_n \frac{V_{in}^C}{P_{in}} \\ D_{n\neq i} &\equiv 4\pi W_n k_n^2 G_n \\ D_i &\equiv 4\pi k_i^2 G_i \end{aligned}$$

so that equation 4.10 can be written as

$$T_{ij} = V_{ij} + \sum_{n=1}^{N} D_n V_{in}^C T_{nj}$$

Defining $M_{in} \equiv D_n V_{in}$ we have

$$T_{ij} = V_{ij} + \sum_{n=1}^{N} M_{in} T_{nj}$$

or in matrix form

$$\begin{aligned} T &= V + MT \\ (1-M)T &= V \end{aligned}$$

just as before. Again, the problem reduces to one of solving for the zero of the determinant of a matrix:

$$\det(1-M) = 0 \tag{4.11}$$

Adding in the strong potential in the single channel case is trivial. If, in equation 4.9 we replace $V_l^C(k',p)$ with $V_l^C(k',p) + V_l^N(k',p)$ we find that the only change in the formalism involves redefining

$$V_{in} \equiv V_{in}^C + V_{in}^N$$

The extension to coupled channels for the case where at least one of the channels is open is nontrivial and we devote the next section to a discussion of that extension.

4.2.3 Extension to Coupled Channels

The extension of the Kwon Tabakin-Lande method to coupled channels is due to Landau [48]. If we think for a moment of the single channel problem and attempt simply to evaluate the matrix M in equation 4.11 for a positive value of E we find that $G_E(k')$ is singular for the on shell value of k' (non-relativistically this occurs when $k'^2/2\mu = E$). It is for this reason that the Kwon Tabakin-Lande subtraction technique doesn't work for the scattering problem where we might expect to be able to simply replace equation 4.11 with

$$T = (1 - M)^{-1} V$$

The singularity in $G_E(k')$ at positive energies yields a singularity in M which for the present is considered unremovable. A similar problem occurs in the bound state problem when the system is coupled to an open channel in that for the open channel the problem is actually a scattering problem. One can work around this problem as long as there is **no Coulomb interaction in the open channel**. The method is most easily understood by considering the open channel alone first, adding a closed channel, and then including the Coulomb interaction within the closed channel. Rewriting the Lippmann-Schwinger equation for the scattering amplitude we have

$$T_l(k', E, k) = V_l(k', k) + 4\pi \int dp\, p^2 \frac{V_l(k', p)\, T_l(p, E, k)}{E - E(p) + i\epsilon} \tag{4.12}$$

The integrand is singular at the on shell point $p = k_0$ where $E = E(k_0)$. The singularity can be removed by adding and subtracting an integral which can be evaluated analytically. Recall that the plus $i\epsilon$ in the denominator of the

integrand is put there to build in the proper scattering boundary conditions (outgoing spherical waves) and that the limit as $\epsilon \to 0$ is to be taken after the integration. The integral to be added and subtracted is

$$\lim_{\epsilon \to 0} 4\pi k_0^2 V_l(k', k_0) T_l(k', k_0) \int_0^\infty \frac{1}{\frac{k_0^2}{2\mu} - \frac{p^2}{2\mu} + i\epsilon} = -4i\pi^2 \mu k_\circ V_l(k', k_0) T_l(k_0, k)$$

Equation 4.12 becomes

$$\begin{aligned} T_l(k', E, k) &= V_l(k', k) \\ &+ 4\pi \int dp \left[p^2 \frac{V_l(k', p)\, T_l(p, E, k)}{E - E(p) + i\epsilon} - k_0^2 \frac{V_l(k', k_0)\, T_l(k_0, E, k)}{\frac{k_0^2}{2\mu} - \frac{p^2}{2\mu} + i\epsilon} \right] \\ &- 4i\pi^2 \mu k_0 V_l(k', k_0) T_l(k_0, k) \end{aligned}$$

in which the integrand is nonsingular. We convert this to a matrix equation as follows: (We suppress the subscript l and use the notation T_{ij} for $T(k_i, E, k_j)$ etc.)

$$\begin{aligned} T_{ij} &= V_{ij} + \sum_{n=1}^{N} 4\pi W_n k_n^2 V_{in} G_n T_{ni} + \\ &\left[-4i\pi^2 \mu k_0 - k_0^2 \sum_{n=1}^{N} \frac{1}{\frac{k_0^2}{2\mu} - \frac{k_n^2}{2\mu}} \right] V_{i0} T_{0j} \end{aligned}$$

Define

$$\begin{aligned} D_n &\equiv 4\pi W_n k_n^2 G_n \quad \text{for } n = 1 \to N \\ D_0 &\equiv \left[-4i\pi^2 \mu k_0 - k_0^2 \sum_{n=1}^{N} \frac{1}{\frac{k_0^2}{2\mu} - \frac{k_n^2}{2\mu}} \right] \end{aligned}$$

We can then write

$$T_{ij} = V_{ij} + \sum_{n=0}^{N} D_n V_{in} T_{nj}$$

If we further define

$$M_{in} \equiv D_n V_{in}$$

we obtain

$$T_{ij} = V_{ij} + \sum_{n=0}^{N} M_{in} T_{nj}$$

which in matrix form is simply

$$T = V + MT$$

or

$$(1 - M)T = V$$

If $E < 0$ the singularity never occurs so the subtraction never has to be made. We can still use the same formalism however just by setting $D_0 = 0$.

4.2.4 The Coulomb Plus Nuclear Coupled Channels Problem

For a given l (subscript suppressed in this section) the coupled channels Lippmann-Schwinger equation can be written

$$T_{\alpha\beta}(k', k) = V_{\alpha\beta}(k', k) + 4\pi \sum_{\gamma=1}^{N_{ch}} \int dp\, p^2 \frac{V_{\alpha\gamma}(k', p)\, T_{\gamma\beta}(p, k)}{E - E(p) + i\epsilon}$$

where the subscripts on T and V indicate the channel and N_{ch} is the total number of coupled channels in the problem. We can remove the singularity in the propagator part of the integrand for open channels using the same method as employed in the single channel case. This yields

$$\begin{aligned} T_{\alpha\beta}(k', k) &= V^{NC}_{\alpha\beta}(k', k) + \\ &\quad 4\pi \sum_{\gamma=1}^{N_{ch}} \int dp \left[p^2 \frac{V^{NC}_{\alpha\gamma}(k', p)\, T_{\gamma\beta}(p, k)}{E - E(p) + i\epsilon} - \right. \end{aligned}$$

$$\Theta(E_\gamma)k_0^2\,\frac{V^N_{\alpha\gamma}(k',k_0)\,T(k_0,E,k)}{\frac{k_0^2}{2\mu}-\frac{p^2}{2\mu}}\Bigg] -$$
$$\Theta(E_\gamma)4i\pi^2\mu_\gamma k_0 V^N_{\alpha\gamma}(k',k_0)T_{\alpha\gamma}(k_0,k) \qquad (4.13)$$

where the step function $\Theta(E_\gamma)$ is inserted so that the procedure used to remove the singularity takes effect only in those channels for which there is a singularity, namely, in the open channels. The superscripts N and NC, where they occur on the potential, indicate "Nuclear" and "Nuclear Plus Coulomb". Expressing

$$V^{NC}_{\alpha\beta} = V^N_{\alpha\beta} + V^C_{\alpha\beta}$$

and using the Kwon Tabakin-Lande subtraction technique to remove the Coulomb singularity we have

$$\begin{aligned} T_{\alpha\beta}(k',k) \;=\; & V^N_{\alpha\beta}(k',k) + V^C_{\alpha\beta}(k',k) + \qquad (4.14)\\ & 4\pi\sum_{\gamma=1}^{N_{ch}}\Bigg\{\int dp\,\Bigg[p^2\,\frac{V^N_{\alpha\gamma}(k',p)\,T_{\gamma\beta}(p,k)}{E-E(p)+i\epsilon}+\\ & V^C_{\alpha\gamma}(k',p)\left(p^2\frac{T_{\gamma\beta}(p,k)}{E_\gamma-E_\gamma(p)}-k'^2\frac{T_{\gamma\beta}(k',k)}{E_\gamma-E_\gamma(k')}\frac{1}{P_l(z_{k'p})}\right)-\\ & \Theta(E_\gamma)k_0^2\,\frac{V^N_{\alpha\gamma}(k',k_0)\,T(k_0,E,k)}{\frac{k_0^2}{2\mu}-\frac{p^2}{2\mu}}\Bigg]+\\ & 4\pi S_{\gamma(k')}\frac{T_{\gamma\beta}(k',k)}{E_\gamma-E_\gamma(k')}-\Theta(E_\gamma)4i\pi^2\mu_\gamma k_0 V^N_{\alpha\gamma}(k',k_0)T_{\alpha\gamma}(k_0,k)\Bigg\} \end{aligned}$$

where $V^C_{\alpha\beta}$ and S_γ are both zero for open channels[7]. Now we put the problem on a grid, that is, we approximate the integral with a sum by letting

$$\begin{aligned} \int_0^\infty dp &\rightarrow \sum_{n=1}^{N} W_n \\ k' &\rightarrow k_i \\ k &\rightarrow k_j \\ p &\rightarrow k_n \end{aligned}$$

Equation 4.15 becomes

$$\begin{aligned} T_{\alpha\beta}(k_i,k_j) &= V^{NC}_{\alpha\beta}(k_i,k_j) + \\ &\quad 4\pi \sum_{\gamma=1}^{N_{ch}} \sum_{n=1}^{N_{grid}} W_n k_n^2 \frac{V^N_{\alpha\gamma}(k_i,k_n) T_{\gamma\beta}(k_n,k_j)}{E_\gamma - E_\gamma(p)} + \\ &\quad 4\pi \sum_{\gamma=1}^{N_{ch}} \sum_{\substack{n=1 \\ n\neq i}}^{N_{grid}} W_n k_n^2 \frac{V^C_{\alpha\gamma}(k_i,k_n) T_{\gamma\beta}(k_n,k_j)}{E_\gamma - E_\gamma(p)} + \\ &\quad D^C_\gamma(k_i) V^{C'}_{\alpha\gamma}(k_i,k_i) T_{\alpha\beta}(k_i,k_j) + D^N_\gamma(k_0) V^N_{\alpha\gamma}(k_i,k_0) T_{\alpha\beta}(k_0,k_j) \end{aligned}$$

where we define

$$\begin{aligned} D^N_\gamma(k_0) &\equiv 4\pi\Theta(E_\gamma) \left[-i\pi\mu_\gamma k_0 - \sum_{\gamma=1}^{N_{ch}} \sum_{n=1}^{N_{grid}} \frac{W_n k_0^2}{\frac{k_0^2}{2\mu_\gamma} - \frac{k_n^2}{2\mu_\gamma}} \right] V^N_{\alpha\gamma}(k_i,k_0) T_{\alpha\beta}(k_0,k_j) \\ D^C_\gamma(k_i) &\equiv 4\pi \frac{k_i^2}{E_\gamma - E_\gamma(p)} \end{aligned}$$

[7] $V^C_{\alpha\beta}$ is 0 whenever α or β represent a channel in which the particles are uncharged which according to our restrictions means whenever α or β represent an open channel. If we used Coulomb states $|k_c\rangle$ such that $\langle k'_c| V^N |k_c\rangle = \langle k'| V^{NC} |k\rangle$ then the potential coupling an uncharged channel to a charged channel would appear as $\langle k'_C| V^N |k\rangle = \sum_p \langle k'_C|p\rangle \langle p| V^N |k\rangle$ We approximate $\langle k'_C|p\rangle \approx \delta_{k'p}$. That is we use no Coulomb interaction in the potential coupling an uncharged channel to a charged one.

and

$$V^{C'}_{\alpha\gamma}(k_i,k_i) \equiv S_\gamma(k_i) - 4\pi \sum_{\gamma=1}^{N_{ch}} \sum_{\substack{n=1 \\ n\neq i}}^{N_{grid}} \frac{V^C_{\alpha\gamma}(k_i,k_n)}{P_l(z_{k_i k_n})} \tag{4.15}$$

If we further define

$$D_\gamma(k_n) = \begin{cases} 4\pi \dfrac{W_n k_n^2}{E_\gamma - E_\gamma(k_n)} & n \neq 0, n \neq i \\ D^N_\gamma(k_0) & n = 0 \\ D^C_\gamma(k_i) & n = i \end{cases} \tag{4.16}$$

and

$$V_{\alpha\gamma}(k_i,k_n) = \begin{cases} V^{NC}_{\alpha\gamma}(k_i,k_n) & n \neq 0, n \neq i \\ V^{N}_{\alpha\gamma}(k_i,k_0) & n = 0 \\ V^{NC'}_{\alpha\gamma}(k_i,k_i) & n = i \end{cases}$$

then we can write

$$T_{\alpha\beta}(k_i,k_j) = V_{\alpha\beta}(k_i,k_j) + 4\pi \sum_{\gamma=1}^{N_{ch}} \sum_{n=0}^{N_{grid}} D_\gamma(k_n) V_{\alpha\gamma}(k_i,k_n) T_{\gamma\beta}(k_n,k_j)$$

Now let

$$\begin{aligned} N_{max} &= N_{ch}(N_{grid}+1) \\ u &= iN_{ch} + \alpha \\ v &= jN_{ch} + \beta \\ w &= nN_{ch} + \gamma \end{aligned}$$

For a given w, the values of n and γ are unique and known from

$$n = \text{trunc}(\frac{w-1}{N_{ch}}) \quad \text{and} \quad \gamma = w - nN_{ch}$$

where trunc(x) gives the greatest integer less than or equal to the real number x. Thus we can write

$$T_{uv} = V_{uv} + \sum_{w=0}^{N_{max}} D_w V_{uw} T_{wv}$$

The coupled channels nuclear plus Coulomb problem has thus been reduced to one of finding the solution of the same type of matrix equation as the one that occurs in the single channel problem.

$$\begin{aligned} M_{uw} &\equiv D_w V_{uw} \\ T &= V + MT \\ (1 - M)T &= T \\ \det(1 - M) &= 0 \end{aligned} \tag{4.17}$$

In practice the problem is easier to solve than this discussion of the formalism would suggest. One chooses a set of N_{grid} grid points (60 is a typical value for N_{grid}) and forms an $(N_{grid} + 1) \times (N_{grid} + 1)$ super matrix of $N_{ch} \times N_{ch}$ (3×3 in our case) submatrices. This makes for a square matrix of side $(N_{grid} + 1)N_{ch}$. For each set of momentum values k_i and k_j, where i and j run from 0 to N_{grid} with "0" corresponding to the on shell point, one computes the value of the potential for each channel and assigns that value to the corresponding matrix element. The strong potential is simply evaluated, the Coulomb potential need not be evaluated at any of the on shell points $i = 0$ or $j = 0$ and one uses equation 4.15 for the Coulomb potential along the diagonal. In addition to the potential matrix a vector of "D-Values" (see equation 4.16) is constructed. The potential matrix becomes the matrix $1 - M$ (see equation 4.17) when each element in row i is multiplied by D_i

for all rows i and the value 1 is added to each of the diagonal elements. The determinant of the matrix is then calculated. The entire process is under control of a search routine which varies the energy and repeats the process until the resulting determinant is zero.

4.3 Kaonic Hydrogen Results

In Figure 40 we show the shift and width of the 1s level in kaonic hydrogen as calculated by Landau and Cheng [48] using potentials determined by HAW [23] and Schick and Gibson [53]. The experimental values are also displayed. These are the same as in Figure 39. The solid lines result from using the potential of HAW fit C [23], the dotted from Schick and Gibson's fit to the K-matrix analysis of Kim and the dashed from Schick and Gibsons fit to the K-matrix analysis of Berley. We note that in all cases the calculated shift is toward the less bound while the experimental shift is toward the more bound. In Figures 41 and 42 we give similar diagrams with the results of our work. The shifts and widths depicted in 41 are determined from the nonrelativistic fits nr1, nr2 and nr3. The shifts and widths depicted in 42 are determined from the relativistic fits r1 and r2.

Here we see that only fit r2 yields a shift of the Coulomb bound state which is in agreement with experiment. It appears that the puzzle has been solved. By including relativistic kinematics in the coupled channels formalism we can reconcile the results of the kaonic hydrogen experiment with the predictions based on low energy scattering.

To further test the consistency of the "new relativistic" fit r2 scattering

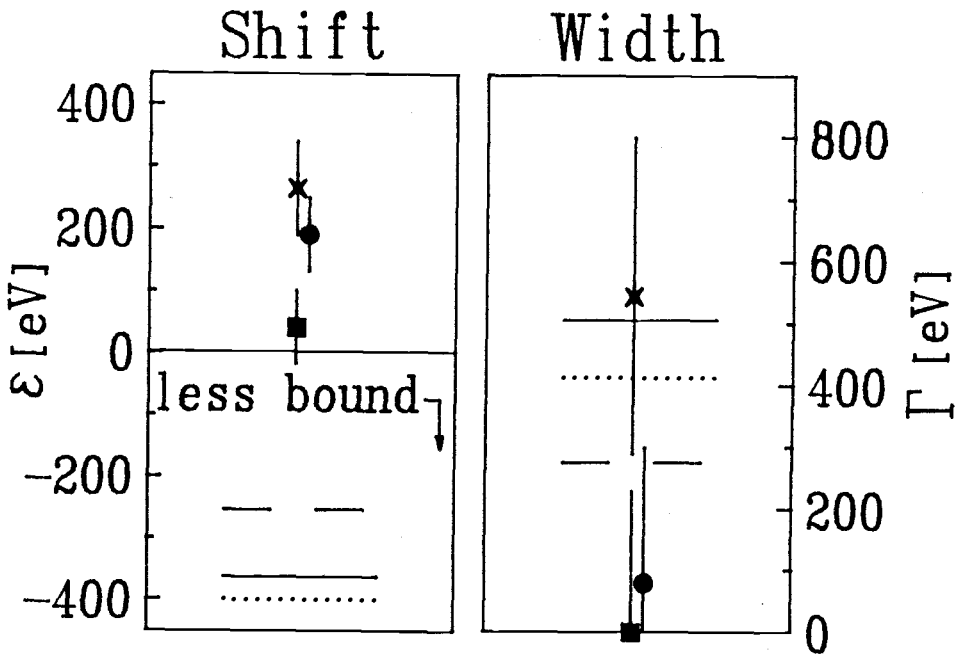

Figure 40. The shifts and widths of the 1S level in kaonic hydrogen as calculated by Landau and Cheng [48] using potentials determined by HAW [23] in their fit C (solid line), Schick and Gibson [53] in their fit to the K-matrix analysis of Kim [35] (dotted line), and in their fit to the K-matrix analysis of Berley [54] (dashed line). The data are the same as in figure 39.

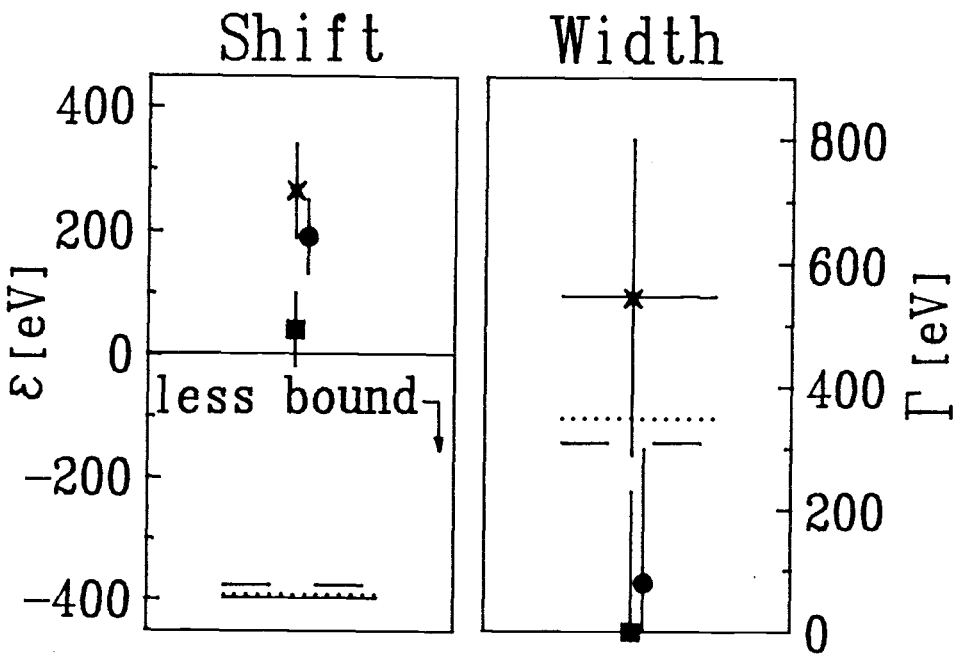

Figure 41. The shifts and widths of the 1S level in kaonic hydrogen based on potential parameters determined from fits nr1 (solid line), nr2 (dashed line), and nr3 (dotted line) to low energy scattering cross sections and the $\pi\Sigma$ mass spectrum. The data are the same as in figure 39.

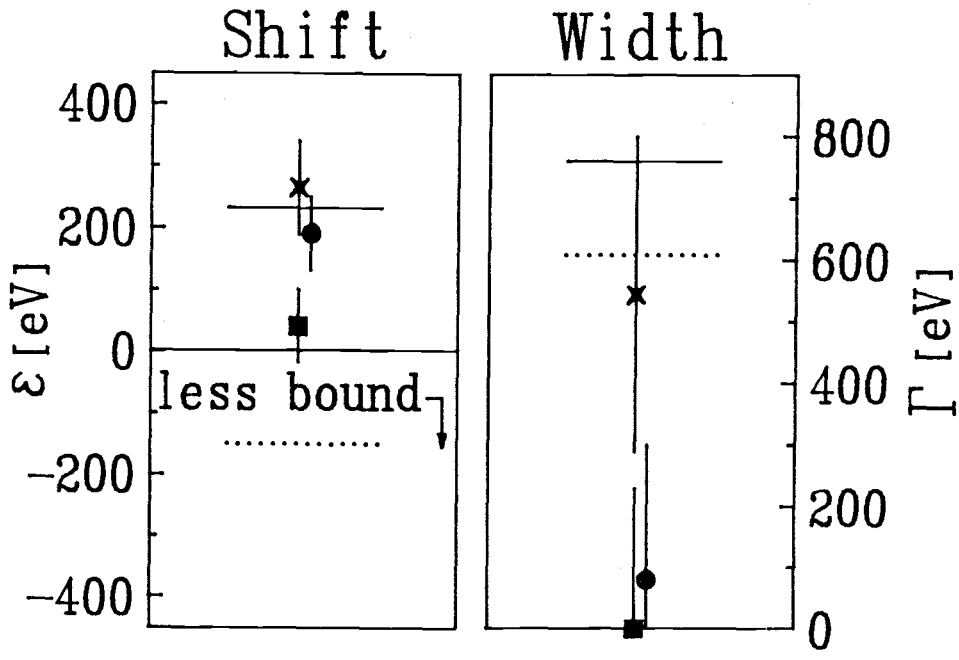

Figure 42. The shifts and widths of the 1S level in kaonic hydrogen based on potential parameters determined from fits r1 (dotted line) and r2 (solid line) to low energy scattering cross sections and the $\pi\Sigma$ mass spectrum. The data are the same as in Figure 39.

amplitude with nature we use this scattering amplitude in the construction of an optical potential to compute the shift and width in the Coulomb levels of heavier kaonic atoms.

Chapter 5

Antikaon-Nucleus Bound States

5.1 Kaonic Atom Experiment

Negatively charged antikaons form a Coulomb bound state with nuclei as well as with protons. In a manner similar to that of the kaonic hydrogen experiment the energy of photons given off when an antikaon makes a transition from a Coulomb level of principal quantum number n to one of principal quantum number $n-1$ can be measured directly. The identification of the levels in the resulting spectrum for nuclei heavier than helium is much easier than for the case of kaonic hydrogen. The 2p helium level is difficult to identify but the results are considered to be more reliable than those of kaonic hydrogen. We investigate the 2p level in kaonic helium-4 and the 2p level in kaonic carbon-12. The relative sizes of the Bohr orbits for the kaonic atoms under investigation, including the hydrogen 1s orbit, are given in Figure 43. The Bohr radius R_B is determined as a function of the number of nucleons in the nucleus Z, the antikaon-nucleus reduced mass μ, and the principal

Level	Atom	Shift[eV]	Width[eV]	Ref.
2p	^4He	-50 ± 12	+100 ± 40	[56]
2p	^4He	-35 ± 12	+30 ± 30	[57]
2p	^4He	-41 ± 33	———	[58]
2p	^{12}C	-590 ± 80	1730 ± 150	[21]

Table 8. Experimental kaonic atom shifts and widths.

quantum number n from

$$R_B = \frac{\hbar c}{Z\alpha\mu c^2} n^2$$

where α is the electromagnetic coupling constant. The shifts and widths for all the transitions measured in kaonic atom x-ray experiments up to the year 1980 are given in a review article by Batty [55]. Those for which we have carried out the calculation are given in Table 8. These include the recent results on kaonic helium by Baird et al. [56].

5.2 Kaonic Atom Theory

In calculating the bound state energy levels for kaonic atoms we use the method described in section 4.2 for the single channel Coulomb plus nuclear bound state problem. The coupling to hypernucleus channels is not treated in the direct manner of the coupled channels calculation but is (partly) accounted for by using a potential derived from the elementary K^-p scattering amplitude which has been determined via a coupled channels calculation. The potential thus has an imaginary part which provides the absorption

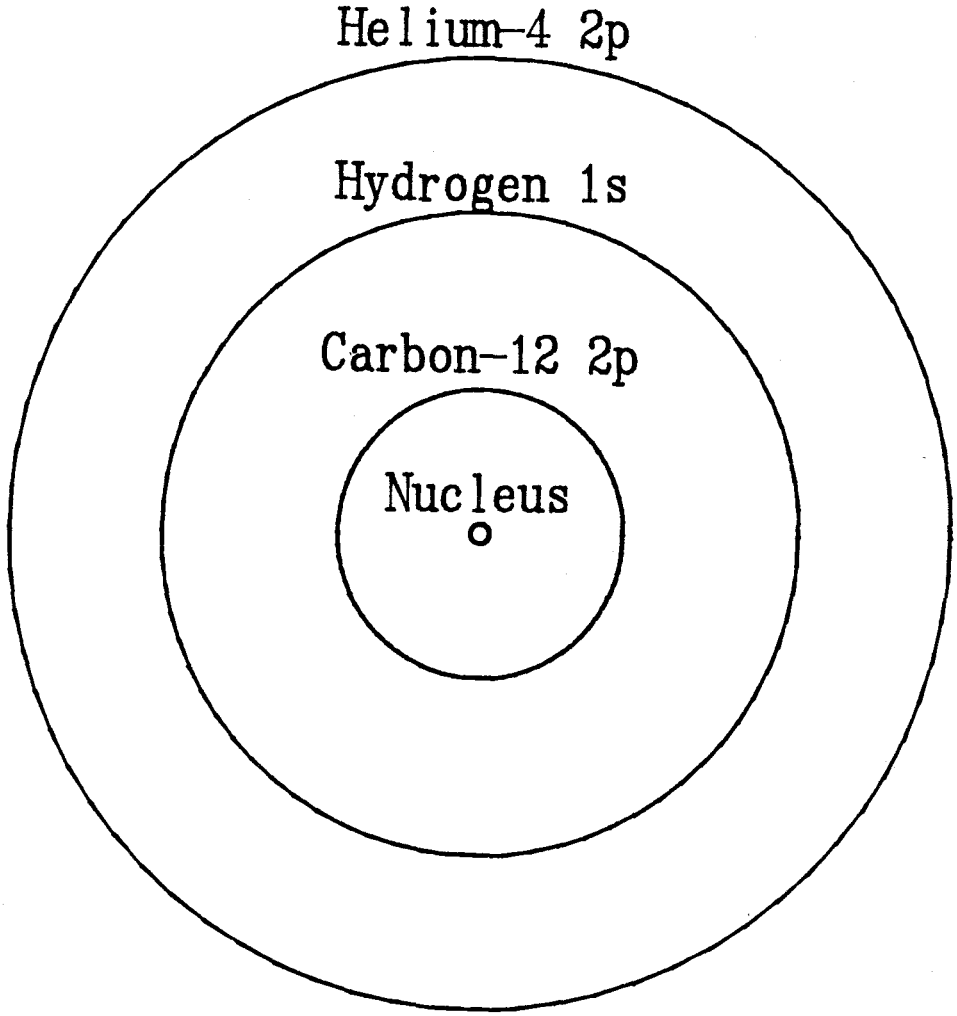

Figure 43. Relative sizes of the Bohr orbits as compared to a representative nuclear radius of 2.5 fm. The actual Bohr radii are; 38 fm for carbon-12 2p, 84 fm for hydrogen 1s, and 124 fm for helium-4 2p.

corresponding to the coupling to hypernucleus channels[8]. The problem of extending the K^-p bound state theory to handle K^-A bound states (" A " designates "nucleus") consists almost entirely of determining the strong potential for the antikaon-nucleus interaction given the antikaon-nucleon scattering amplitude.

5.2.1 The Optical Potential

In developing the optical potential methodology it is convenient to think in terms of the scattering problem. The operator form of the Lippmann-Schwinger equation for the T-matrix is

$$\begin{aligned} T &= V + VGT \\ (1 - VG)T &= V \\ T &= (1 - VG)^{-1}V \end{aligned} \tag{5.18}$$

In this framework the condition for a bound state is that the T-matrix is singular (while the potential is not) or

$$det(1 - VG) = 0 \tag{5.19}$$

The problem is identical up to the point where one must decide whether to solve equation 5.18 or 5.19. Thus it is reasonable to determine V with the scattering problem in mind and then use it in equation 5.19 to solve for the

[8]In general the imaginary part can come from nucleon knockout and coupling to the $\overline{K}^0 n$ channel (charge exchange) as well. We will be evaluating the potentials at energies below the K^-A threshold (bound state energies) where these processes cannot occur.

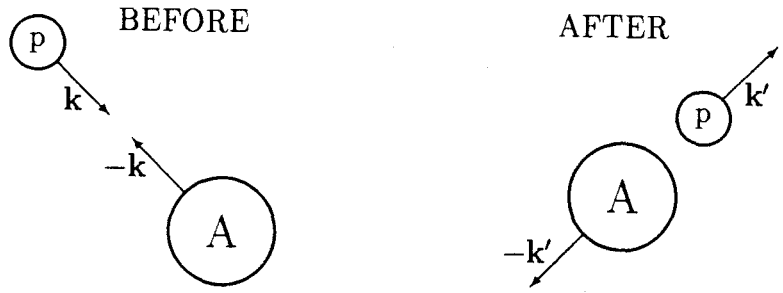

Figure 44. The projectile-nucleus scattering problem.

bound state energy. Indeed the physical situation of a particle bound to a nucleus can be viewed as one in which the particle is continuously scattering from the nucleus.

The scattering problem to be discussed is depicted in Figure 44. A target nucleus consisting of A nucleons is struck by a projectile p. In the overall center of mass frame the projectile has an initial momentum $\mathbf{k}$ and the target nucleus momentum $-\mathbf{k}$. After the interaction the projectile has momentum $\mathbf{k}'$ and the target momentum $-\mathbf{k}'$.

We consider elastic scattering so that $|\mathbf{k}| = |\mathbf{k}'|$ and the target nucleus is in its ground state before, after, and during the collision. The latter condition implies that we are developing a first order optical potential. We assume that the projectile interacts with the individual nucleons. The nuclear medium effects (of the interaction of the nucleon and the projectile with the nuclear core) on the projectile-nucleon interaction are taken into account approximately. In general we make use of the factored approximation (to be described) but some of the calculations have been carried out without it.

The operator form of the Lippmann-Schwinger equation is again

$$T = V + VGT$$

where

$$G = \frac{1}{E - K_A - K_p} \tag{5.20}$$

with K_A the kinetic energy operator for the target nucleus and K_p the kinetic energy operator for the projectile. Considering the overall interaction to be the sum of the interactions of the projectile with the individual nucleons we have

$$T = \sum_{i=1}^{A} v_i + \sum_{i=1}^{A} v_i G T \tag{5.21}$$

This can be expanded in a Born series as

$$T = \sum_{i=1}^{A} v_i + \sum_{i=1}^{A} v_i G \sum_{j=1}^{A} v_j + \sum_{i=1}^{A} v_i G \sum_{j=1}^{A} v_j G \sum_{k=1}^{A} v_k + \cdots \tag{5.22}$$

We would like to express the T-matrix for the projectile-target interaction in terms of the projectile-nucleon t-matrix. To this end we write the Lippmann-Schwinger equation for the projectile interacting with a nucleon which is bound to the nucleus as

$$\tau_i = v_i + v_i G \tau_i \tag{5.23}$$

This too can be expanded in a Born series as

$$\tau_i = v_i + v_i G v_i + v_i G v_i G v_i + \cdots \tag{5.24}$$

The propagator G can also be written as (compare equation 5.20)

$$G = \frac{1}{\omega - K_{pN}^{\text{relative}}}$$

where K_{pN}^{relative} is the kinetic energy operator for the relative motion of the projectile p and the nucleon N. ω is the energy of the projectile and nucleon in the 2-body center of mass frame that obtains when E is the energy in the projectile-nucleus center of mass frame. When evaluated between states, ω is a very complicated function (even in the projectile-nucleus center of mass frame) involving the nucleon-core and projectile-core potentials. The methods used in approximating ω, in particular the inclusion of binding energy corrections requires some discussion. This is carried out in section 5.2.1. If we substitute the Born series for τ (equation 5.24) into the expression

$$T = \sum_{i=1}^{A} \tau_i + \sum_{i=1}^{A} \tau_i G \sum_{\substack{j=1 \\ j\neq i}}^{A} \tau_j + \sum_{i=1}^{A} \tau_i G \sum_{\substack{j=1 \\ j\neq i}}^{A} \tau_j G \sum_{\substack{k=1 \\ k\neq j}}^{A} \tau_k + \cdots \tag{5.25}$$

we retrieve equation 5.22. Thus, by writing equation 5.25 we have succeeded in expressing T in terms of the elementary t-matrix τ_i. Now we have to get this into the form $T = V + VGT$ where the potential V is made up of elementary t-matrices. There are two methods of carrying this out. The first method consists of ignoring the restrictions on the summations and defining the first order optical potential by

$$U = A\tau \tag{5.26}$$

so that

$$T \approx U + UGT$$

The T-matrix calculated by this method corresponds to a direct solution of the Schrödinger equation and thus has the advantage of being unitary. The method is due to Watson [59]. The second method is due to Kerman, McManus, and Thaler [60] and is described as follows: In that the overall wave

function for the nucleus has to be symmetric with respect to the interchange of two nucleons and since the operators in equation 5.25 are to be evaluated between nuclear states we can replace $\sum_{i=1}^{A} \tau_i$ with $A\tau$. If we define the first order optical potential U as

$$U = (A-1)\tau \tag{5.27}$$

we can write

$$T' = U + UGT'$$

where the factor $(A-1)$ in equation 5.27 has made it so that the conditions $j \neq i$, $k \neq j$, etc. on the summations, are met. It has also introduced an overall factor of $(A-1)/A$ so that we obtain the final T-matrix by solving

$$\begin{aligned} T &= \frac{A}{A-1}T' \\ &= A\tau + A(A-1)\tau G\tau + A(A-1)^2\tau G\tau G\tau + \cdots \end{aligned}$$

Since we do not calculate the T-matrix itself in the bound state problem, we use the first method in most of our calculations and check our results for some cases against the results obtained using the KMT approach. In practice we allow for different K^-p versus K^-n interactions by replacing equation 5.26 with

$$U = Z\tau_{K^-p} + N\tau_{K^-n}$$

where Z is the number of protons in the nucleus and N the number of neutrons.

The discussion up to this point has been carried out in terms of the operators. We must now face the task of evaluating these operators between the initial and final projectile-target states.

We evaluate the optical potential operator between initial and final states $|\mathbf{k}, \Psi_0(\mathbf{P})\rangle$ and $\langle\Psi_0(\mathbf{P}'), \mathbf{k}'|$ where $\mathbf{k}$ represents the momentum of the projectile and $\mathbf{P}$ that of the target. We mix the notation in writing $\Psi_0(\mathbf{P})$ within the ket to emphasize that the nucleus is in the ground state. The states are product states which can be written $|\mathbf{k}\rangle\,|\Psi_0(\mathbf{P})\rangle$ where the target state is the product of individual nucleon states

$$\begin{aligned} |\Psi_0(\mathbf{P})\rangle &= |\mathbf{p_1}\rangle\,|\mathbf{p_2}\rangle\cdots|\mathbf{p_A}\rangle \\ &= |\mathbf{p_1}, \mathbf{p_2}, \ldots, \mathbf{p_A}\rangle \end{aligned}$$

We describe the evaluation of the optical potential between initial and final states in the Watson formalism. The optical potential can be written as

$$\langle\Psi_0(\mathbf{P}')\mathbf{k}'|\,U\,|\mathbf{k}\Psi_0(\mathbf{P})\rangle = A\,\langle\Psi_0(-\mathbf{k}')\mathbf{k}'|\,\tau^{pN}\,|\mathbf{k}\Psi_0(-\mathbf{k})\rangle$$

where we have substituted the momenta of the nucleus, $\mathbf{P} = \mathbf{k}$ and $\mathbf{P}' = \mathbf{k}'$, with the understanding that all the momenta are given in the projectile-nucleus center of mass frame. The superscripts on τ are there to emphasize that τ is the projectile-nucleon t-matrix. We evaluate this by using the completeness relation

$$1 \equiv \int d^3p_1 d^3p_2 \cdots d^3p_A\,|\mathbf{p_1}, \mathbf{p_2}, \ldots, \mathbf{p_A}\rangle\,\langle\mathbf{p_1}, \mathbf{p_2}, \ldots, \mathbf{p_A}|$$

on either side of τ^{pN} to obtain

$$\begin{aligned} U/A &= \int\int d^{3A}p\, d^{3A}p'_1\,\langle\Psi_0(-\mathbf{k}')|\mathbf{p}'_1, \mathbf{p}'_2, \ldots, \mathbf{p}'_A\rangle \times \\ &\quad \langle\mathbf{p}'_1, \mathbf{p}'_2, \ldots, \mathbf{p}'_A, \mathbf{k}'|\,\tau^{pN}\,|\mathbf{k}\mathbf{p}_1, \mathbf{p}_2, \ldots, \mathbf{p}_A\rangle \times \\ &\quad \langle\mathbf{p}_1, \mathbf{p}_2, \ldots, \mathbf{p}_A|\Psi_0(-\mathbf{k})\rangle \end{aligned} \tag{5.28}$$

In that the matrix element $\langle \mathbf{p'}_i \mathbf{k'} | \tau^{pN} | \mathbf{k} \mathbf{p}_i \rangle$ is independent of i for a totally antisymmetric nuclear wave function we can choose to allow τ^{pN} to act on $|\mathbf{p}_1\rangle$ so that

$$\langle \mathbf{k'}, \mathbf{p'}_1, \mathbf{p'}_2, \ldots, \mathbf{p'}_A | \tau^{pN} | \mathbf{p}_1, \mathbf{p}_2, \ldots, \mathbf{p}_A, \mathbf{k} \rangle = \prod_{i=2}^{A} \delta(\mathbf{p'}_i - \mathbf{p}_i) \langle \mathbf{p'}_1 \mathbf{k'} | \tau^{pN} | \mathbf{p}_1 \mathbf{k} \rangle$$

With this substitution equation 5.28 becomes

$$\begin{aligned} U/A &= \int\int d^{3A}p d^3p' \langle \Psi_0(-\mathbf{k'}) | \mathbf{p'}_1, \mathbf{p}_2, \mathbf{p}_3, \ldots, \mathbf{p}_A \rangle \times \\ &\quad \langle \mathbf{p'}_1 \mathbf{k'} | \tau^{pN} | \mathbf{k} \mathbf{p}_1 \rangle \langle \mathbf{p}_1, \mathbf{p}_2, \ldots, \mathbf{p}_A | \Psi_0(-\mathbf{k}) \rangle \end{aligned} \tag{5.29}$$

Now we introduce the momentum transfer $\mathbf{q} = \mathbf{k'} - \mathbf{k}$ which occurs in the elementary interaction such that the effect of t_{pN} on $|\mathbf{p}_1 \mathbf{k}\rangle$ is to produce a state $|\mathbf{p}_1 - \mathbf{q}, \mathbf{k} + \mathbf{q}\rangle$ times a transition amplitude $\tau^{pN}(\mathbf{p}_1 - \mathbf{q}, \mathbf{k} + \mathbf{q}; \mathbf{p}_1, \mathbf{k})$ so that

$$\langle \mathbf{p'}_1 \mathbf{k'} | \tau^{pN} | \mathbf{k} \mathbf{p}_1 \rangle = \tau^{pN}(\mathbf{p}_1 - \mathbf{q}, \mathbf{k} + \mathbf{q}; \mathbf{p}_1, \mathbf{k}) \delta[\mathbf{p'}_1 - (\mathbf{p}_1 - \mathbf{q})]$$

Then equation 5.29 becomes

$$\begin{aligned} U/A &= \int d^{3A}p \langle \Psi_0 | \mathbf{p}_1 - \mathbf{q}, \mathbf{p}_2, \mathbf{p}_3, \ldots, \mathbf{p}_A \rangle \times \\ &\quad \langle \mathbf{p}_1, \mathbf{p}_2, \ldots, \mathbf{p}_A | \Psi_0 \rangle \tau^{pN}(\mathbf{p}_1 - \mathbf{q}, \mathbf{k} + \mathbf{q}; \mathbf{p}_1, \mathbf{k}) \end{aligned}$$

By the closure relation on the nucleon state vectors $|\mathbf{p}\rangle$ we have[9]

$$\int \Psi_0^*(\mathbf{p}_i)\Psi_0(\mathbf{p}_i)d^3p_i = 1 \tag{5.30}$$

so that

$$U/A = \int d^3p\, \Psi_0^*(\mathbf{p}-\mathbf{q})\, \Psi_0(\mathbf{p})\, \tau^{pN}(\mathbf{p}-\mathbf{q}, \mathbf{k}+\mathbf{q}; \mathbf{p}, \mathbf{k}) \tag{5.31}$$

where we have dropped the subscript "1" on $\mathbf{p}_1$ since the expression is independent of which nucleon we choose.

The Factored Approximation

The product of nucleon wave functions

$$\Psi_0^*(\mathbf{p}-\mathbf{q})\Psi_0(\mathbf{p})$$

represents the probability amplitude for finding a nucleon in the nucleus with momentum $\mathbf{p}$ and replacing it with a nucleon with momentum $\mathbf{p}-\mathbf{q}$. In many cases this product peaks at a particular value of the momentum $\mathbf{p} = \mathbf{p}_0$. For Gaussian wave functions

$$\Psi_0(\mathbf{p}) \propto e^{-\alpha|\mathbf{p}|^2}$$

[9]We have implicitly assumed that the wave functions for the nucleons within the nucleus are functions of a momentum measured with respect to the nuclear center of mass. Since we are discussing the projectile-nucleus scattering problem in the projectile-nucleus overall center of mass and the nucleus recoils, there are actually two nuclear center of mass frames in the problem and equation 5.30 can only be considered an approximation which becomes exact in the limit of an infinitly heavy nucleus. We ignore recoil corrections here but consider them for the active nucleon. The choice of $\mathbf{p_0}$ in equation 5.32 includes recoil effects.

this occurs at [61]

$$\mathbf{p}_0 = -\frac{\mathbf{k}}{\mathbf{A}} + \frac{A-1}{2A}\mathbf{q} \tag{5.32}$$

Most of the contribution to the integral occurs at this value of $\mathbf{p}_0$ so that if the elementary t-matrix $\tau^{pN}(\mathbf{p}-\mathbf{q},\mathbf{k}+\mathbf{q};\mathbf{p},\mathbf{k})$ does not vary too rapidly in the neighborhood of $\mathbf{p}=\mathbf{p}_0$ it is a good approximation to pull the t-matrix outside the integral and evaluate it at $\mathbf{p}=\mathbf{p}_0$. Equation 5.31 thus becomes

$$U/A \approx \tau^{pN}(\mathbf{p}_0-\mathbf{q},\mathbf{k}+\mathbf{q};\mathbf{p}_0,\mathbf{k}) \int d^3p \Psi_0^*(\mathbf{p}-\mathbf{q})\Psi_0(\mathbf{p})$$

This approximation is referred to as the factored approximation. The resulting integral is called the form factor $F(\mathbf{q})$

$$F(\mathbf{q}) = \int d^3p \Psi_0^*(\mathbf{p}-\mathbf{q})\Psi_0(\mathbf{p}) \tag{5.33}$$

The form factor is the Fourier transform of the density distribution of nucleons in the nucleus. It is a measured quantity. The data is typically fit to a function which is the product of a polynomial and a Gaussian. This form results from the use of harmonic oscillator wave functions in equation 5.33. If one chooses not to make the factored approximation then the wave function must be known. In these cases we use the harmonic oscillator wave functions themselves in equation 5.31.

In evaluating

$$\tau^{pN}(\mathbf{p}_0-\mathbf{q},\mathbf{k}+\mathbf{q};\mathbf{p}_0,\mathbf{k})$$

which we write as

$$\tau^{pN}(\mathbf{p'}_0,\mathbf{k'}|\omega|\mathbf{p}_0,\mathbf{k})$$

to show the dependence on the two-body energy ω, we first need to determine the two-body center of mass momenta κ' and κ at which to evaluate the

known 2-body t-matrix and what the relationship is between the known 2-body t-matrix

$$t^{pN}(\kappa'|\tilde{\omega}|\kappa)$$

and the desired one

$$\tau^{pN}(\mathbf{p'}_0, \mathbf{k'}|\omega|\mathbf{p}_0, \mathbf{k})$$

We shall now use a Lorentz invariance argument to show that

$$\tau^{pN}(\mathbf{p'}_0, \mathbf{k'}|\omega|\mathbf{p}_0, \mathbf{k}) = \gamma\tau^{pN}(\kappa'|\tilde{\omega}|\kappa) \tag{5.34}$$

and to determine γ. We consider the situation in which a system makes a transition from an initial state "i" to a final state "f". We can write the transition probability $P(f \leftarrow i)$ for a system of N particles in a frame independent form in terms of the S-matrix as

$$P(f \leftarrow i) = \int \frac{d^3k_1}{E_1}\frac{d^3k_2}{E_2}\cdots\frac{d^3k_N}{E_N}(E_1^f E_2^f \cdots E_N^f)(E_1^i E_2^i \cdots E_N^i)|S_{fi}|^2$$

where

$$(E_1^f E_2^f \cdots E_N^f)(E_1^i E_2^i \cdots E_N^i)|S_{fi}|^2$$

is invariant. The S-matrix can be written in terms of the T-matrix as

$$S_{fi} = \delta_{fi} - 2\pi i\delta^4(p_f - p_i)\,\langle T_{fi}\rangle$$

In that the two delta functions in this expression are invariant with respect to Lorentz transformations the expression

$$[(E_1^f E_2^f \cdots E_N^f)(E_1^i E_2^i \cdots E_N^i)]^{\frac{1}{2}}T_{fi}$$

is also invariant. In the projectile-nucleon case that we have been discussing this means that

$$\sqrt{E_p(\kappa')E_N(\kappa')E_p(\kappa)E_N(\kappa)}\,\langle\kappa'|\,t(\tilde{\omega})\,|\kappa\rangle = \sqrt{E_p(k')E_N(p')E_p(k)E_N(p)}\,\langle\mathbf{k'p'}|\,t(\omega)\,|\mathbf{kp}\rangle$$

This can be written as equation 5.34 with

$$\gamma = \sqrt{\frac{E_p(\kappa')E_N(\kappa')E_p(\kappa)E_N(\kappa)}{E_p(k')E_N(p')E_p(k)E_N(p)}}$$

In order to determine the values of the two-body center of mass momenta κ' and κ at which to evaluate $\langle\kappa'|\,t(\tilde{\omega})\,|\kappa\rangle$ we carry out a Lorentz transformation for the on shell case and generalize the result to apply to the off shell case. In the special situation under study in this paper the two-body interaction is considered to be pure S-wave so that we only need to determine the magnitudes of the vectors κ' and κ. This simplifies the discussion considerably and we will confine our attention to this special case.

In carrying out the arguments we use four-vector notation and the Mandelstam invariant s. The invariant s is given in terms of the projectile p and target nucleon N four momenta p_p^μ and p_N^μ by the function

$$\begin{aligned} s(\mathbf{p}_p,\mathbf{p}_N) &= (p_p^\mu + p_N^\mu)^2 \\ &= (E_p + E_N)^2 - (\mathbf{p}_p - \mathbf{p}_N)^2 \end{aligned}$$

Since s is invariant we can determine κ from

$$s \equiv s(\mathbf{k},\mathbf{p}) = s(\kappa,-\kappa)$$

and κ' from

$$s' \equiv s(\mathbf{k}', \mathbf{p}') = s(\kappa', -\kappa')$$

yielding

$$\kappa = \left\{ \frac{[s - (m_p + m_N)^2][s - (m_p - m_N)^2]}{4s} \right\}^{\frac{1}{2}}$$

and

$$\kappa' = \left\{ \frac{[s' - (m_p + m_N)^2][s' - (m_p - m_N)^2]}{4s'} \right\}^{\frac{1}{2}}$$

The Two-Body Energy ω

The determination of ω is carried out in two different approximations yielding two different expressions for ω. We will present results based on the use of each method. Here we describe the two methods. In the first method we use the on shell expression

$$\omega^2 = s(\mathbf{k}_0, \mathbf{p}) = [E_p(\mathbf{k}_0) + E_N(\mathbf{p})]^2 - (\mathbf{k}_0 + \mathbf{p})^2$$

where $\mathbf{p}$ is the nucleon momentum in the projectile-nucleus center of mass and $\mathbf{k}_0$ is the on shell momentum of the projectile satisfying

$$E = \sqrt{m_p^2 + k_0^2} + \sqrt{m_N^2 + k_0^2}$$

(where E is the energy parameter appearing in the Lippmann-Schwinger equation propagator). In the factored approximation we use the optimal momentum

$$\mathbf{p} = \mathbf{p}_0 = -\frac{\mathbf{k}}{\mathbf{A}} + \frac{A-1}{2A}\mathbf{q}$$

Otherwise the three components of $\mathbf{p}$ are variables of integration. In order to take into account the fact that the interaction between the projectile and

the nucleon takes place while both particles are under the influence of the nuclear core we subtract a binding energy E_B from the resulting ω. In our model E_B is a free parameter. We expect it to be on the order of the single nucleon separation energy and thus in the range 0–50 MeV. Aside from these questions of nuclear medium effects this choice of ω is clearly correct on shell where $\mathbf{k}' = \mathbf{k} = \mathbf{k}_0$ and its use off shell is a straight forward generalization. However, experience with the three-body problem tends to indicate that it is not the best generalization. The second method of determining ω involves treating the projectile-nucleus problem as a three body problem consisting of the projectile, an active nucleon, and a nuclear core made up of all the other nucleons. Equation 5.20 gives the propagator G for the case of a projectile p interacting with a nucleus A. This is the same propagator which appears in equation 5.23. This Lippmann-Schwinger equation is for the case of a projectile interacting with a single nucleon in the nucleus. In order to use the propagator in this equation, we need it in a form which involves the kinetic energy operator for the relative motion of the projectile and the nucleon. The Schrödinger equation for a projectile interacting with a single nucleon in a nucleus can be written in terms of operators as

$$(K_p + H_A + V_{pN}) |\Psi\rangle = E_{\text{tot}} |\Psi\rangle \tag{5.35}$$

where K_p is the kinetic operation for the projectile, H_A the Hamiltonian operator for the nucleus, V_{pN} the potential operator for the projectile-nucleon interaction, E_{tot} the eigenenergy of the problem and $|\Psi\rangle$ the wave function for the complete system. If we consider the three body problem of a system consisting of a projectile interacting with a single nucleon which is bound to

a nuclear core of $A-1$ nucleons we can write the Hamiltonian H_A as

$$H_A = H_C + K_C + K_N + V_{NC}$$

where H_C is the Hamiltonian for the interactions of the nucleons making up the core with each other, K_C is the kinetic energy operator for the motion of the core center of mass, K_N is the nucleon kinetic energy operator, and V_{NC} is the potential operator for the interaction between the nucleon and the core. Equation 5.35 becomes

$$(K_p + H_C + K_C + K_N + V_{NC} + V_{pN})\,|\Psi\rangle = E_{\text{tot}}\,|\Psi\rangle$$

We consider this equation in the overall center of mass frame i.e. the frame in which the center of mass of the projectile-nucleus system is at rest. If we rewrite the kinetic energy operators of the core and the nucleon in terms of kinetic energy operators for their relative and center of mass motion, K_{NC}^{rel} and K_{NC}^{COM}, we have

$$[(K_p + K_{NC}^{\text{COM}} + V_{pN}) + (K_{NC}^{\text{rel}} + V_{NC})]\,|\Psi\rangle = (E_{\text{tot}} - H_C)\,|\Psi\rangle \qquad (5.36)$$

The operators on the left obey the Schrödinger equations

$$(K_p + K_{NC}^{\text{COM}} + V_{pN})\,|\Psi\rangle = E\,|\Psi\rangle \qquad (5.37)$$

$$(K_{NC}^{\text{rel}} + V_{NC})\,|\Psi\rangle = -|E_B|\,|\Psi\rangle \qquad (5.38)$$

where E is the same energy that appears in equation 5.20 and $|E_B|$ is the nucleon core binding energy which we write with the absolute values symbol to indicate that it is a positive energy. Equation 5.36 can thus be written

$$[(K_p + K_{NC}^{\text{COM}} + V_{pN}) + (K_{NC}^{\text{rel}} + V_{NC})]\,|\Psi\rangle = (E - |E_B|)\,|\Psi\rangle$$

Having established this, we go back to the individual particle kinetic energy operators for the nucleon and core so that

$$(K_p + K_N + V_{NC} + K_C + V_{pN})\,|\Psi\rangle = (E - |E_B|)\,|\Psi\rangle$$

Now we write the kinetic energy operators of the projectile and the nucleon in terms of their relative and center of mass kinetic energy operators $K_{pN}^{\rm rel}$ and $K_{pN}^{\rm COM}$ and rearrange the terms obtaining

$$[(E - |E_B| - V_{NC} - K_C + K_{pN}^{\rm COM}) - K_{pN}^{\rm rel}]\,|\Psi\rangle = V_{pN}\,|\Psi\rangle \qquad (5.39)$$

For the asymptotic states between which the propagator is to be evaluated this becomes

$$[(E - |E_B| - K_C - K_{pN}^{\rm COM}) - K_{pN}^{\rm rel}]\,|\mathbf{k}\Psi_0(\mathbf{p})\rangle = V_{pN}\,|\mathbf{k}\Psi_0(\mathbf{p})\rangle \qquad (5.40)$$

and we can identify the propagator G as

$$G = \frac{1}{\omega - K_{pN}^{\rm rel}}$$

with

$$\omega = E - |E_B| - K_C - K_{pN}^{\rm COM} \qquad (5.41)$$

defining the two body energy at which the Lippmann-Schwinger equation for the projectile-nucleon interaction needs to be solved.

We have ignored the interaction of the projectile with the core (passive core model). It can be taken into account approximately by considering the binding energy to be a free parameter. The eigenvalues of the kinetic energy operators on the right hand side of equation 5.41 can be evaluated

in a straight forward manner in the projectile-nucleus center of mass for a given projectile momentum $\mathbf{k}$ and nucleon momentum p_N. Here we use the same symbols for the kinetic energy eigenvalues as we did for the operators. The mass of the core is

$$m_C = m_A - m_N + |E_B|$$

The core momentum is

$$\mathbf{p}_C = -\mathbf{k} - \mathbf{p}_N$$

since the momentum of the nucleus is $-\mathbf{k}$. Thus, the total energy of the core is

$$E_C = \sqrt{m_C^2 + p_C^2}$$

and

$$K_C = E_C - m_C$$

The nucleon energy is

$$E_N = \sqrt{m_N^2 + p_N^2}$$

K_{NC}^{rel} is determined from the invariant mass

$$\begin{aligned} s_{NC} &= (E_N + E_C)^2 - (\mathbf{p}_N + \mathbf{p}_C)^2 \\ &= (E_N + E_C)^2 - k^2 \end{aligned}$$

as

$$K_{NC}^{\text{rel}} = \sqrt{s_{NC}} - m_N - m_C$$

The projectile energy is

$$E_p = \sqrt{m_p^2 + k^2}$$

and we can write the kinetic energy operator for the motion of the projectile-nucleon center of mass in terms of the invariant mass

$$s_{pN} = (E_p + E_N)^2 - (\mathbf{p}_N + \mathbf{k})^2$$

as

$$K_{pN}^{\mathrm{COM}} = E_p + E_N - \sqrt{s_{pN}}$$

Pauli Effects

We include Pauli Effects in computing the kaon-nucleon t-matrix by including the Brueckner Q operator in the two-body propagator

$$G = \frac{1}{\omega - E(p) + i\epsilon} \rightarrow \frac{Q}{\omega - E(p) + i\epsilon}$$

Q is determined via the Fermi gas model for the nucleus. In the Lippmann-Schwinger equation

$$t(\mathbf{k}', E, \mathbf{k}) = V(\mathbf{k}', \mathbf{k}) + (\hbar c)^3 \int d^3p \, \frac{V(\mathbf{k}', \mathbf{p})\, Q(\mathbf{p})\, t(\mathbf{p}, E, \mathbf{k})}{E - E(\mathbf{p}) + i\epsilon} \qquad (5.42)$$

Q is 0 for the case where $\mathbf{p}$ designates a state which is occupied by another nucleon and 1 for states which are unoccupied. In the Fermi gas model states with momentum of magnitude less than the Fermi momentum p_F in the nuclear center of mass frame are occupied and those with momentum greater than p_F are unoccupied. In solving equation 5.42 the variable of integration is $\mathbf{p}$, the relative projectile-nucleon momentum. For a given $\mathbf{k}$ and $\mathbf{k}'$ (projectile-nucleus relative momentum before and after the interaction) we need to find the momentum of the nucleon relative to the center of mass of the

nucleus for each value of the integration variable $\mathbf{p}$ and compare its magnitude with p_F. The Fermi gas model is only appropriate for heavier nuclei. We will only consider it for A=12. Thus, we can neglect the motion of the nucleus. Also since the Fermi momentum is small compared to the rest mass of a nucleon we can use nonrelativistic kinematics. The velocity of the nucleon in the nucleus center of mass is then just the sum of projectile-nucleon relative velocity and the velocity of the center of mass of the projectile-nucleon pair

$$\frac{\mathbf{P}}{m_p + m_N}$$

where m_N is the mass of the nucleon, m_p is the mass of the projectile and $\mathbf{P}$ is the combined projectile-nucleon momentum in the center of mass of the nucleus. Thus,

$$\mathbf{p}_N = \frac{m_N}{m_p + m_N}\mathbf{P} + \mathbf{p}$$

and

$$\begin{aligned} Q = \ & 0 \quad \left|\frac{m_N}{m_p + m_N}\mathbf{P} - \mathbf{p}\right| > p_F \\ Q = \ & 1 \quad \text{otherwise} \end{aligned}$$

We can expand Q in terms of Legendre polynomials as

$$Q(\mathbf{P}, \mathbf{p}) = \sum_l Q_l(P, p)\, P_l(\hat{p} \cdot \hat{P})$$

Since we consider only s-waves in the antikaon-nucleon interaction we just need the $l = 0$ term

$$\begin{aligned} Q_0(P, p) &= 0 \ \text{ for } \ \xi P + p < p_F \\ &= 1 \ \text{ for } \ |\xi P - p| > p_F \end{aligned}$$

$$= \left[(\xi P + p)^2 - p_F^2\right] / 4\xi P p$$

otherwise

where

$$\xi \equiv \frac{m_N}{m_p + m_N}$$

We determine p_F using a local density in the Fermi gas model

$$p_F = \left[\frac{3\pi^2}{2}\rho(r_0)\right]^{\frac{1}{3}}$$

Where $\rho(r)$ is the nuclear matter density as a function of radial position r and r_0 is the radial position of maximum overlap of the kaon and nuclear wave functions. This occurs at the maximum of the product

$$r^2|\Psi(r)|^2 r^2\rho(r)$$

where $\Psi(r)$ is the radial kaon atomic (pure Coulomb) wave function. In Figure 45 we show the probability for finding a kaon in a kaonic carbon-12 2p level at r, in the upper plot of Figure 46 we show the probability for finding a nucleon at radius r, and in the lower plot of Figure 46 we show the product of the two. The latter peaks at $r_0 = 3.2$ fm. This corresponds to a density of 0.024 nucleons/fm^3 in the harmonic oscillator model of the density. This yields a Fermi momentum of 140 MeV/c. Again, this value is for the 2p level of kaonic carbon.

Partial Wave Projection

The optical potential given in the last few sections is a function of the vectors $\mathbf{k}', \mathbf{p}', \mathbf{k}$, and $\mathbf{p}$ where $\mathbf{k}$ and $\mathbf{k}'$ are the initial and final momenta of the

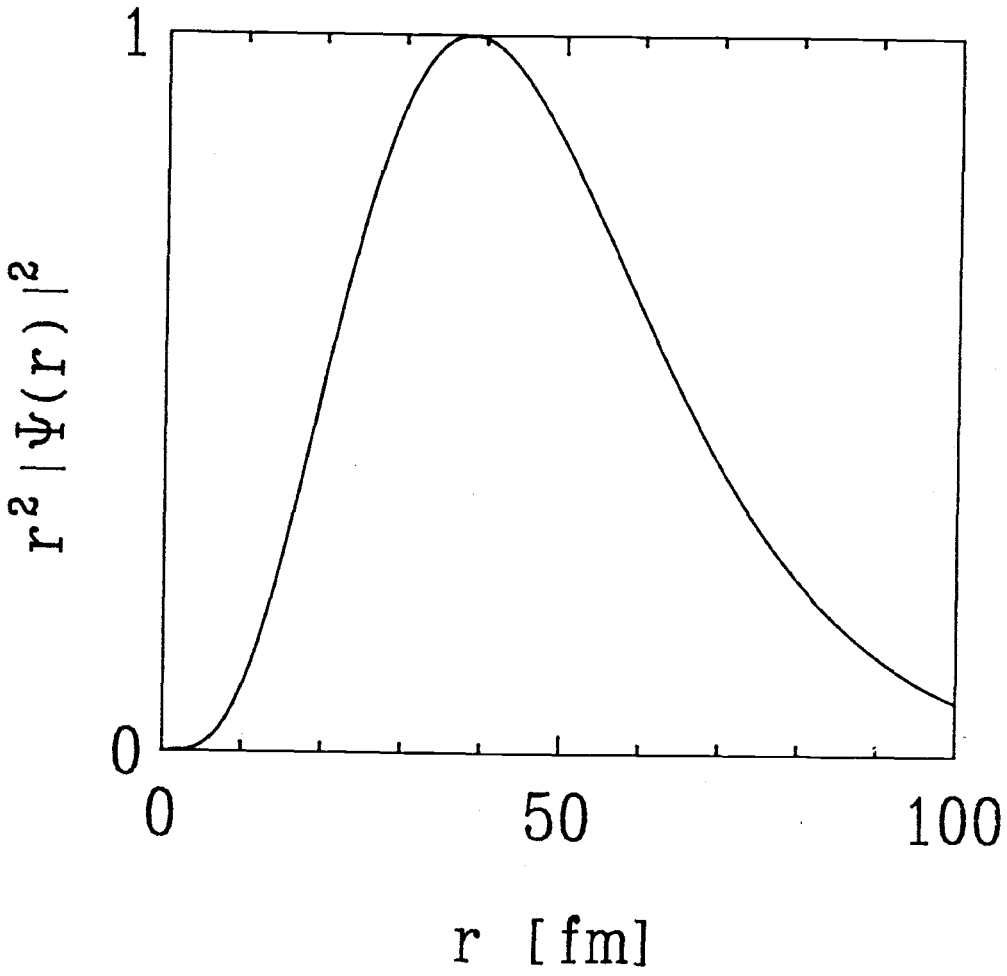

Figure 45. The probability for finding a kaon in the kaonic carbon-12 2p orbit at radius r (arbitrary normalization).

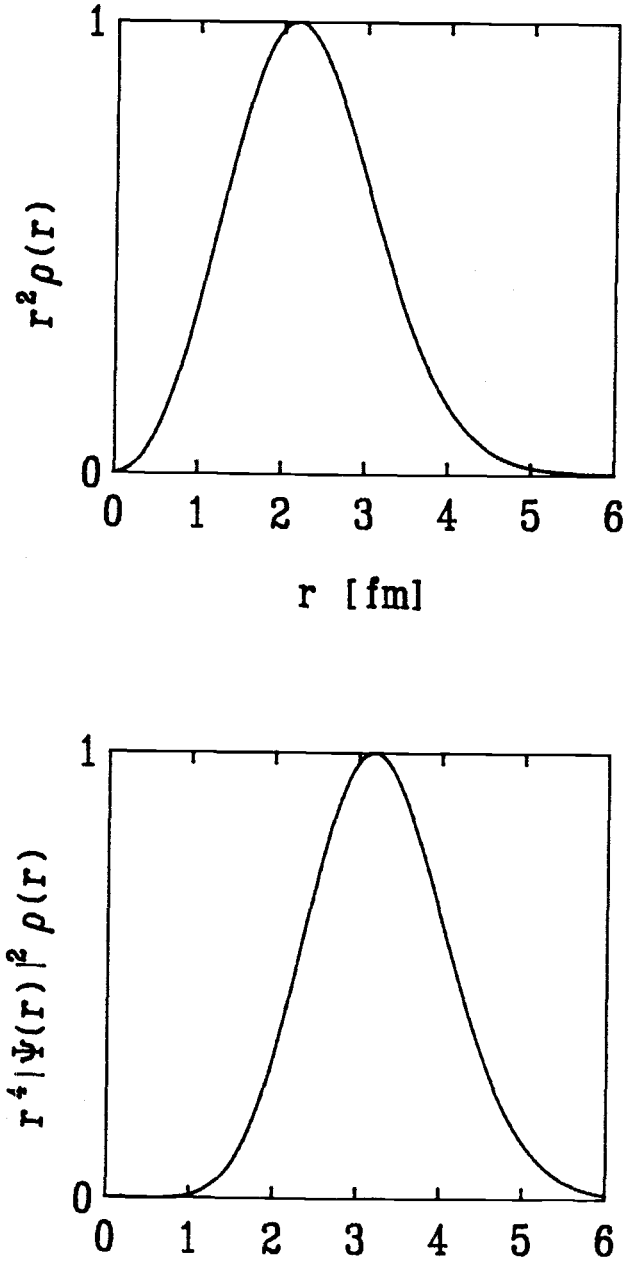

Figure 46. The probability for finding a nucleon in carbon-12 at radius r (upper graph) and the product probability for finding a nucleon and a kaon at radius r (lower graph).

projectile and $\mathbf{p}$ and $\mathbf{p}'$ are the initial and final momenta of the target nucleus. In that these momenta are all given in the projectile-nucleus center of mass we have $\mathbf{p}' = -\mathbf{k}'$ and $\mathbf{p} = -\mathbf{k}$ so that the optical potential is actually just a function of $\mathbf{k}$ and $\mathbf{k}'$. Further, for the case of an elementary interaction which is pure s-wave and form factors with azimuthal symmetry the optical potential is a function only of the magnitudes of the initial and final projectile momenta and the angle between them. Thus we can write

$$U(\mathbf{k}', \mathbf{p}'|\mathbf{k}, \mathbf{p}) = U(k', k, \cos\theta)$$

This means that we can expand the potential in a Legendre Polynomial series as

$$U(\mathbf{k}', \mathbf{p}'|\mathbf{k}, \mathbf{p}) = \frac{1}{2\pi^2} \sum_{l=0}^{\infty} (2l+1) U_l(k', k) P_l(\cos\theta)$$

with

$$U_l(k', k) = \int_{-1}^{1} U(k', k, \cos\theta) P_l(\cos\theta) d\cos\theta \tag{5.43}$$

Now even though the elementary 2-body t-matrix is pure s-wave the optical potential is not because the energy at which we evaluate the 2-body t-matrix depends on θ and the form factor is in general a function of theta. In this work we consider p waves, $l = 1$. The projection in equation 5.43 is carried out numerically.

Form Factors

We calculate the shift and width of the Coulomb bound states for ^{4}He and ^{12}C. The functions used to describe the form factors are different for these two cases and we describe each.

^{4}He The form factor for ^{4}He is given in terms of $q \equiv |\mathbf{k}' - \mathbf{k}|$ by Frosch et al. [62] as

$$\rho(q) = \frac{(1 - a_{cm}^{12} q^{12}) e^{-a_{ch}^2 q^2/4}}{f^p(q)}$$

where the proton form factor $f^p(q)$ is given by [63]

$$f^p(q) = (1 + q^2/18.2\text{fm}^{-2})^{-2}$$

and

$$\begin{aligned} a_{ch} &= 1.362\text{fm} \\ a_{cm} &= 0.316\text{fm} \end{aligned}$$

^{12}C For ^{12}C we use the density distribution for nucleons given by the harmonic oscillator model. In coordinate space the density appears as

$$\tilde{\rho}(r) = \tilde{\rho}_0 \left[1 + \frac{Z-2}{3}(\frac{r}{a_{cm}})^2\right] e^{-r^2/a_{ch}^2}$$

where Z is the number of protons in the nucleus. By Fourier transform we obtain the form factor as

$$\rho(q) = \left(1 - \frac{Z-2}{6} a_{cm}^2 q^2\right) e^{-a_{ch}^2 q^2/4}$$

We use the fit of ref. [64] in which

$$\begin{aligned} a_{ch} &= 1.649\text{fm} \\ a_{cm} &= 1.705\text{fm} \end{aligned}$$

where these values apply specifically to ^{12}C.

5.3 Kaonic Carbon Results

For each set of potential parameters determined on the basis of low energy K^-p scattering and $\pi p \rightarrow \pi\Sigma K^0$ mass spectrum we have constructed the optical potential and used it to calculate the shift and width of the 2p level in kaonic carbon. The results are given as a function of the one free parameter in the theory, the binding energy E_B, implemented to account for nuclear medium effects on the antikaon-nucleon interaction. In Figure 47 we show the results for the HAW and nr1 parameter sets. At $E_B \approx 25$ MeV both sets provide reasonable agreement with experiment. The agreement is not good but we cannot rule out either set of potential parameters on the basis of this comparison. We note that the values of the width are significantly smaller than the experimental values. This trend is observed for all the potential parameter sets and was also reported by HAW [23] in a coordinate space study of the same problem. They concluded that more absorption was needed in the optical potential. We propose that this additional absorption would come about naturally if the bound state problem were treated as a coupled channels problem. Recall that we treat the elementary K^-p interaction as a coupled channels problem and the channel coupling is the source of the absorption in the bound antikaon-nucleus problem which we treat as a single channel problem. In the absence of nuclear form factors for the nucleus which results when the reaction $K^-p \rightarrow \pi\Sigma$ occurs in the nucleus we consider the full coupled channels antikaon-nucleus problem to be beyond the state of the art.

The shift resulting from the parameter set nr2 yields a shift that is roughly

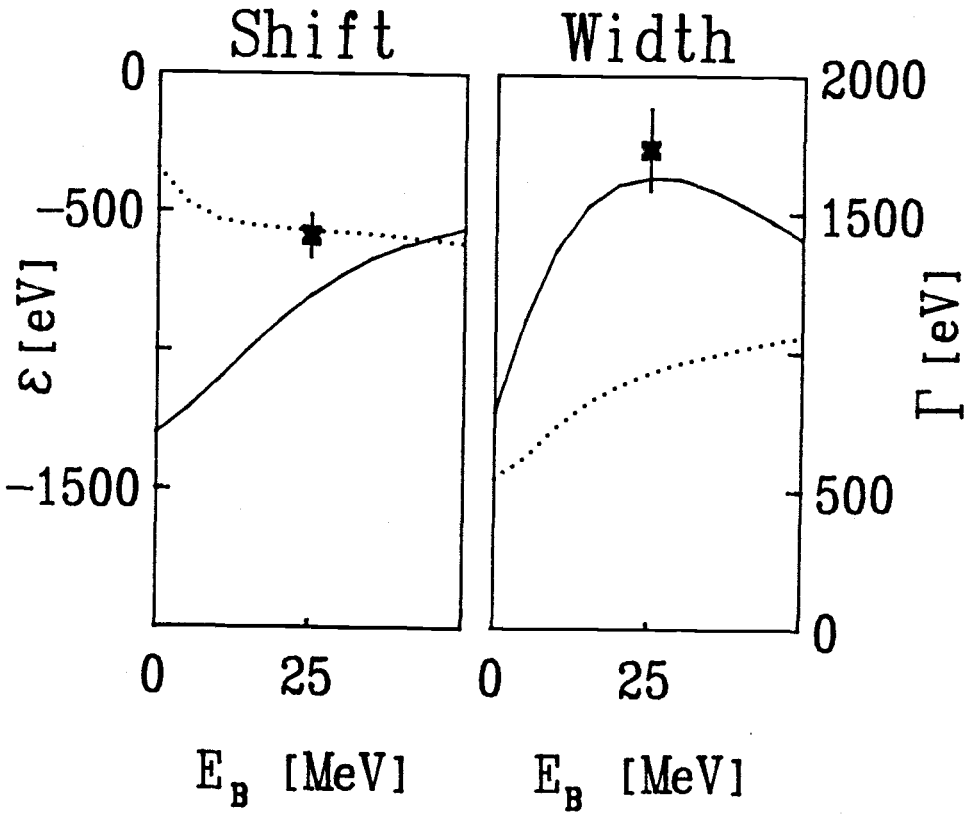

Figure 47. The energy levels corresponding to the shift and width of the 2p level in kaonic carbon-12. The data are from ref. [21]. The calculated values are plotted as a function of the binding energy parameter (the abscissas apply only to the calculated values, not the data). The solid lines correspond to the HAW potential parameters for the K^-p interaction and the dotted lines to the nrl parameters.

a factor of three greater than the measured shift. (See Figure 48.) We conclude that this set can be ruled out as describing the K^-p interaction which occurs in nature even though it corresponded to our best fit to the low energy scattering data and $\pi\Sigma$ mass spectrum. The situation for parameter set nr3 is even worse. The shift is on the order of +3000 eV (in the wrong direction) and the width is greater than 4000 eV. The nr3 parameters are the ones that yielded a good fit to the low energy scattering data and the spectrum but did not show an $I = 0$ $\pi\Sigma$ resonance corresponding to the $\Lambda(1405)$. The poor agreement with the carbon data shows that this resonance deserves the four star rating assigned to it in the particle data booklet [44].

The shift and width of the 2p level in kaonic carbon computed with the relativistic parameter sets r1 and r2 are shown in Figure 49. Neither of these parameter sets can be discarded on the basis of the carbon experiment. In particular, the new relativistic fit r2 remains the only fit which does not contradict any experimental data.

5.4 Kaonic Helium Results

In the case of kaonic helium the shift and width calculated with any of the potential parameter sets are small compared to experimental results. The calculated values are fairly constant as a function of E_B over a subrange of the values on the interval 0–50 MeV so we are able to present the results in tabular form (see Table 9). Note that the experimental values themselves (see Table 8 on page 96) are a small fraction of the Coulomb binding energy for the 2p level (11.6 KeV). It is not surprising that the nuclear force has a

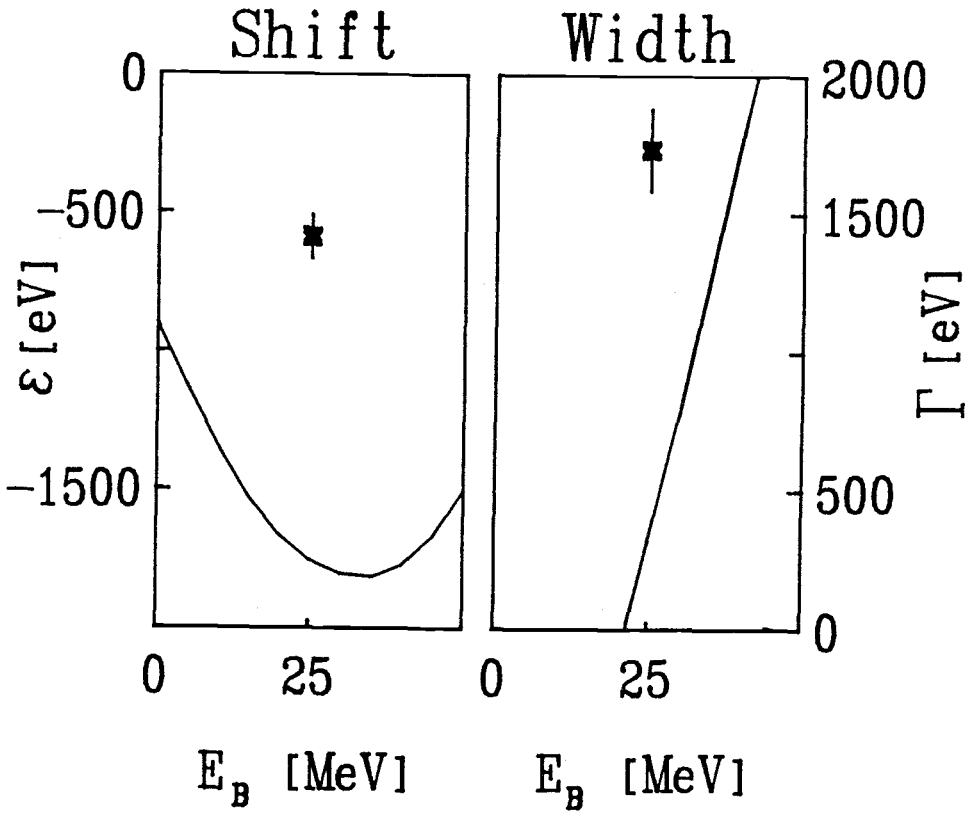

Figure 48. The energy levels corresponding to the shift and width of the 2p level in kaonic carbon-12. The data are from ref. [21]. The solid solid lines represent the results of a calculation using the nr2 potential parameters for the K^-p interaction.

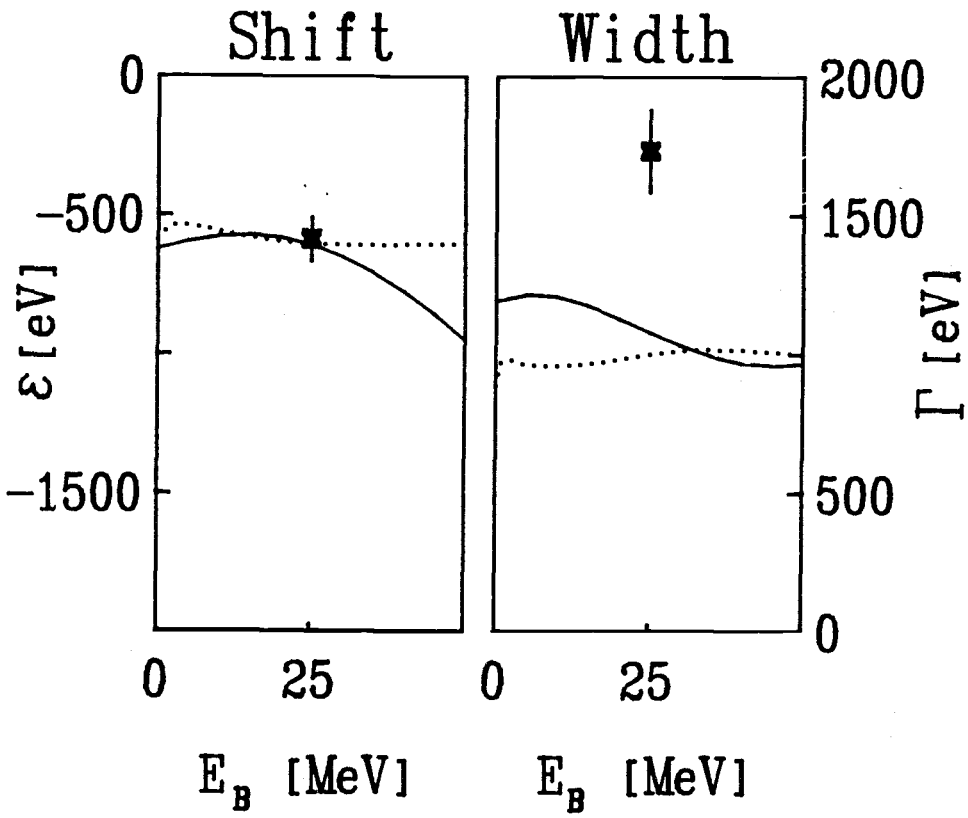

Figure 49. The energy levels corresponding to the shift and width of the 2p level in kaonic carbon-12. The data are from ref. [21]. The calculated values are plotted as a function of the binding energy parameter (the abscissas apply only to the calculated values, not the data). The solid solid lines correspond to the r2 potential parameters for the K^-p interaction and the dotted lines to the r1 parameters.

Fit	Shift[eV]	Width[eV]
nr1	-5.6	1.6
nr2	-6.5	0.5
nr3	-6.8	0.8
HAW	-6.1	2.0
r1	-6.0	0.7
r2	-5.2	0.7

Table 9. The shifts and widths of the 2p level in kaonic helium based on fits nr1, nr2, nr3, r1, and r2 of the present work and fit HAW (fit c of ref. [23]).

small effect on this atomic state in that the Bohr radius is 124 fm, roughly 70 times the size of the nucleus. An attempt to predict this small an effect in a few body system with a many body theory is perhaps overly ambitious. The omitted recoil corrections which are small for carbon may not be so small for an atom whose mass is only eight times that of the kaon. We have experimented with various form factors, with the inclusion of Pauli effects, and with full three dimensional Fermi folding (no factored approximation) as well as allowing the binding energy to vary well outside the expected range of validity. Because the calculated values remain small over such a wide variety of circumstances it appears that minor improvements to the model will not account for the discrepancy with experiment. It appears that something special must be occurring in the kaonic helium system. This view is supported by previous work. In a theoretical study quite different from the

present work Batty [65] also found values for the shift and width in kaonic helium-4 which were small compared to the measured values. In that study the parameters of an optical potential of the form

$$V(r) = \frac{2\pi\hbar^2}{\mu}\left(1 + \frac{\mu}{m}\right)\bar{a}\rho(r)$$

[where μ is the reduced mass for the kaon-nucleon system, m is the mass of a nucleon, $\bar{a}$ is the complex scattering length (an adjustable parameter), and ρ is the nuclear density] were obtained from an analysis of all available data for heavier nuclei. This potential was then used to predict the values $\epsilon = -0.2$ eV and $\Gamma = 2$ eV for the shift and width of the 2p level in kaonic helium-4. Thus, two very different theoretical approaches yield similar results. Baird et al. [56] have determined the optical potential parameters needed to fit the kaonic helium data and conclude that the strength of the imaginary part of the potential must be very small to reproduce experimental results. We investigated the possibility that the imaginary part of our kaonic helium optical potential was too large relative to the real part by multiplying it by a factor allowed to very from 0 to 1. We found that using only a fraction of the imaginary part of the optical potential made very little difference and indeed the small effect that it did have was to reduce the magnitude of the shift and width even further. We conclude that our potential is simply too weak overall to produce the experimental values. Several workers have investigated the possibility that the anomalous shift and width are due to the presence of a nuclear bound state [8,13,66]. Staronski and Wycech [67] have shown the importance of the interaction of the pion resulting from $K^-p \rightarrow \pi\Sigma$ with the nucleus in determining the shift and width. Again

it appears that an improvement to our model should involve the explicit treatment of the coupled channels in the kaon-nucleus system. In that all the potential parameter sets gave essentially the same results the failure to obtain agreement with experiment points out a weakness in the theory as opposed to a problem with the understanding of the elementary $\bar{K}N$ interaction. Thus the kaonic helium atom has not proved to be a discriminating testing ground for the various descriptions of the $\bar{K}N$ interaction.

Chapter 6

Summary/Conclusions

6.1 Summary of Results

We have presented an s-wave scattering amplitude (based on the potential parameter set r2) for the $K^-p, \overline{K}^0n, \pi\Sigma$ coupled channels system which is consistent with low energy K^-p scattering, the $\pi^-p \rightarrow \pi\Sigma K^0$ production data, kaonic hydrogen x-ray emission and heavier kaonic atoms x-ray emission. The scattering amplitude is derived from a potential model and thus has the desired properties of unitarity and analyticity (dispersion relations are built in). This scattering amplitude provides a solution to the puzzle consisting of the discrepancy between the measured kaonic hydrogen shift and that predicted on the basis of low energy K^-p scattering. The importance of using relativistic kinematics in describing a system which is coupled strongly to a channel in which the particles are at relativistic energies even at the threshold energy of the original system is revealed by the fact that only with relativistic kinematics were we able to obtain scattering amplitudes consistent with all the data. The fact that we were able to obtain agreement with

experiment in a model which has at its heart a Yukawa potential binding an antikaon to a nucleon and a pion to a sigma hyperon supports the view [43] that the $\Lambda(1405)$ resonance is predominantly a composite particle consisting of a meson and a baryon as opposed to an elementary 3-quark state.

6.2 Future Directions

6.2.1 Experiment

The best alternative to our solution to the kaonic hydrogen shift puzzle assumes that the results of all three kaonic hydrogen x-ray experiments are wrong. A definitive x-ray experiment would go a long way in supporting or ruling out this possibility and is thus considered crucial to work in this area. The experiment proposed by van Eijk and Hollander [68] may provide the answer.

6.2.2 Theory

The framework in which this study has been carried out allows room for several extensions to the study. The effect of higher partial waves in the two body interaction could prove a fruitful avenue for future investigation. There is some evidence that p-waves may be important even at low energies. Furthermore the inclusion of higher partial waves would extend the validity of the method to higher energies where the results could be tested against more data, in particular, data from the Coulomb nuclear interference experiments and low energy antikaon-nucleus scattering. It appears that this high energy data when fitted by s-wave plus higher partial wave scattering amplitudes

constrains the s-wave amplitude even at subthreshold energies. This statement is based on the fact that Kim [35] was able to predict the existence of the $\Lambda(1405)$ resonance based on the results of K-matrix analyses of the scattering data out to 550 MeV. Kim used s, p, and d waves.

One could include the Coulomb force in the elementary interaction. This is not expected to be important in s-waves. In including p-waves however, the Coulomb interaction and in particular Coulomb nuclear interference may play a large role in determining the angular distribution of differential cross sections.

The optical potentials determined in the present work could be used in an investigation of strong kaonic bound states or low energy antikaon-nucleus scattering.

The present framework is ideal for testing models of the elementary two-body interaction such as potentials based on specific meson exchange or quark models. This is probably the most important direction for the theoretical work to take. One simply builds the physics into the two-body potential and attempts to generate scattering amplitude that meet all the criteria herein. The success or failure will determine the relevance of the physics built into the interaction.

Another possible extension to the present work involves an improved method for handling the kaonic atom problem for $A > 1$. One could solve a coupled channels problem here as is done for the elementary interaction. More information on the form factor of nuclei in which one of the protons has turned into a sigma particle would have to be developed but the calculations could be expected to yield more quantitative results.

BIBLIOGRAPHY

[1] E. H. S. Burhop, Nucl. Phys. **B1**, 438 (1967).

[2] S. D. Bloom, M. H. Johnson, and E. Teller, Phys. Rev. Lett. **23**, 28 (1969).

[3] H. A. Bethe and P. J. Siemens, Nucl. Phys. **B21**, 589 (1970).

[4] K. Aslam and J. R. Rook, Nucl. Phys. **B20**, 397 (1970).

[5] T. E. O. Ericson and F. Scheck, Nucl. Phys. **B19**, 450 (1970).

[6] S. Wycech, Nucl. Phys. **B28**, 541 (1971).

[7] Max Krell, Phys. Rev. Lett. **26**, 584 (1971).

[8] Justus H. Koch, Morton M. Sternheim, and James F. Walker, Phys. Rev. Lett. **26**, 1465 (1971).

[9] J. R. Rook and S. Wycech, Phys. Lett. **39B**, 469 (1972).

[10] E. H. S. Burhop, Nucl. Phys. **B44**, 445 (1972).

[11] B. Brook, Nucl. Phys. **B36**, 345 (1972).

[12] G. Backenstoss, A. Bamberger, I. Bergström, P. Bounin, T. Bunaciu, J. Egger, S. Hultberg, H. Koch, M. Krell, U. Lynen, H. G. Ritter, A. Schwitter, and R. Stearns, Phys. Lett. **38B**, 181 (1972).

[13] Ryoichi Seki, Phys. Rev. C **5**, 1196 (1972).

[14] W. A. Bardeen and E. Wayne Torigoe, Phys. Lett. **38B**, 135 (1972).

[15] Y. Eisenberg and D. Kessler, Phys. Rev. **130**, 2352 (1963).

[16] G. R. Burleson, D. Cohen, R. C. Lamb, D. N. Michael, R. A. Schluter, and T. O. White, Jr., Phys. Rev. Lett. **15**, 70 (1965).

[17] Clyde E. Wiegand and Dick A. Mack, Phys. Rev. Lett. **18**, 685 (1967).

[18] D. H. Davis, S. P. Lovell, M. Csejthey-Barth, J. Sacton, G. Schorochoff, and M. O'Reilly, Nucl. Phys. **B1**, 434 (1967).

[19] G. Backenstoss, A. Bamberger, J. Egger, W. D. Hamilton, H. Koch, U. Lynen, H. G. Ritter, and H. Schmitt, Phys. Lett. **32B**, 399 (1970).

[20] R. Kunselman, Phys. Lett. **34B**, 485 (1971).

[21] G. Backenstoss, J. Egger, H. Koch, H. P. Povel, A. Schwitter, and L. Tauscher, Nucl. Phys. **B73**, 189, (1974).

[22] P. D. Barnes, R. A. Eisenstein, W. C. Lam, J. Miller, R. B. Sutton, M. Eckhause, J. R. Kane, R. E. Welsch, D. A. Jenkins, R. J. Powers, A. R. Kunselman, R. P. Redwine, and R. E. Segel, Nucl. Phys. **A231**, 477 (1974).

[23] M. Alberg, E. M. Henley, and L. Wilets, Ann. Phys. **96**, 43 (1976).

[24] J. D. Davies, G. J. Pyle, G. T. A. Squier, C. J. Batty, S. F. Biagi, S. D. Hoath, P. Sharman, and A. S. Clough, Phys. Lett. **83B**, 55 (1979).

[25] M. Izycki, G. Backenstoss, L. Tauscher, P. Blüm, R. Guigas, N. Hassler, H. Koch, H. Poth, K. Fransson, A. Nilsson, P. Pavlopoulos, and K. Zioutas, Z. Phys. A **297**, 11 (1980).

[26] P. M. Bird, A. S. Clough, K. R. Parker, G. J. Pyle, G. T. A. Squier, S. Baird, C. J. Batty, A. I. Kilvington, F. M. Russell, and P. Sharman, Nucl. Phys. **A404**, 482 (1983).

[27] C. J. Batty, Nukleonika **25**, 545 (1980).

[28] H. H. Brouwer, J. W. de Maag, and L. P. Kok, Z. Phys. A **318**,1 (1984).

[29] William E. Humphrey and Ronald R. Ross, Phys. Rev. **127**, 1305 (1962).

[30] K. Schlosser, B. Buschbek-Czapp, H. Hromadnik, and G. Otter, Phys. Lett. **17**, 334 (1965).

[31] P. Baillon, C. Bricman, M. Ferro-Luzzi, P. Jenni, J. M. Perreau, R. D. Tripp, and T. Ypsilantis, Nucl. Phys. **B105**, 365 (1976).

[32] A. D. Martin, Phys. Lett. **65B**, 346 (1976).

[33] Terry S. Mast, Margaret Alston-Garnjost, Roger O. Bangerter, Angela S. Barbaro-Galtieri, Frank T. Solmitz, and Robert D. Tripp, Phys. Rev. D **14**, 13 (1976).

[34] W. Kittel, G. Otter, and I. Wacek, Phys. Lett. **21**, 349 (1966).

[35] Jae Kwan Kim, Phys. Rev. Lett. **19**, 1074 (1967).

[36] T. S. Mast, M. Alston-Garnjost, R. O. Bangerter, A. S. Barbaro-Galtieri, F. T. Solmitz, and R. D. Tripp, Phys. Rev. D **11**, 3078 (1975).

[37] R. O. Bangerter, M. Alston-Garnjost, A. Barbaro-Galtieri, T. S. Mast, F. T. Solmitz, and R. D. Tripp, Phys. Rev. D **23**, 1484 (1981).

[38] A. D. Martin, Nucl. Phys. **B179**, 33 (1981).

[39] J. Ciborowski, J. Gwizdz, D. Kielczewska, R. J. Nowak, E. Rondio, J. A. Zakrzewski, M. Goossens, G. Wilquet, N. H. Bedford, D. Evans, G. P. Fleming, Y. A. Hamam, J. V. Major, J. H. Bartley, D. H. Davis, D. J. Miller, D. N. Tovee, and T. Tymieniecka, J. Phys. G **8**, 13 (1982).

[40] D. Evans, J. V. Major, E. Rondio, J. A. Zakrzewski, J. E. Conboy, D. J. Miller, and T. Tymieniecka, J. Phys. G **9**, 885 (1983).

[41] J. Ciborowski, J. Gwizdz, D. Kielczewska, R. J. Nowak, E. Rondio, J. A. Zakrzewski, M. Goossens, G. Wilquet, N. H. Bedford, D. Evans, G. P. Fleming, Y. A. Hamam, J. V. Major, J. H. Bartley, D. H. Davis, D. J. Miller, D. N. Tovee, and T. Tymieniecka, in *Proceedings of the International Conference on Hypernuclear and Kaon Physics,* edited by B. Povh, Max-Planck-Institute für Kernphysik, Heidelberg, Federal Republic of Germany, 243 (1982).

[42] D. W. Thomas, A. Engler, H. E. Fisk, and R. W. Kraemer, Nucl. Phys. **B56**, 15 (1973).

[43] E. A. Veit, B. K. Jennings, A. W. Thomas, and R. C. Barrett, Phys. Rev. D **31**, 1033 (1985).

[44] C. G. Wohl, R. N. Cahn, A. Rittenberg, T. G. Trippe, G. P. Yost, F. C. Porter, J. J. Hernandez, L. Nontanet, R. E. Hendrick, R. L. Hendrick, R. L. Crawford, M. Roos, N. A. Törnqvist, G. Höhler, M. Aquilar-Benitez, T. Shimada, M. J. Losty, G. P. Gopal, Ch. Walck, R. E. Shrock, R. Frosch, L. D. Roper, W. P. Trower, and B. Armstrong, Rev. Mod. Phys. **56**, S39 (1984).

[45] *Introduction to Nuclear and Particle Physics* by Hans Frauenfelder, Lecture Notes, University of Illinois, p. 4.17 (1966).

[46] W. Krzyzanowski, J. Wrzecionko, and S. Wycech, Acta Phys. Pol. **B6**, 259 (1975).

[47] R. C. Barret, J. Phys. G **9**, 355 (1983).

[48] Rubin H. Landau, Phys. Rev. C **28**, 1324 (1983); R. H. Landau and Beato Cheng, Phys. Rev. C **33**, 734 (1986).

[49] J. Thaler, J. Phys. G **10**, 1037 (1984).

[50] T. L. Trueman, Nuc. Phys. **26**, 57 (1961).

[51] *Handbook of Mathematical Functions*, edited by Milton Abramowitz and Irene A. Stegun, National Bureau of Standards Applied Mathematics Series 55, 916 (1972).

[52] Yong Rae Kwon and F. Tabakin, Phys. Rev. C **18**, 932 (1978).

[53] L. H. Schick, B. F. Gibson, Z. Phys. A **288**, 307 (1978).

[54] D. Berley, S. P. Yamin, R. R. Kofler, A. Mann, G. W. Meisner, S. S. Yamamoto, J. Thompson and W. Willis, Phys. Rev. D **1**, 1996 (1970); D **3**, 2297 (1971).

[55] *Exotic Atoms; A Review* by C. J. Batty, Rutherford and Appleton Laboratories, Chilton, Didcot, Oxon, U. K., RL-80-94 (1980).

[56] S. Baird, C. J. Batty, F. M. Russell, P. Sharman, P. M. Bird, A. S. Clough, K. R. Parker, G. J. Pyle, and G. T. A. Squier, Nuc. Phys. **A392**, 297 (1983).

[57] C. J. Batty, S. F. Biagi, S. D. Hoath, P. Sharman, J. D. Davies, G. J. Pyle, and G. T. A. Squier, Nuc. Phys. **A326**, 455 (1979).

[58] Clyde E. Wiegand and Richard H. Pehl, Phys. Rev. Lett. **27**, 1410 (1971).

[59] *Collision Theory*, by M. L. Goldberger and K. M. Watson, John Wiley & Sons, Inc., New York, 679 (1964).

[60] A. K. Kerman, H. McManus, and R. M. Thaler, Ann. Phys. **8**, 551 (1959).

[61] R. H. Landau and A. W. Thomas, Nuc. Phys. **A302**, 461 (1978).

[62] R. F. Frosch, J. S. McCarthy, R. E. Rand, and M. R. Yearian, Phys. Rev. **160**, 874 (1967).

[63] B. Bartoli, F. Felicetti, and V. S. Silvestrini, Rev. Nuovo Cimento **2**, 241 (1972).

[64] I. Sick and J. S. McCarthy, Nuc. Phys. **A150**, 631 (1970).

[65] C. J. Batty, Nuc. Phys. **A372**, 418, 433 (1981).

[66] Justus H. Koch, Morton M. Sternheim and James F. Walker, Phys. Rev. C **5**, 381 (1972).

[67] R. Staronski and S. Wycech, Czech. J. Phys. B **36**, 903 (1986).

[68] C. W. E. van Eijk and R. W. Hollander, (Experiment Proposal 87.629), Instrumentatie Stralingssonderzoek, Vakgroep Spectroscopie en Stralingstechnologie, Faculteit der Technische Natuurkunde, TU Delft (1987).

APPENDIX

Appendix A

$\pi p \rightarrow \pi\Sigma K^0$ Reaction Kinematics

The energies of all the particles in the reaction

$$\pi p \rightarrow \pi\Sigma K^0$$

are to be evaluated in the $\pi\Sigma$ center of mass frame. Where convenient we refer to the $\pi\Sigma$ pair as a single particle Λ. Viewed in the πp center of mass frame the interaction appears as in Figure 50 which serves to define the angle theta. We use unprimed kinematic variables for quantities in the πp center of mass frame and primed variables for quantities in the $\pi\Sigma$ center of mass frame. The symbol p is used to specify a four momentum and $\mathbf{p}$ is used to specify a 3-momentum.

A.1 Determination of E'_p and E'_π

The Mandelstam variable t can be written in terms of variables in the πp center of mass as

$$\begin{aligned} t &= (p_p - p_\Lambda)^2 \\ &= (E_p - E_\Lambda)^2 - |\mathbf{p}_p|^2 - |\mathbf{p}_\Lambda|^2 + 2|\mathbf{p}_p|\,|\mathbf{p}_\Lambda|\cos\theta \end{aligned} \qquad \text{(A.44)}$$

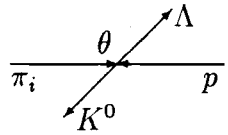

Figure 50. The $\pi p \rightarrow \pi\Sigma K^0$ scattering problem in the πp center of mass. The symbol Λ represents the $\pi\Sigma$ pair.

Given the total energy E (established in the experiment) we can compute all the quantities on the right except $\cos\theta$ by first solving

$$E = \sqrt{|\mathbf{p}_p|^2 + m_p^2} + \sqrt{|\mathbf{p}_p|^2 + m_\pi^2}$$

for $|\mathbf{p}_p|^2$ (which $= |\mathbf{p}_{\pi_i}|^2$) to obtain

$$E_p = \sqrt{|\mathbf{p}_p|^2}$$

and then solving

$$E = \sqrt{|\mathbf{p}_\Lambda|^2 + m_{K^0}^2} + \sqrt{|\mathbf{p}_\Lambda|^2 + M_\Lambda^2}$$

for $|\mathbf{p}_\Lambda|^2$ (which $= |\mathbf{p}_{K^0}|^2$) to obtain

$$E_\Lambda = \sqrt{|\mathbf{p}_p|^2}$$

The Mandelstam variable t can also be written in the $\pi\Sigma$ center of mass frame as

$$t \;=\; (p'_p - p'_\Lambda)^2$$

$$
\begin{aligned}
&= (E'_p - E'_\Lambda)^2 - (\mathbf{p}'_p - \mathbf{p}'_\Lambda)^2 \\
&= (E'_p - E'_\Lambda)^2 - |\mathbf{p}'_p|^2 \\
&= M_\Lambda^2 - 2E'_p M_\Lambda + m_p^2 \qquad \text{(A.45)}
\end{aligned}
$$

Equating the two expressions for t (equations A.44 and A.45) we find

$$E'_p = \frac{E_p E_\Lambda - |\mathbf{p}_p|\,|\mathbf{p}_\Lambda|\cos\theta}{M_\Lambda}$$

Choosing

$$t = (p_{\pi_i} - p_{K^0})^2$$

we carry out the same steps to find

$$E'_{\pi_i} = \frac{E_{\pi_i} E_{K^0} - |\mathbf{p}_{\pi_i}|\,|\mathbf{p}_{K^0}|\cos\theta}{m_{K^0}}$$

In practice we use a forward peaking approximation in which $\cos\theta$ is set equal to 1.

A.2 Determination of E'_{K^0}

E'_{K^0} is determined with the aid of the Mandelstam invariant s by

$$
\begin{aligned}
E^2 &= s \\
&= (p'_{K^0} + p'_\Lambda)^2 \\
&= (E'_{K^0} + M_\Lambda)^2 - |\mathbf{p}'_{K^0}|^2
\end{aligned}
$$

Substituting

$$|\mathbf{p}'_{K^0}|^2 = E'^2_{K^0} - m^2_{K^0}$$

we can solve for E'_{K0} obtaining

$$E'_{K^0} = \frac{E^2 - (M_\Lambda^2 + m^2_{K^0})}{2m_2}$$

A.3 Determination of E'_π and E'_Σ

E'_π and E'_Σ can be determined simply by solving

$$\begin{aligned} M_\Lambda^2 &= (E'_\pi + E'_\Sigma)^2 \\ &= (\sqrt{|\mathbf{p}'_\Sigma|^2 + m_\Sigma^2} + \sqrt{|\mathbf{p}'_\Sigma|^2 + m_{\pi_f}^2})^2 \end{aligned}$$

for $|\mathbf{p}'_\Sigma|^2$ and using

$$\begin{aligned} E'_\Sigma &= \sqrt{|\mathbf{p}'_\Sigma|^2 + m_\Sigma^2} \\ |\mathbf{p}'_\pi|^2 &= |\mathbf{p}'_\Sigma|^2 \\ E'_\pi &= \sqrt{|\mathbf{p}'_\pi|^2 + m_\pi^2} \end{aligned}$$

Note that M_Λ is the abscissa variable in Figure 10 and is thus to be considered a given for the purpose of these calculations.